



IERS TECHNICAL NOTE 28

High frequency to subseasonal variations in Earth Rotation

Kolaczek B., Schuh H., Gambis D., (Eds)

September 2000

Central Bureau of IERS - Observatoire de Paris
61, avenue de l'Observatoire
F-75014 PARIS France

IERS Technical Notes

This series of publications gives technical information related to the IERS activities, e.g., reference frames, excitation of the Earth rotation, computational or analysis aspects, models, etc. It also contains the description and results of the analyses performed by the IERS Analysis Centres for the Annual Report global analysis.

Back issues still available

- No 14: P. Charlot (ed.). Earth orientation, reference frames and atmospheric excitation functions submitted for the 1992 IERS Annual Report.*[Superseded by T.N. 17]*
- No 16: J.O. Dickey and M. Feissel (eds.). Results from the SEARCH'92 Campaign
- No 17: P. Charlot (ed.). Earth orientation, reference frames and atmospheric excitation functions submitted for the 1993 IERS Annual Report.*[Superseded by T.N. 19]*
- No 19: P. Charlot (ed.). Earth orientation, reference frames and atmospheric excitation functions submitted for the 1994 IERS Annual Report
- No 21: D.D. McCarthy (ed.). IERS Conventions (1996)
- No 22: C. Reigber and M. Feissel (eds.). IERS missions, present and future. Report on the 1996 IERS Workshop
- No 24: C. Boucher, Z. Altamimi, P. Sillard (eds.). Results and Analysis of the ITRF96.
- No 25: J. Ray (ed.). Analysis Campaign to Investigate Motions of the Geocenter.
- No 26: D. Salstein, B. Kolaczek, D. Gambis (eds.). The impact of El Niño and other low-frequency signals on Earth rotation and global Earth system parameters.
- No 27: C. Boucher, Z. Altamimi, P. Sillard (eds.). The 1997 International Terrestrial Reference Frame (ITRF97)
- No 28: B. Kolaczek, Schuh H., Gambis D. (eds.). High frequency to subseasonal variations in Earth Rotation

Contents

	Page
- IERS Technical Notes	ii
- Introduction	v
Updated model of short-period tidal variations in Earth rotation	
<i>Ray Richard D.</i>	
Space Geodesy Branch, NASA Goddard Space Flight, USA	1
Diurnal and sub-diurnal variations of the Earth rotation	
<i>Zharov Vladimir E. (1), Gambis Daniel (2), Bizouard Christian (2)</i>	
(1) Sternberg State Astronomical Institute, Moscow, Russia	
(2) Observatoire de Paris, IERS, Paris, France	5
Estimation of subdiurnal tidal terms in UT1-UTC from VLBI data analysis	
<i>Titov Oleg</i>	
Saint-Petersburg University, Russia	11
Interpretation of high frequency polar motion and length of day variations	
<i>Arfa-Kaboodvand K.(1), Groten Erwin (1), Varga Peter (2), Zavoti J.(2)</i>	
(1) Darmstadt University of Technology, Institute for Physical Geodesy, Germany	
(2) Geodetic and Geophysical Research Institute of Hungarian Acad. of Sciences, Hungary	15
The short period nutations of the Earth	
<i>Souchay Jean (1) and Marta Folgueira (2)</i>	
(1) Observatoire de Paris, Paris, France	
(2) Instituto de Astronomia y Geodesia (UCM-CSIC), Madrid, Spain	27
Short periods in Earth rotation seen in VLBI data analysed by the least-squares collocation method	
<i>Titov Oleg(1) and Schuh Harald (2)</i>	
(1) Saint-Petersburg University, Russia	
(2) Institut für Geodäsie und Geophysik, Technische Universität Wien, Austria	33
Contribution of the GPS to monitor Earth Orientation Parameters	
<i>Weber Robert (1), Rothacher Markus (2), Beutler Gerhard (3)</i>	
(1) University of Geodesy and Geophysics, TU-Vienna	
(2) Forschungseinrichtung Satellitengeodäsie, TU-Munich, Germany	
(3) Astronomical Institute, University of Berne,	43
High frequency atmospheric excitation of Earth rotation	
<i>Brzezinski Aleksander</i>	
Space Research Centre, Polish Acad. of Sciences, Warsaw, Poland	53
Irregular short period variations in Earth rotation	
<i>Kosek Wieslaw</i>	
Space Research Centre, Polish Academy of Sciences, Warsaw, Poland	61

Wavelet analysis of stochastic signals*Michael Schmidt*

Deutsches Geodätisches Forschungsinstitut, Germany

65

Abilities of wavelet analysis for investigating short-period variations of Earth rotation*Michael Schmidt, Harald Schuh*

Deutsches Geodätisches Forschungsinstitut, Germany

73

Comparison between spectro-temporal analysis methods on the Earth rotation parameters and their atmospheric excitation functions*Kosek Wiesław (1), Popinski Waldemar (2)*

(1) Space Research Centre, Polish Academy of Sciences Warsaw, Poland

(2) Department of Standards, Central Statistical Office, Warsaw, Poland

81

Modes of variability in high-frequency atmospheric excitation for polar motion*Nastula Jolanta (1) and David A. Salstein (2)*

(1) Space Research Centre, Polish Acad. Of Sciences, Warsaw, Poland

(2) Atmospheric and Environmental Research, Inc. Cambridge, MA, USA

85

Introduction

At the XXIV EGS General Assembly held in The Hague in 19-23 April 1999, Session G18 on "High frequency and subseasonal oscillations of Earth rotation" was organized in order to present and discuss recent results concerning determinations and interpretations of these oscillations.

Fourteen papers were presented at the Session of which nine are published here. Four additional papers were added to this volume.

High frequency and subseasonal oscillations of Earth rotation have been extensively studied over the last decade thanks to the achievement of high accuracy and resolution in the space-geodetic techniques of VLBI, SLR and GPS. These signals can now be determined with an accuracy better than one millisecond of arc with a time resolution of a few hours.

Analyses of Earth Orientation Parameters (EOP) using Wavelet Transform (WT) and Fourier Transform Band Pass Filter (FTBPF) techniques have been used to determine and study time variations of high frequency variations of both Earth rotation and of effective atmospheric angular momentum functions (EAAM) which are highly correlated.

Results concerning high frequency oscillations of Earth rotation, including those on diurnal and semidiurnal scales, have yielded significant improvements in theories of tides and nutation. Furthermore, the effect of different geophysical phenomena on Earth rotation has been better understood because of the EAAM results.

Papers of this volume deal with the following problems.

- Methods of analyses of EOP and EAAM data and their results (Schmidt, Schuh and Schmidt, Kosek and Popinski, Nastula and Salstein)
- Determinations of EOP data by VLBI and GPS (Titov and Schuh, Weber and Rothacher)
- Atmospheric excitation of high frequency oscillations of ERP (Brzezinski)
- Irregular variations of EOP (Kosek)
- Improvements in nutation theory (Souchay and Folgueiza, Weber and Rothacher)
- Improvements in tidal terms in Earth rotation (Ray, Titov, Zharov *et al.*, Arfa-Kaboodvand *et al.*)

UPDATED MODEL OF SHORT-PERIOD TIDAL VARIATIONS IN EARTH ROTATION

Ray Richard D. - Space Geodesy Branch, NASA Goddard Space Flight Center Greenbelt, MD, USA

INTRODUCTION

The ocean tides are the dominant cause of short-period (daily and subdaily) variations in the Earth's rotation rate and polar motion (Chao et al., 1996). The tides directly perturb the Earth's inertia tensor as well as exchange angular momentum with the solid mantle. Both mechanisms are important for understanding the rotation variations, which are well observed by modern methods of space geodesy (Brosche et al., 1991; Herring and Dong, 1994; among others).

Over the past decade there have been a number of estimates of tidally driven Earth-rotation variations based on various kinds of ocean tide models. The most accurate of these are models constrained by direct oceanic measurements, usually either tide gauges (Ray et al., 1994) or satellite altimetry (Chao et al., 1996). Models based upon strictly numerical hydrodynamic methods (i.e., those that use only bathymetry data and the known astronomical potential) have been less successful. The reason for this is the difficulty of accurately modeling the ocean's barotropic response to very short-period forcing. When the basic mechanisms of tidal energy dissipation are still unresolved (Munk, 1997), it is not surprising that strictly numerical models are found wanting. By far the most accurate models of ocean tides are nowadays those based on direct tidal estimates from the Topex/Poseidon satellite altimeter. Hydrodynamic theories are still required for deducing current velocities, and also for modeling tides in polar seas, but the direct estimates from T/P have been a great boon to tidal accuracies.

Chao et al. (1996) published tidal Earth-rotation predictions based on three models constrained by T/P observations. All these models were based on 3 or fewer years of T/P measurements. As of this writing the T/P satellite has accumulated slightly more than 7 years of measurements, and updated (second generation) tidal models are now appearing. Moreover, methods of analysis have been improving, as have methods of deducing barotropic tidal currents from the measured elevations. This report tabulates updated predictions of tidal rotation variations from one such new model.

IMPROVED ESTIMATES OF TIDAL HEIGHTS AND CURRENTS

Goddard Ocean Tide model GOT99.2 is based on 232 10-day cycles of Topex/Poseidon altimeter measurements, processed as a correction to a prior tide model consisting of several hydrodynamic models, primarily FES94.1 of Le Provost et al. (1994) plus several regional models for various shallow and inland seas. (All polar seas above the T/P inclination of 66° rely on the FES model.) The Earth's body tide and load (radial displacement) tide were removed from the altimeter data by use of (strictly real) Love and loading numbers h_2 and h_n' . For further details of this tidal height model, including data processing steps, adopted geophysical constants, and final global cotidal charts, see Ray (1999).

The GOT99.2 elevations are clearly superior to the models used by Chao et al. (1996). This is especially evident in some shallow sea areas, such as the Gulf of Maine and the South and East China Seas. The model is also marginally better in the deep ocean. For example, in a comparison with 102 deep-sea tide gauges and bottom-pressure recorders, the new model has an rms discrepancy in M_2 of 1.47 cm, compared with 1.64 cm for CSR3.0 and 1.55 cm for CSR4.0 (which are two widely used models based on T/P).

Barotropic (depth-averaged) tidal currents were computed from the GOT99.2 elevations by a least-squares procedure that fits both the hydrodynamic equations of momentum and continuity. The momentum equations included terms for self-attraction and loading and a linearized bottom frictional stress for dissipation (with frictional coefficient $r = 0.01$ m/s). The resulting currents are clearly superior to two of the three models used by Chao et al. and are comparable to the third (their "Model C"—the TPXO.2 model of Egbert et al., 1994). Comparisons with 77 deep-ocean moored current meters and with two deep-ocean acoustic tomography arrays suggest that the new currents are comparable to TPXO.2 and slightly less accurate than TPXO.3 (although the elevations are more accurate). Further details of the methodology used for deriving the currents are described in Ray (2000).

IMPLIED TIDAL VARIATIONS IN EARTH ROTATION

The new model of tidal heights and currents has been used to compute ocean tidal angular momentum (Table 1) and the implied variations in UT1 and polar motion (Table 2). The procedure followed is precisely the same as that used by Chao et al. (1996). Note that the Z component of angular momentum is computed directly from the Y_2^0 spherical harmonic component of the model; this avoids a small inaccuracy stemming from a slight nonconservation of mass (see discussion in Ray et al., 1997). The conversion from angular momentum to UT1 and polar motion follows Gross (1993), including his adopted values for Love numbers and FCN and Chandler Wobble frequencies. The phase convention used in Tables 1 and 2 is consistent with that used by both Gross (1993) and Chao et al. (1996); the phases used for angular momentum and for UT1 are phase lags and are consistent with the Doodson convention for Greenwich phase lags used by most oceanographers.

While the GOT99.2 tidal heights and currents are certainly improved over the models used by Chao et al. (1996), as noted by *in situ* comparisons of oceanic heights and currents, there is no comparable way to assess the accuracy in the extremely long wavelength band (e.g., the degree-2 heights) which affects Earth rotation. Yet it seems likely that these components must also be improved. Comparisons with space-geodetic Earth orientation measurements are probably the most direct test. No such detailed tests have yet been performed, but cursory comparisons (e.g., UT1 comparisons for M_2 , O_1 , and K_1 with the VLBI estimates of Gipson [1996]) do suggest marginal improvement in model estimates.

The Δ UT1 phasor diagram for the M_2 tide is of special interest because of the possible detection of Earth libration, which results from tidal forcing of the triaxial solid Earth and is estimated to contribute approximately 1.9 μs (Chao et al., 1991) to UT1 (based on the Earth's C_{22} and S_{22} Stokes coefficients). Figure 1 shows the components of tidal heights, currents, and libration contributing to Δ UT1, plus the VLBI estimate of Gipson (1996). (Other published VLBI estimates are similar to Gipson's but with larger error circles; published estimates based on GPS and SLR observations, however, are not consistent with the VLBI; see Chao et al., 1996.) The total of tides plus libration falls almost within 2σ of the VLBI measurement of UT1, which is a small improvement to the results shown in Chao et al. (1996). The error circle for the tidal estimates is unknown but is surely as large (more likely, larger) than the VLBI estimate (preliminary calculations by G. Egbert based on inverse methods of tidal analysis suggest an error circle 50% larger than Gipson's).

REFERENCES

- Brosche, P., J. Wünsch, J. Campbell, H. Schuh, *Astron. Astrophys.*, 25, 676–682, 1991.
- Chao, B. F., D. N. Dong, H. S. Liu, T. A. Herring, *Geophys. Res. Lett.*, 18, 2007–2010, 1991.
- Chao, B. F., R. D. Ray, J. M. Gipson, G. D. Egbert, C. Ma, *J. Geophys. Res.*, 101, 20151–20163, 1996.
- Egbert, G. D., A. F. Bennett, M. G. G. Foreman, *J. Geophys. Res.*, 99, 24821–24852, 1994.
- Gipson, J. M., *J. Geophys. Res.*, 101, 28051–28064, 1996.
- Gross, R. S., *Geophys. Res. Lett.*, 20, 293–296, 1993.
- Herring, T. A., D. Dong, *J. Geophys. Res.*, 99, 18051–18071, 1994.

- Le Provost, C., M. L. Genco, F. Lyard, P. Vincent, P. Caneil, *J. Geophys. Res.*, 99, 24777–24797, 1994.
- Munk, W. H., *Prog. Oceanogr.*, 40, 7–36, 1997.
- Ray, R. D., D. J. Steinberg, B. F. Chao, D. E. Cartwright, *Science*, 264, 830–832, 1994.
- Ray, R. D., B. F. Chao, Z. Kowalik, A. Proshutinsky, *J. Geod.*, 71, 344–350, 1997.
- Ray, R. D., A global ocean tide model from Topex/Poseidon altimetry: GOT99.2, NASA Tech. Memo. 209478, 58 pp., 1999.
- Ray, R. D., Inversion of oceanic tidal currents from measured elevations, to appear, 2000.

Table 1. Oceanic tidal angular momentum (OTAM)
Amplitudes and phase lags.

		X	Y	Z
Q1	heights	1.1, 342°	2.6, 216°	0.7, 134°
	currents	0.7, 296°	0.7, 206°	1.3, 109°
O1	heights	4.7, 328°	11.7, 221°	2.0, 151°
	currents	2.9, 318°	3.9, 214°	5.9, 118°
P1	heights	1.6, 309°	4.6, 223°	0.4, 40°
	currents	1.7, 284°	2.5, 190°	2.5, 129°
K1	heights	4.6, 307°	13.8, 223°	1.4, 31°
	currents	5.2, 288°	7.5, 192°	7.7, 130°
N2	heights	1.2, 347°	0.4, 232°	0.5, 78°
	currents	1.1, 247°	2.3, 157°	3.0, 328°
M2	heights	5.1, 12°	3.6, 305°	6.0, 86°
	currents	9.8, 258°	17.5, 164°	16.0, 321°
S2	heights	1.1, 40°	2.7, 7°	2.4, 133°
	currents	5.2, 301°	9.4, 202°	7.1, 342°
K2	heights	0.4, 40°	0.9, 0°	0.7, 120°
	currents	1.4, 298°	2.6, 198°	2.2, 342°

Amplitudes in 10^{24} kg m²/s; Greenwich phase lags in degrees.

Table 2. Tidal variations in UT1 and
Prograde and Retrograde Polar Motion.

	ΔUT1	Progr. PM	Retr. PM
Q1	4.7, 26.2°	29, 76°	44, 302°
O1	20.5, 34.6°	139, 65°	102, 307°
P1	6.7, 31.9°	57, 57°	880, 134°
K1	19.8, 31.9°	169, 56°	9840, 132°
N2	4.0, 244.3°	15, 136°	37, 269°
M2	18.9, 246.1°	82, 125°	245, 269°
S2	7.4, 261.8°	29, 92°	122, 303°
K2	2.3, 263.3°	7, 92°	32, 301°

Amplitudes of ΔUT1 are μs.

Amplitudes of polar motion are μas.

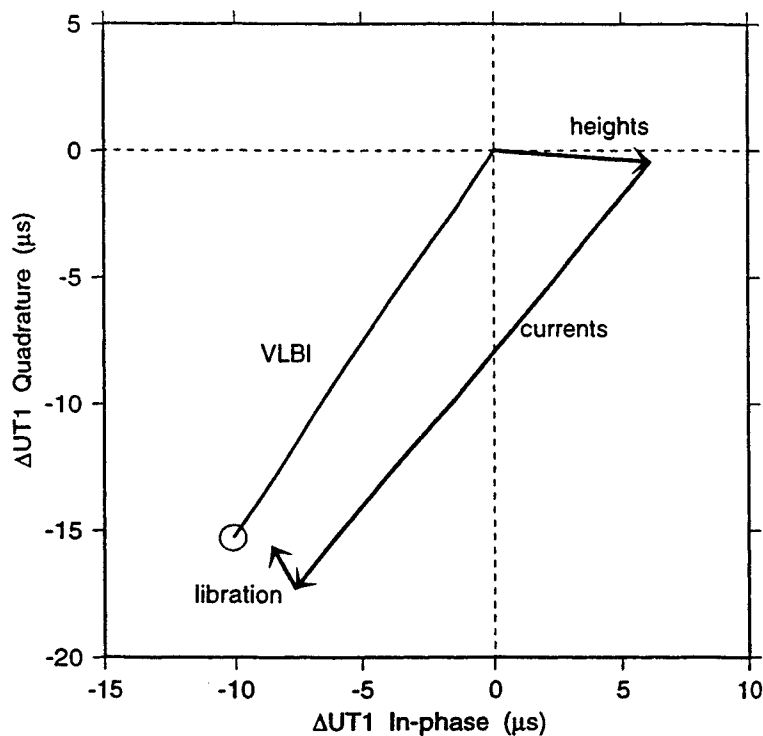


Figure 1. ΔUT1 phasor diagram for M_2 , in microseconds. Tidal heights and currents correspond to model GOT99.2. Libration is $1.9 \mu\text{s}$, with phase lag 120° . VLBI is “constrained” solution of Gipson (1996).

DIURNAL AND SUB-DIURNAL VARIATIONS OF THE EARTH ROTATION

Zharov V.E.(1), D. Gambis (2), Ch. Bizouard (2)

(1) Sternberg State Astronomical Institute, Universitetskij prospect 13, 119899 Moscow, Russia

(2) Observatoire de Paris, UMR8630, IERS, 61 Avenue de l'Observatoire, 75014, Paris, France

1. INTRODUCTION

The oceanic variability is responsible of most of the variations on polar motion (PM) and on the angular velocity of the Earth in the diurnal and semidiurnal frequency bands. Theoretical evaluations of the ocean tidal effect on PM and UT1 were made by various authors (Gross (1993), Ray et al. (1994), Chao et al. (1996)). The new techniques based on Very Long Baseline Interferometry (VLBI) and Global Positioning System (GPS) have recently shown their ability to derive LOD or UT1 and PM with hourly resolutions (IERS TN16, 1994).

Estimation of the diurnal and semidiurnal tidal parameters were made from VLBI analysis by various authors (Sovers et al., 1993; Herring and Dong, 1994; Ma and Gipson 1995; Gipson, 1996) Chao et al. (1996) showed that eight major tides ($Q_1, O_1, P_1, K_1, N_2, M_2, S_2, K_2$) explain nearly 60% of the total variance in sub-daily polar motion and are responsible for as much as 90% of the sub-daily power of the UT1 variations.

The objective of the present paper is twofold: first to compare different sets of estimates of the coherent tidal oscillations in UT1 and PM on one hand and theoretical ones on the other hand. This was done using both VLBI and GPS series. Secondly, to determine to which extent the atmosphere explains the discrepancy between theory and observations.

2. DATA

Since 1995, the CODE Analysis Center is providing PM and LOD estimates with a one-hour time resolution (Beutler and Rothacher, 1999). Three years of this series (January 2, 1995 - February 14, 1998) were used in this analysis.

In order to calculate the effect of the atmospheric tides on the Earth's rotation we used the 6-hourly series of the effective atmospheric angular momentum (EAAM) computed by NCEP/NCAR reanalysis project (Kalnay et al., 1996).

3. ANALYSIS AND RESULTS

Both the ocean and atmospheric tides are the effects by the luni-solar gravitational forces; the phase φ_j^p of the j -th prograde tide depends on the five fundamental lunisolar arguments (l, l', F, D, Ω) . φ_j^p can be written as:

$$\varphi_j^p = a_j l + b_j l' + c_j F + d_j D + e_j \Omega + n_j (GMST + \pi),$$

where a_j, b_j, c_j, d_j, e_j are integer constants, n_j is integer equals to -1 or -2 for diurnal and

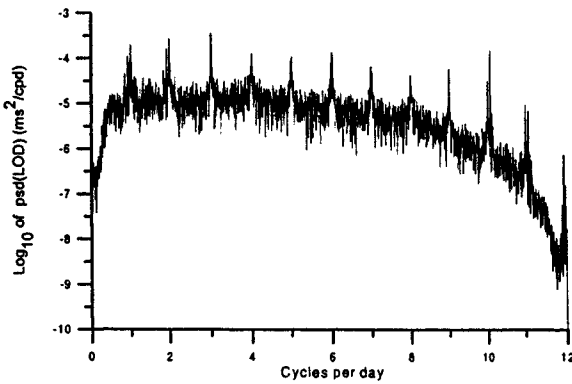


Figure 1: Power spectral density estimates from a seven-point smoothing of the LOD residuals periodogram

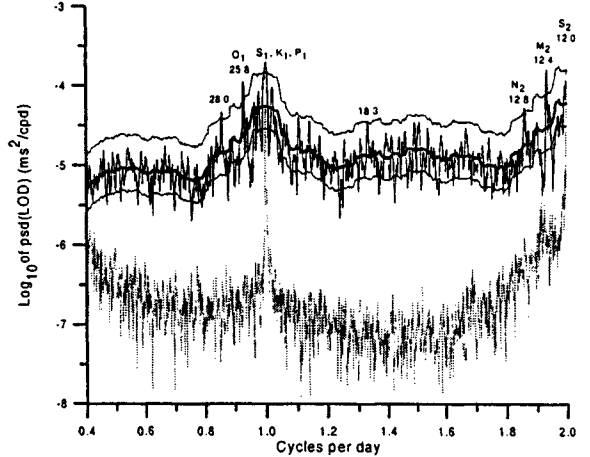


Figure 2: Power spectral density estimates of the LOD residuals (upper graph) and χ_3 (lower graph) periodograms. The bold solid line is highly smoothed surrounded by 95% confidence interval.

semidiurnal waves, respectively, *GMST* is the Greenwich mean sidereal time. Using this representation the prograde tidal variations in UT1, PM and the AAM χ functions can be expressed as:

$$\begin{aligned}\delta(\text{UT1}) &= \sum_j (u_j^{cp} \cos \varphi_j^p + u_j^{sp} \sin \varphi_j^p), \\ \delta(\text{PM}) &= \delta x - i \delta y = - \sum_j (p_j^{cp} + i p_j^{sp}) e^{i \varphi_j^p}, \\ \delta \chi &= \chi_1 + i \chi_2 = - \sum_j (\chi_j^{cp} + i \chi_j^{sp}) e^{i \varphi_j^p}.\end{aligned}\quad (1)$$

The retrograde variations can be obtained using the opposite sign of the tidal phase: $-\varphi^p = \varphi^r$. In the following, we denote the retrograde amplitudes of UT1 and PM as $u_j^{cr}, u_j^{sr}, p_j^{cr}, p_j^{sr}$. We also use the alternative representation for PM:

$$\delta x = \sum_j (A_{xj} \cos \varphi_j + B_{xj} \sin \varphi_j), \quad (2)$$

$$\delta y = \sum_j (A_{yj} \cos \varphi_j + B_{yj} \sin \varphi_j), \quad (3)$$

where

$$A_{xj} = -p_j^{cp} - p_j^{cr}, B_{xj} = -p_j^{sp} + p_j^{sr}, A_{yj} = p_j^{sp} + p_j^{sr}, B_{yj} = -p_j^{cp} + p_j^{cr}.$$

Expressions (2-3) do not include the retrograde diurnal components of the PM spectrum because they are not accessible to the GPS. Solutions obtained from VLBI observations do not contain them neither since they are estimated as celestial pole offsets.

In order to estimate the coefficients $u_j^{cp}, u_j^{sp}, A_{xj}, B_{xj}, A_{yj}, B_{yj}$ in eqs.(1-3) from the CODE series for the eight major tides and tide S_1 , we removed at first the low-frequency variations.

The estimates of the components u_j^{cp} and u_j^{sp} for UT1 are shown in Table 1 (6^{th} column).

The influence of the atmospheric tides was estimated from the axial atmospheric angular momentum function. The estimates are given in the last column.

Next, we removed the effects of the oceans tides (according to Chao et al, 1996) from the LOD series. The spectra of the residuals is shown in Figures 1. Figure 2 represents LOD residuals (CODE minus ocean model) and function χ_3 from NCEP/NCAR analysis power spectral density

Table 1: The UT1 cosine u^c and sine u^s amplitudes (in $0.1\mu\text{s}$). In columns 2,3,4,5 we showed estimates from VLBI observations, as provided by Sovers et al. (1995), Herring and Dong (1994), Ma and Gipson (1994), Gipson (1996). In column 6, the mean of all these estimates is given. In column 7 are the corresponding values of the ocean tide effects, from the model proposed by Chao et al. (1996) and recommended by IERS as standard. In column 8 is given the difference between the mean value of the observed and theoretical ocean tide amplitudes : $\Delta = \bar{u} - u^{ocean}$.

Tide	Sovers	Herring/ Dong	Ma/ Gipson	Gipson	CODE	$\sum u_j/n$	Ocean model	Δ	χ_3
u^c									
K_2	-9	8	3	7	-12	-0.6 ± 9.3	-3.8	3.2	0
S_2	-4	-1	-12	-8	-7	-6.4 ± 4.2	-4.0	-2.4	?
M_2	-104	-108	-85	-104	-82	-96.6 ± 12.1	-72.0	-24.6	-1
N_2	-23	-16	-44	-19	-19	-24.2 ± 11.3	-15.4	-8.8	0
K_1	35	65	75	90	66	66.2 ± 20.1	86.4	-20.2	-1
P_1	-32	-39	-35	-25	-20	-30.2 ± 7.7	-28.6	-1.6	0
O_1	-135	-173	-156	-133	-111	-141.6 ± 23.7	-121.0	-20.6	0
Q_1	-40	-31	-34	-29	-18	-30.4 ± 8.1	-24.5	-5.9	0
S_1	-	18	6	-4	-18	-0.5 ± 15.3	-	-0.5	-9
u^s									
K_2	26	37	39	28	15	29.0 ± 9.6	19.6	9.4	0
S_2	52	86	87	80	67	74.4 ± 14.8	75.9	-1.5	?
M_2	149	143	123	154	155	144.8 ± 13.1	161.7	-16.9	-3
N_2	20	28	12	32	34	25.2 ± 9.1	38.0	-12.8	1
K_1	151	178	167	163	157	163.2 ± 10.3	177.1	-13.9	-3
P_1	-64	-59	-54	-53	-69	-59.8 ± 6.8	-51.6	-8.2	-1
O_1	-166	-162	-168	-177	-137	-162.0 ± 15.0	-160.5	-1.5	1
Q_1	-53	-44	-39	-48	-44	-45.6 ± 5.2	-50.3	4.7	0
S_1	-	13	19	11	16	14.8 ± 3.5	-	14.8	-5

estimates. Power law of LOD residuals spectrum is shown by the thick solid line (middle curve). It is surrounded by 95% confidence interval. Spectral peaks at periods of 28.0 hours, 25.8 hours (tide O_1), central peak (combination of tides S_1, K_1, P_1), 18.3 hours, 12.8 hours (N_2), 12.4 hours (M_2) have non-random origin (with 95% probability). According to this estimate of LOD residual spectrum, the semidiurnal atmospheric signal must be detected with a high accuracy level. Unfortunately the estimation of the amplitude of the semidiurnal tide from NCEP data is impossible because of the linmiting 6-hour time-resolution. The spectrum of the residuals for PM (CODE - Oceanic model) is shown on Figure 3; Table 2 gives the PM variations due to the ocean tides obtained from both the GPS and VLBI observations, as provided by Herring and Dong (1994), Ma and Gipson (1994), Gipson (1996). The mean of all these estimates was done. In the last column the tidal oceanic effects, as modeled by Chao et al. (1996), are given.

The differences between observed mean PM variations and theoretical model of Chao et al. (1996) are shown in Table 3.

4. DISCUSSION

The various peaks appearing in the spectra of LOD (Fig. 1) and PM (Fig. 3) are the higher harmonics of the diurnal frequency. One possible explanation is the orbital effects which have typical period of 12 hours. In the AAM series, besides the main terms with frequencies of 1,2 cpd connected with S_1 and S_2 tides, other peaks appear with frequencies of 4,8 cpd, but their power is very small. Other signals are present with frequencies 3,5,7,etc. cpd not separable from the noise. The existence of all these harmonics can be predicted by the excitation of the thermal sub-diurnal tides in the atmosphere by the sub-diurnal harmonics of the heating function (Zharov, 1998) but their power is not sufficient to explain the observed residuals with respect tidal oceanic model in CODE series.

For LOD (Figure 2), we remark an increase of power near the semidiurnal frequency band but the power level of χ_3 remains 10 times smaller than those observed by GPS. According to

Table 2: The PM cosine A and sine B amplitudes for x- and y-components (in μas)

Tide	Herring/ Dong		Ma/ Gipson		Gipson		CODE		Mean value		Ocean model	
	A_x	B_x	A_x	B_x	A_x	B_x	A_x	B_x	A_x	B_x	A_x	B_x
x-component												
K_2	-13	21	-7	21	4	27	-19	51	-9 ± 10	30 ± 14	17	36
S_2	64	111	84	117	85	124	66	125	75 ± 11	119 ± 7	64	145
M_2	9	323	-45	357	-13	331	-45	303	-24 ± 26	329 ± 22	-28	330
N_2	-3	59	36	89	3	57	-15	47	6 ± 22	63 ± 18	-13	57
K_1	-133	74	-125	38	-129	47	-116	64	-126 ± 7	56 ± 16	-152	78
P_1	49	-35	54	-26	49	-28	60	-25	53 ± 5	-29 ± 5	50	-25
O_1	178	-89	136	-64	133	-69	104	-33	138 ± 31	-64 ± 23	133	-49
Q_1	33	-11	34	-18	34	-11	27	-8	32 ± 3	-12 ± 4	26	-6
S_1	-	-	-	-	-	-	-32	-43	-	-	-	-
	A_y	B_y	A_y	B_y	A_y	B_y	A_y	B_y	A_y	B_y	A_y	B_y
y-component												
K_2	12	-65	10	-38	5	-27	13	-7	10 ± 4	-34 ± 24	22	-18
S_2	87	-69	95	-69	93	-64	91	-64	92 ± 3	-67 ± 3	87	-59
M_2	208	-12	213	-15	215	-20	201	-43	209 ± 6	-23 ± 14	196	-37
N_2	35	-21	28	-13	27	-7	35	-9	31 ± 4	-13 ± 6	33	-11
K_1	-74	-133	-38	-125	-47	-129	-64	-116	-56 ± 16	-126 ± 7	-78	-152
P_1	35	49	26	54	28	49	25	60	29 ± 5	53 ± 5	25	50
O_1	89	178	64	136	69	133	33	104	64 ± 23	138 ± 31	49	133
Q_1	11	33	18	34	11	34	8	27	12 ± 4	32 ± 4	6	26
S_1	-	-	-	-	-	-	43	-32	-	-	-	-

Table 3: Difference between observed PM variations and ocean tidal model (Chao et al, 1996). Unit is μas)

	K_2	S_2	M_2	N_2	K_1	P_1	O_1	Q_1	S_1
A_x	-26	11	4	19	26	3	5	6	-32
B_x	-6	-26	-1	6	-22	-4	-15	-6	-43
A_y	-12	5	13	-2	22	4	15	6	43
B_y	-16	-8	14	-2	26	3	5	6	-32

the results shown in Table 1 there is a systematic difference between observations and theoretical ocean tides. It means that some unknown processes, not linked to atmospheric tides, were nor taken into account. The explanation is probably the mismodeling of the ocean tides. We assume that the amplification of the tides M_2, N_2, O_1 due to the coincidence of their frequencies with those of the normal modes of the oceans (Sündermann, 1982) could improve the agreement between both the observations and the model. As stated previously, non-tidal signals exist in the spectrum of the LOD residuals (Fig.2). The term with a period of 28.0 hours can be connected with normal mode of the world ocean with a period of 28.7 hours. The reality of this signal is confirmed by independent analysis of VLBI data (Titov, 1999). The origin of the large discrepancy of the K_1 amplitudes is still unknown. power near the sub-diurnal frequencies. Most powerful The amplitude of this questionable.

The comparison of the LOD variations from CODE analysis with ocean tidal model is shown on Figure 4 for two time intervals. Variance of residuals (observation minus model) is equals to $\sigma = 0.12$ ms for the first one (MJD 49990-50005) and to $\sigma = 0.19$ for the second one (MJD 50255-50270) intervals. Significant scatter of residuals exceeding 3σ is observed during the period ranging from MJD 50262 to 50268. A similar effect is observed for PM variations too. It is one example when over one week the amplitude of LOD and PM variations is significantly increasing with respect to the model. The atmosphere cannot be responsible for such an effect because the variations of χ_3 function 10 times smaller.

According to Table 3 the largest discrepancies between PM and tidal estimates are observed for K_1 ($34\mu\text{as}$ in amplitude) and S_1 ($45\mu\text{as}$ in amplitude) and K_2 tides. Here again, these

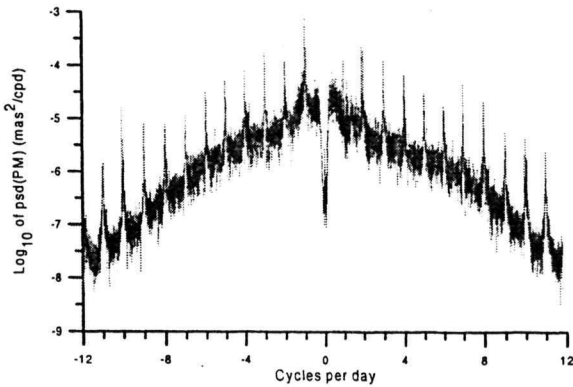


Figure 3: Power spectral density estimates from a seven-point smoothing of the PM residuals periodogram.

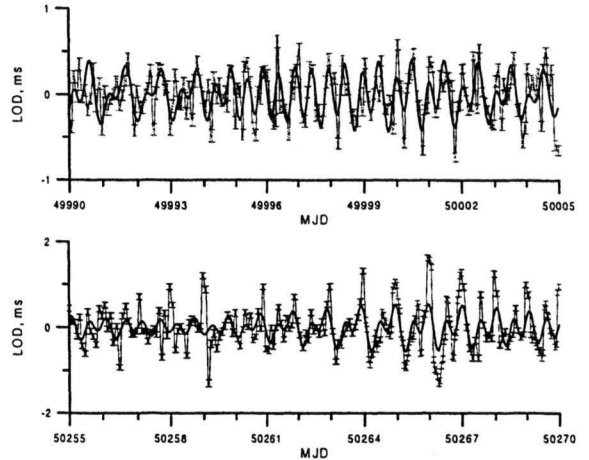


Figure 4: LOD estimates from CODE analysis and ocean tidal model for different intervals

atmospheric effects are not sufficient, since they do not exceed $10\mu\text{as}$ (Petrov, 1998; Brzezinsky and Bizouard, 2000).

The agreement of the mean value of amplitudes of M_2, N_2, O_1 tides with theoretical values is fair but the scatter of the amplitudes in different series is large. It could be explained by the variable amplification of these tides.

5. CONCLUSION

The tidal coherent waves in UT1 and PM were estimated from GPS CODE series. The values obtained for UT1 are consistent with those deduced from VLBI observation, with discrepancies within $1\mu\text{s}$, except for tides of K_1, O_1 for which the discrepancies exceed $2\mu\text{s}$. We have shown that almost all tidal coherent waves of UT1 (especially K_1, O_1, M_2, N_2) exceed their prediction from oceanic tidal model. The atmospheric effect is ten time smaller, and can not explain such a discrepancy. One possible explanation is the coincidence of the frequencies of the tides M_2, N_2, O_1 with the frequencies of the normal modes of the world ocean. More generally, this systematic difference shows that another effect has to be taken into account.

Similar conclusion can be given for PM variations. The largest difference in amplitude between observations and model is found for K_1, S_1, K_2 tides. No explanation could be given.

Acknowledgments We kindly thank Dr. R. Weber for providing the CODE PM and LOD series. One of us (V.E.Z.) thanks the Paris Observatory and Central Bureau of IERS for financial support during visit to IERS. This work was supported by the Russian Foundation of Basic Research under grant 98-05-64797.

4. REFERENCES

- Beutler G. and Rothacher M., Polar motion and subdaily time resolution. Submitted to Proc. IAU Colloq. N178, Cagliari, 1999
- Brzezinsky A. and Bizouard C., Influence of the atmosphere on the Earth rotation: what new can be learned from the recent atmospheric angular momentum estimations, Geophysical Survey, to be published.
- Chao B.F., Ray R.D., Gipson J.M., Egbert G.D., Ma C., Diurnal/semdiurnal polar motion excited by oceanic tidal angular momentum. *J. Geophys. Res.* 1996. V.101. P.20151-20163.
- Gipson J.M., VLBI determination of neglected tidal terms in high-frequency Earth orientation variation. *J. Geophys. Res.* 1996. V.101. P.28051-28064.

- Gross R.S., The effect of ocean tides on the Earth's rotation as predicted by the results of an ocean tide model. *Geophys. Res. Lett.* 1993. V.20. P.293-296.
- Herring T.A. and Dong D., Measurement of diurnal and semidiurnal rotational variations and tidal parameters of Earth. *J. Geophys. Res.* 1994. V.99. P.18051-28071.
- IERS Technical Note 16. Observatoire de Paris. 1994.
- Kalnay E., Kanamitsu M., Kistler R., Collins W., Deaven D., Gandin L., Iredell M., Saha S., White G., Woolen J., Zhu Y., Chelliah M., Ebisuzaki W., Higgins W., Janowiak J., Mo K.C., Ropelewski C., Wang J., Leetmaa A., Reynolds R., Jenne R., Joseph D., The NMC/NCAR 40-year reanalysis project. *Bull. Amer. Met. Soc.* 1996. V.77. No.3. P.437-471.
- Ma C., Gipson J.M., Earth orientation from VLBI during SEARCH'92. IERS Technical Note 16. Observatoire de Paris. 1994. P.III9-III15.
- Petrov S.D., *Modeling geophysical excitation of Earth rotation : stochastic and nonlinear approaches*, Ph.d. Thesis, Space Research Centre of the Polish Acad. of Sciences, Warsaw, Poland. 1998.
- Ray R.D., Steinberg D.J., Chao B.F., Cartwright D.E., Diurnal and semidiurnal variations in the Earth's rotation rate induced by oceanic tides. *Science* 1994. V.264. P.830-832.
- Sovers O.J., Jacobs C.S., Gross R.S., Measuring rapid ocean tidal Earth orientation variations with Very Long Baseline Interferometry. *J. Geophys. Res.* 1993. V.98. N B11. P.19959-19971.
- Sündermann J., 1993. The resonance behaviour of the world ocean. In *Tidal Friction and the Earth's Rotation* ed. by P.Brosche and J.Sündermann. Springer-Verlag, Berlin, Heidelberg, 1982. P.165-174.
- Titov O. Private communication. 1999.
- Zharov V.E. Rotation of the Earth and dynamics of the atmosphere. Doctoral thesis, S.Petersburg university, 1998.

ESTIMATION OF SUBDIURNAL TIDAL TERMS IN UT1-UTC FROM VLBI DATA ANALYSIS

Titov Oleg · Saint-Petersburg University, Russia

INTRODUCTION

Subdiurnal UT1–UTC variations arisen from oceanic forced effect have been estimated since 1989. Brosche et al. [1991] presented their results for four terms only (O1, K1, M2, S2) using one-year observational data set. Currently, it is possible to detect UT1–UTC oceanic tidal terms with accuracy 1-3 μ sec due to progress in VLBI observations performance. Gipson [1996] published estimates for 41 tidal terms in UT1–UTC and for 57 tidal terms in polar motion using 1.6 billion delays from 1979 till 1996.

There are two ways for estimation of subdiurnal tidal terms in EOP. The first way foresees preliminary estimation of long-term EOP time series with high time resolution and subsequent adjustment using conventional least squares technique [Brosche et al., 1991; Titov, 2000]. The second one makes a direct adjustment of all tidal terms under analysis without intermediate calculation of time series [Herring, Dong, 1994; Haas et al., 1995]. The former approach is very useful if we want to receive the EOP subdiurnal variations and seek for non-tidal effects. Obvious oceanic effects can be demonstrated visually. It is appeared that the EOP time series a sensitive to chosen a priori information. As a result, the estimates of oceanic tidal terms can be unstable on level of a few μ sec. Therefore, from general point of view, the latter approach looks more preferable because we do not need any a priori information about EOP behavior on subdiurnal time scale.

Another problem is a strong correlation between main band and sidebands because it can bias an estimates. Historical limit on observational data set prevents an appropriate reducing of correlation between close effects. It can be shown that the correlation coefficients are depend on choice of a priori information.

GLOBAL ADJUSTMENT

Let consider parametrical model of observations

$$Ax + By + Cz + w = l, \quad (1)$$

where l – vector of observations (O–C); w – vector of observations. Three types parameters to be considered: 'global' (tidal terms) – vector x ; 'arc' or 'daily' (site positions, EOP) – vector y ; 'stochastic' (clock offset, troposphere) – vector z . Here A, B, C are matrixes of partial derivatives. For each single VLBI session the following matrix of normal equations can be constructed

$$A^T Q A x = A^T Q l \quad (2)$$

where covariance matrix Q is a combination of matrixes

$$Q = Q_0^{-1} - Q_0^{-1} B (B^T Q_0^{-1} B)^{-1} B^T Q_0^{-1} \quad (3)$$

where Q_0 as follows

$$Q_0 = CQ_zC^T + Q_w. \quad (4)$$

Matrix Q_z can be calculated using information about covariance functions of stochastic parameters (see below). Q_w – diagonal covariance matrix of observational dispersions. Full matrix Q_0 (size $N \times N$, N – the amounts of VLBI sessions under analysis) to be inverted. Making a sum on all VLBI sessions we are able to get an solution of global parameters vector

$$\hat{x} = \left(\sum_{i=1}^n (A^T Q A)_i \right)^{-1} \cdot \sum_{i=1}^n (A^T Q I)_i, \quad (5)$$

where n – the amounts of VLBI sessions under analysis. Estimates of vectors y and z for each VLBI session are given by

$$\hat{y} = (B^T Q_0^{-1} B)^{-1} B Q_0^{-1} (I - A \hat{x}) \quad (6)$$

$$\hat{z} = Q_z C^T (C Q_z C^T + Q_w)^{-1} (I - A \hat{x} - B \hat{y}). \quad (7)$$

It means that the y and z parameters can be estimated after adjustment of global parameter vector only. Procedure for a priori covariance function calculation is discussed at the paper "Full covariance matrix for least squares collocation method" (see this volume).

Three solutions have been obtained using different dispersion for wet delay as well as clock offset variations. Table 1 contains list of a priori dispersion for wet delay and clock offset.

Parameter	Solution 1	Solution 2	Solution 3
Wet delay	2.5	12.5	12.5
Clock offset	2	10	2

Table 1. A priori dispersion for wet delay and clock offset (cm**2).

SOLUTION

Regular observational VLBI data (IRIS-A, NEOS-A) from 1984 till 1999 have been used for global adjustment procedure. Celestial reference frame has been fixed by radiosources coordinates (ICRF 1997). Terrestrial reference frame has been fixed by coordinates of Wettzell, direction from Wettzell to another VLBI station and vertical component of third station. We process 898 VLBI sessions (more than 546.000 time delays) using OCCAM 3.4 software [Titov, Zarraoa, 1997] and estimate 34 tidal terms by LSCM. No special constraints for reducing of correlation has been applied for solution. Table 2 contains coefficients of correlation between main tidal terms and their sidebands. Upper triangle shows the coefficients for cosines components, low triangle – for sinus ones.

	O1'	O1	K1"	K1	K1'
O1'	-	0.42			
O1	0.42	-			
K1"			-	0.38	-0.13
K1			0.38	-	0.37
K1'			-0.09	0.37	-

	M2'	M2	K2	K2'
M2'	-	0.33		
M2	0.34	-		
K2			-	0.32
K2'			0.36	-

Table 2. Coefficient of correlation.

Other sidebands demonstrate the analogous level of correlation. Suddenly, it has been discovered significant correlation between 2Q1 and S1 terms (up to 0.45) as well as 2N2 and R2 terms (up to 0.35). Probably, it can be explained by closeness of fundamental arguments (l , l' , F , Ω , θ) combination $l'-\theta \approx 1 + 2F + 2\Omega - \theta$ for time interval 1984 – 1999.

DISCUSSION

A few LSCM estimates of tidal amplitudes are compared with the same terms from IERS Conventions [McCarthy, 1996] and paper by Gipson [1996]. Table 3 demonstrates that the values estimates do not essentially depend on a priori dispersions from Table 1. Generally, all estimates for diurnal tidal terms are in a good accordance with ones from IERS Conventions 1996. Disagreement with results by Gipson is on level 1-2 μ sec in diurnal time band. In semidiurnal band all LSCM estimates exceed the alternatives on 1-6 μ sec. The essential disagreement indicates that more detailed research must be done in future.

ACKNOWLEDGEMENTS

The work has been supported by Russian Foundation of Basic Research (RFBI) (grant 99-02-18059).

	Tide	IERS Conv. 1996	Gipson (1996) constrained	Gipson (1996) unconstrained	Solution 1	Solution 2	Solution 3
1	Q1	5.6	5.9	6.7	5.6	5.6	5.7
2	O1'		4.2	3.3	4.3	4.3	4.3
3	O1	20.1	22.5	22.8	20.6	20.8	20.6
4	K1"		0.3	2.2	3.0	3.0	3.4
5	K1	19.7	18.5	15.3	19.2	19.3	18.9
6	K1'		2.6	4.1	4.3	4.3	3.9
7	N2	4.1	3.9	3.8	4.9	5.0	4.8
8	M2'		0.6	1.4	2.2	2.0	2.2
9	M2	17.7	18.3	17.4	22.8	23.4	21.3
10	S2	7.6	7.8	7.8	10.8	11.0	10.4

Table 3. Estimates of amplitudes of main UT1–UTC tides and sidebands (in μ sec).

REFERENCES

1. Brosche, P., J. Wünsch, J. Campbell, H. Schuh, 1991, Ocean tide effects in Universal Time detected by VLBI, *Astron. Astrophys.*, 245, 676–682.
2. Gipson, J., 1996, Very long baseline interferometry determination of neglected tidal terms in high-frequency Earth orientation variation, *Journal of Geophys. Res.*, 101, 28.051–28.064.
3. Haas, R., J. Campbell, H. Schuh, 1995, Geodynamical Parameters Determined by VLBI, In R. Lanotte (ed.), *Proceedings of the 10-th Working Meeting on European VLBI for Geodesy and Astrometry*, 91–102.
4. Herring, T.A., D. Dong, 1994, Measurements of diurnal and semidiurnal rotational variations and tidal parameters of Earth, *Journal of Geophys. Res.*, 99, 18.051–18.071.
5. McCarthy D., (ed.), 1996, IERS Conventions 1996, IERS Technical notes 21, Paris Observatory.
6. Titov, O., 2000, Estimation of the subdiurnal UT1–UTC variations by least squares collocation method, *Astronomical and Astrophysical Transactions*, v.19, 113–126.
7. Titov, O., N. Zarraoa, 1997, OCCAM 3.4. User's guide, *Communication of IAA*, 69, Saint-Petersburg.

INTERPRETATION OF HIGH FREQUENCY POLAR MOTION AND LENGTH OF DAY VARIATIONS

Arfa-Kaboodvand K.(1), Grotens E.(1), Varga P.(2), Zavoti J.(2)

(1) Darmstadt University of Technology, Institute for Physical Geodesy, Petersenstrasse 13,
D-64287 Darmstadt, Germany

(2) Geodetic and Geophysical Research Institute of Hungarian Academy of Sciences,
Csatkai E., u. 6-8, H-9400 Sopron, Hungary

Abstract: The continuous GPS observations of 1995 completed by the International GPS Service are analysed in terms of polar motion (PM) and length of day (LOD) in view of diurnal and subdiurnal periods first of all.

The complex study of these two phenomena shows, that

- the most prominent diurnal and subdiurnal components of the record can be found at the tidal frequencies. In case of PM the zonal (long periodic) tides were not detected due to the fairly high noise level. The tesseral waves are of Earth tidal origin (their amplitudes are around 1 mas). The sectorial tidal peaks are generated by oceanic tides and are the order of 0.1–1 mas. The most significant LOD spectral amplitude is at the frequency of the fortnightly M_f wave ($\sim 10^{-3}$ s) but significant LOD variations occur in the semi-diurnal band: for: M_2 780.1 mas was found.
- regular not explained yet high frequency anomalies were detected in the frequency band 3-11 cycles/day. It can not be excluded that such effects are present at tidal frequency band too. This circumstance not allows an unambiguous interpretation of the Lunisolar spectral peaks.
- The LOD time series was carefully compared with the seismological data catalogue of the US Geological Survey. It was not possible to find any short periodic (diurnal-subdiurnal) signal which can be connected to earthquake activity.

Keywords: Earth rotation, polar motion, tides, Fourier and wavelet analysis.

1. INTRODUCTION

The study of the short periodic variations of the irregularities of the Earth rotation started in 1935, when Pavel and Uhink (1935) discovered the annual term in this phenomenon. The study of variations in the subannual frequency band of the Earth rotation and its interpretation became possible with the appearance of very long baseline interferometry (VLBI) and methods of space geodesy like satellite and lunar laser ranging (SLR and LLR) (Eubanks et al., 1988; Dickey et al., 1994; Gross, 1993; Hide et al., 1991, Kolaczek, 1995; Popinski et al., 1994). Precise LOD measurements have showed variations in angular frequency down to days and even sub-daily (Chao et al., 1995a,c ; Barnes et al., 1983; Kotaczek, 1995). In the paper of Chao and Gross (1995) the short periodic changes in the Earth's rotational energy, which induce earthquakes, are given.

In the study of short-periodic variations of LOD and polar motion (PM) the GPS hourly values of these phenomena produced by the International GPS Service (IGS) are of first importance. The IGS starts its activity in June 1992. At present the formal errors of its EOP data are less than 10 microseconds of arc (μ as) and in the case of LOD data they are less than 10 microseconds (μ s) (Springer et al., 1999). The IGS data are based on the world-wide network of globally distributed GPS tracking stations (Neilan, 1998; Weber, 1999).

The aim of the present work is the complex study of the PM together with LOD in the tidal frequency band with the use of IGS data set for 1995.

2. NUMERICAL METHODS USED TO STUDY THE HIGH FREQUENCY PART OF PM AND LOD SPECTRA

The data processing procedure used in this study can be subdivided into four steps:

- a) Determination and removal of the annual part.
- b) Data filtering to obtain the high frequency components.
- c) Power spectra calculation for PM and LOD based on Fourier analysis and Wavelet technique.

a) Determination and removal of the annual part

Before examining the high frequency processes the trend has to be removed from the original data set. It was found that the accurate removal of the annual term improves significantly the analysis results at high (diurnal, subdiurnal) frequencies. For this purpose polynomials of different degrees are recommended by various authors. An uncertainty is resulting here from the choice of the degree of the polynomial. It was proved by our experience that using a polynomial of degree 10 selected by least-squares adjustment gives satisfactory results. To prove this also a generalized spline interpolation method was developed for long-term trend removal. The conventional interpolation procedures show undesirable oscillations, especially at the beginning and the end of the records. This boundary problem is not present in the method described below. The time series is divided into three subintervals of approximately equal length. For each subintervals polynomials of degree 3 were determined by least-squares adjustment. To ensure the continuity of the function of the interpolation, the interpolant and its derivatives have to satisfy appropriate equations. The procedure is iterative: in the course of the consecutive steps the coordinates of the pole receive a correction in inverse ratio to their distance from the trend function. With the use of this method the gross errors (outliers) can be detected and removed.

b) Data filtering to obtain the diurnal and subdiurnal components

The next step in the data processing is the filtering of the given frequency range of the pole-coordinates and LOD data. There are many solutions described in the literature for filtering polar motion and length of day data (e.g. Gambis 1992; Gilbert et al. 1998; Kosek 1995). In the present study two different methods were used: the Butterworth high-pass filter and the trigonometric interpolation. In the second case the pole coordinates and the LOD data sets constitute a stochastic process with a zero mean value and the interpolant is a cosine function with unknown amplitude and phase, but with a positive integer period. The amplitude and phase are estimated from the observed GPS data with the least-squares method. This procedure allows to remove components of a given period. For the purpose of present study periods longer than 30 days were removed from the records.

c) Determination of the power spectra of PM and LOD

The Fourier transformation is a common procedure in digital data processing. The Fourier transformation method has some significant limitations such as the requirement of uninterrupted and evenly input data. Another limitation is connected with the stationarity. For a stationary process the frequency decomposition generally produces sufficient information. Processes in the nature, however, are usually not stationary: the characteristics of the analysed signal may show time dependency. This phenomenon is not expressed in Fourier spectra. (Arfa-Kaboodvand, Grotens, 1999).

Wavelet analysis with Morlet and Mexican hat mother functions

In case of phenomenon for which the spectral composition changes in time, it is necessary to use time-dependent frequency analysis. The PM and LOD temporal variations are typically such a process. In this case, our goal was to apply to the pole coordinates and to the length of day data the wavelet transformation acting in the time-frequency domain. The main advantage of the wavelet transformation is that it identifies time and frequency concurrently. The signal to be analysed (in case of present work the PM and LOD) is evaluated by a mother function in both time and frequency domain. In the frame of present study different basis functions have been used for the wavelet analysis of the Earth's pole position and of the length of day (Morlet, Arfa-Kaboodvand and Groten, 1998). Further investigations could be done to answer the question: what is the highest resolution of GPS data to obtain useful information in frequency domain?

3. GEODYNAMICAL PROCESSES INFLUENCING THE POLAR MOTION AND LENGTH OF DAY IN TIDAL FREQUENCY DOMAIN

a) *Earth tides*

With the use of two horizontal components of the Earth tidal acceleration the latitude φ dependence of the tides can be expressed as follows:

	X (longitudinal) component	Y (meridional) component
Long-periodic tide	$1.5 A \sin 2\varphi$	0
Diurnal tide	$A \cos 2\varphi$	$A \sin \varphi$
Semi-diurnal tide	$0.5 A \sin 2\varphi$	$A \cos \varphi$
(A is the amplitude)		

It follows from above expressions, that the horizontal acceleration components of the Earth tide do not generate PM neither in the case of zonal, long-periodic waves (the two principal long-periodic tidal constituents are the monthly M_m and the fortnightly M_f) nor in the case of the semi-diurnal, sectorial waves (the biggest constituents are the principal lunar M_2 , the principal solar S_2 and the principal lunar ellipsoidal N_2). The tesseral, diurnal waves (the main waves are the main lunar O_1 and the lunar-solar declinational K_1) are able to produce polar motion. Their amplitudes are $-7.3 \cdot \sin 2\delta$ mas in case of X(N-S) and $17.3 \cdot \sin 2\delta$ mas in case of Y(E-W) components (δ is the declination of the tide generating body) (Melchior, 1981). From physical point of view, it is clear that the long-periodic and semi-diurnal earth tides – due to their symmetry relative to the poles – are not able to generate any PM.

The long-periodic tide causes axis-symmetric tidal bulge of the solid Earth that produce directly changes in the polar moment of inertia of the Earth. According to the third law of Euler on the angular moment conservation the product of the Earth's polar moment of inertia (C) and the angular velocity (ω) is constant. Consequently

$$\frac{\Delta C}{C} = -\frac{\Delta \omega}{\omega} = \frac{\Delta(\text{LOD})}{\text{LOD}} \quad (1)$$

The variation of LOD appears in case of Earth tides for the zonal, long-periodic waves alone. The amplitude of the monthly M_m and the fortnightly M_f constituents is of the order of 2-3 ms. The one year long GPS data set used in this study seems to be not optimal for the study of the long-periodic zonal tidal effects on LOD (the period of M_m wave is ~27.6 days that of M_f is 13.6 days).

b) Oceanic tides

The amplitude of PM, generated by the oceanic tides, can be obtained with the use of tidal load theory. Let us consider a spherical layer on the surface of the Earth characterised by a centri angle $\alpha = \frac{\Delta\phi\Delta\lambda}{\pi}$ (where λ is the longitude). In this case at the Ψ angular distance from the centre of the loaded area the generated potential V_L is

$$V_L = \frac{4\pi G R_E \rho}{g(R_E)} \sum_{n=0}^{\infty} H_n(\Psi) \frac{1}{2n+1} \quad (2)$$

Here G is the gravitational constant, R_E is the mean Earth's radius, ρ is the density of the seawater, g is the gravity, while

$$H_n(\psi) = \frac{1}{2} H \sum_{n=0}^{\infty} [P_{n-1}(\cos\alpha) - P_{n+1}(\cos\alpha)] \cdot P_n(\cos\psi) \quad (3)$$

Where H is the amplitude of the tide on the loaded spherical layer characterised with centri angle α and P_n is the n -th Legendre polynomial. Taking into account the features of the Legendre polynomials (Hobson, 1955) the potential of the load can be written as

$$\begin{aligned} V_L &= 2\pi G \rho R_E H \sum_{n=0}^{\infty} \frac{1}{2n+1} [P_{n-1}(\cos\alpha) - P_{n+1}(\cos\alpha)] P_n(\cos\Psi) = \\ &= 2\pi G \rho R_E H \left[1 - \cos\alpha + \sum_{n=1}^{\infty} \frac{\sin^2\alpha}{n(n+1)} \frac{dP_n(\cos\alpha)}{d(\cos\alpha)} \cdot P_n(\psi) \right] \end{aligned} \quad (4)$$

The radial and the horizontal displacements X and Y can be written in the following form for an elastic Earth (Pertzev et al., 1991):

$$\begin{aligned} S_r &= \frac{2\pi G \rho R_E H}{g(R_E)} \sum_{n=1}^{\infty} \frac{h'_n}{2n+1} [P_{n-1}(\cos\alpha) - P_{n+1}(\cos\alpha)] P_n(\cos\psi) \\ S\varphi &= \frac{2\pi G \rho R_E H}{g(R_E)} \sin^2\alpha \sin\varphi \sum_{n=1}^{\infty} n(n+1) \frac{\ell'_n}{n(n+1)} \frac{dP_n(\cos\alpha)}{d(\cos\alpha)} \frac{dP_n(\cos\psi)}{d(\cos\psi)} \\ S_\lambda &= 0 \end{aligned} \quad (5)$$

where h'_n and ℓ'_n are the load numbers.

With the use of above expressions for the displacements the strain components are

$$\begin{aligned} e_{\varphi\varphi} &= \frac{S_r}{R_E} + \frac{1}{R_E} \frac{\partial S\varphi}{\partial\varphi} \\ e_{\lambda\lambda} &= \frac{S_r}{R_E} + co\operatorname{tg}\varphi \frac{S_\varphi}{R_E} \end{aligned} \quad (6)$$

The amplitude value H can be obtained from the co-tidal maps, the load numbers h'_n and ℓ'_n can be found in may theoretical studies (e.g. Jentzsch, 1997; Grafarend et al., 1997). To estimate the magnitude of the polar motion $r = \sqrt{x^2 + y^2}$ due to oceanic tide the co-tidal maps of Schwiderski (1989) for M_2 and O_1 waves have been divided by 420 spherical segments $10^\circ \times 10^\circ$. It was found that the amplitude of PM generated by M_2 tide is of the order of $15 \cdot 10^{-4}$ as while the polar displacement by the oceanic O_1 wave is 10 times smaller. It follows from considerations of this chapter that the PM in case of diurnal tides can be generated mainly by Earth tides, while in case of semi-diurnal tides by the oceanic ones.

4. INTERPRETATION OF VARIATIONS IN POLAR MOTION AND IN LENGTH OF DAY

The radius of the "annual polar motion circle" varied during 1995 between (0.2-0.4) as. After the removal of the "annual" component the total residual can be characterised by radius 10 to 20 mas.

According to signal to noise studies carried out in frame of present study the PM data provided by the IGS are accurate to about 0.1 mas.

For the better understanding of the physical background of daily and subdaily variations the temporal changes of DM and LOD in frequency band of tidal variations were investigated. Figure 1 shows PM energy spectra for the long periodic, diurnal, semi-diurnal and subtidal frequencies.

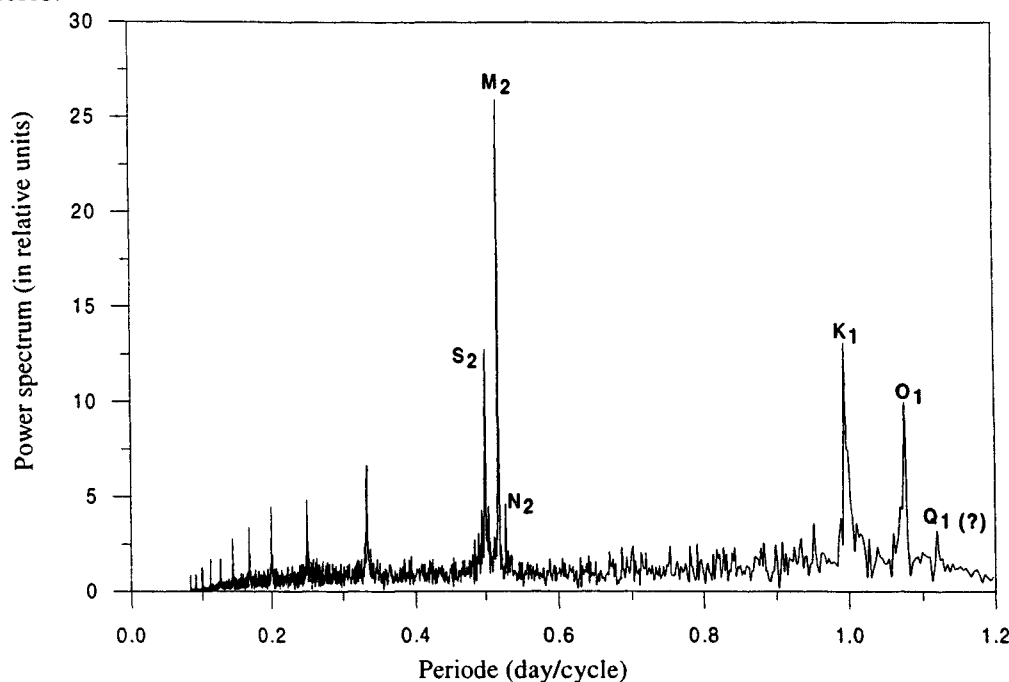


Fig. 1. Power spectrum of polar motion data of the semi-diurnal and diurnal frequency bands. Similar energy spectra for LOD are collected together in Fig. 2.

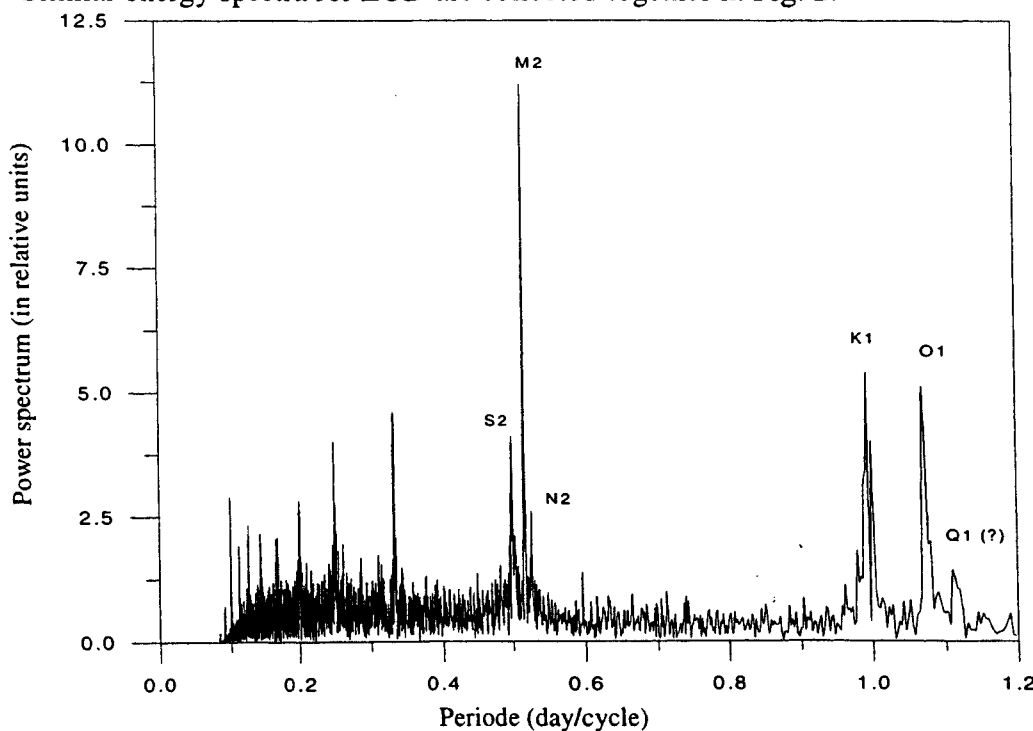


Fig. 2. Power spectrum of LOD data of the semi-diurnal and diurnal frequency bands. In Table 1 PM and LOD spectral peak amplitudes are shown in four different frequency bands.

Table 1. Amplitudes of tidal and non-tidal harmonic components for polar motion (PM) (in 10^{-4} as) and length of day (LOD) (in 10^{-4} s). Frequencies are in °/h

Frequencies	PM	LOD	Comments
Long periodic terms			
0.5444	not detected	4.55	M_m (27.55d)
1.0983	not detected	11.40	M_f (13.66d)
Diurnal components			
13.9430	8.05	3.71	O_1
15.0410	9.10	3.81	K_1
Semi-diurnal components			
28.4397	3.38	1.92	N_2
28.9841	17.10	7.75	M_2
30.0000	9.52	2.61	S_2
Subtidal frequencies			
45.	4.10	2.80	
60.	2.80	2.40	
75.	3.10	1.80	
90.	2.10	1.10	
105.	3.10	1.10	
120.	2.10	1.30	
135.	1.90	1.85	
150.	1.10	1.80	

In the frequency band of long-periodic tides (up to 0.2 cycles/day) LOD data were detected. The PM spectrum at this range is fairly noisy. The most significant LOD peaks are connected with M_m and M_f tidal waves. To obtain realistic spectral peaks for long-periodic band of PM a significant section of it was filtered out. This way a reliable peak for the fortnightly wave M_f was detected.

PM anomalies of diurnal frequency band – as it follows from section 3 – may be of Earth tidal origin. The oceanic tidal influence in principle can generate semi-diurnal LOD components. In semi-diurnal frequency band the biggest anomaly coincides with the frequency of the main lunar wave M_2 . It is remarkable that the S_2 constituent, together with S_1 , is much bigger as it is acceptable on the basis of the theory of terrestrial and oceanic tides. This phenomenon possibly can be explained with meteorological influences to a and less extent by atmospheric tides (Zharov et al., 1996). Systematic, until now not explained, anomalies were found in the PM and LOD spectra in higher frequencies as the tidal frequency bands, i.e. for 3, 4, 5, 6, 7, 8, 9 and 10 cycles/day (the corresponding angular frequencies are 45, 60, 75, 90, 105, 120, 135, 150 °/h). The amplitudes in this part of Fourier spectra are significantly big.

Some examples of wavelets calculated by base functions Morlet are shown on Fig. 3.

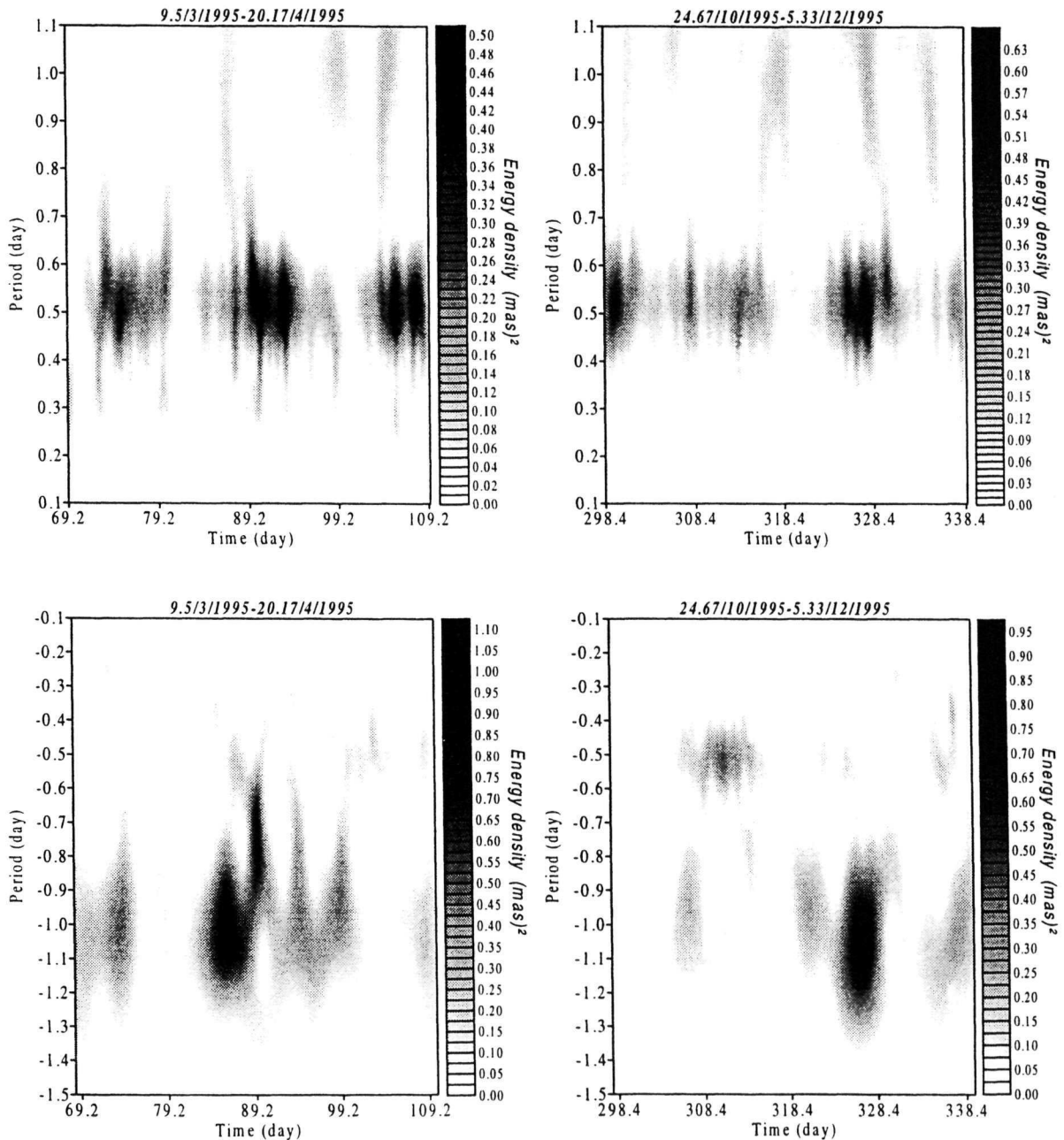


Fig. 3. Energy density values of Earth rotation data (1995) based on Morlet Wavelet technique; maximum prograde (upper diagrams, positive periods) energy density value lies with the time span and the maximum retrograde (lower diagrams, negative periods) energy density value lies with the time span.

It should be mentioned here, that two different wavelet base functions – Morlet and Mexican hat (Arfa-Kaboodvand, Grotens, 1998) show similar results. For the PM it can be concluded that – the strongest and most stable signals are the semi-diurnal prograde and the diurnal retrograde one. Anomalies of another frequency bands – like the diurnal prograde and semi-diurnal retrograde – are present only temporarily. This circumstance proves, that the tidal signal in PM undergo significant irregular – possibly meteorological – influences (Arfa-Kaboodvand, et al., 1999). In the diurnal/semi-diurnal frequency band no significant non-tidal signals were detected above the noise level of 0.1 mas.

5. STUDY OF THE POSSIBLE INFLUENCE OF EARTHQUAKE ON LOD

The influence of earthquakes on short periodic PM and LOD is discussed in many scientific publications (Manshina et al., 1967; Runcorn, 1970; Smylie et al., 1971; Chao et al., 1995).

For the purpose of present research the catalogue of seismic events for 1995 published by the US Geological Survey National Earthquake Information Center has been used. In spite of the fact that during the year 1995 many significant events occurred (first of all should be mentioned the Kuril islands event on 2nd December with a magnitude $M_w = 7.8-7.9$) until now there were not LOD anomalies detected in the frame of present research which can be connected to seismic events without doubt.

From Eqs 2 and 3 – if instead of H the normal hydrostatic stress $P_N = \rho g H$ is introduced the following surface level variation of the loaded area with centri angle α can be obtained (Varga, 1988):

$$D_N = \frac{4\pi G R_E}{g^2} \sum_{n=0}^{\infty} \frac{h_n^N}{2n+1} P_N(\cos \psi) \quad (7)$$

Similar equation holds for the horizontal stress caused surface level variations:

$$D_T = \frac{4\pi G R_E}{g^2} \sum_{n=0}^{\infty} \frac{h_n^T \cdot n \cdot (n+1)}{2n+1} P_M(\cos \psi) \quad (8)$$

In above two equations h_n^N and h_n^T are the normal and horizontal spheroidal stress load numbers, which describes stress accumulation not connected to mass load (Varga, 1988). P_N and P_M have the meaning as holds in Eq. 7 for level variations. Changes in LOD are directly connected to the variations of the polar moment of inertia due to the stress load acting on a spherical segment:

$$\begin{aligned} \Delta C &= \int_r^{r+D} \int_{\varphi_1}^{\varphi_2} \int_{\lambda_2}^{\lambda_1} \rho r^4 \cos^3 \varphi dr d\varphi d\lambda = \\ &= \frac{(r+d)^5 - r^5}{5} \rho \Delta \lambda \left[(\sin \varphi_2 - \sin \varphi_1) - \frac{1}{3} (\sin^3 \varphi_2 - \sin^3 \varphi_1) \right] \end{aligned} \quad (9)$$

Since

$$(r+D)^5 - r^5 \approx r^5 \left[\left(1 + \frac{D}{r} \right)^5 - 1 \right] \approx 5r^4 D \quad (10)$$

ΔC can be written as

$$\Delta C \approx r^4 D \rho \Delta \lambda \left[(\sin \varphi_2 - \sin \varphi_1) - \frac{1}{3} (\sin^3 \varphi_2 - \sin^3 \varphi_1) \right] \quad (11)$$

Actually the area involved in the surface level variation is sufficiently larger than the territory where the stress accumulation takes place. So the integration along the Earth surface in case of loaded by D_N squares $10^\circ \times 10^\circ$, $1^\circ \times 1^\circ$ and $0.1^\circ \times 0.1^\circ$ leads to following results:

Area of stress Accumulation	Corresponding LOD variation
$10^\circ \times 10^\circ$ ($\sim 10^6 \text{ km}^2$)	$10^{-4} - 10^{-5} \text{ s}$
$1^\circ \times 1^\circ$ ($\sim 10^4 \text{ km}^2$)	$10^{-6} - 10^{-7} \text{ s}$
$0.1^\circ \times 0.1^\circ$ ($\sim 10^2 \text{ km}^2$)	$10^{-7} - 10^{-8} \text{ s}$

As it was mentioned in Section 4 the accuracy of the dataset of LOD is accurate to about 10^{-8} s . Due to the fact that no short periodic subdiurnal LOD anomaly was detected above this level in case of Kurill event of 0.2.12.1995 it can be concluded that the area involved into stress accumulation – even in case of such a significant earthquake – is not bigger as 100 km^2 , because the corresponding ΔLOD is less than 10^{-8} s .

6. CONCLUSIONS

The usual way of the study of short periodic variations in Earth rotation is connected with LOD investigations. In this paper changes in length of day were studied together with polar motion data. The following conclusions were formulated.

- a) The strongest peaks of high frequency part of the LOD and PM data appears at lunisolar frequencies. The amplitudes of the other anomalies of Fourier spectra are smaller.
- b) The nature of systematically distributed anomalies at frequencies 3, 4, 5, 6, 7, 8, 9 and 10 cycle/day is not explained satisfactory yet.
- c) In the LOD data set for 1995 it was not possible to find any signal which can be connected to earthquakes without doubt.

Acknowledgements

We appreciate support of Internation Büro of BMBF/Bonn and Deutsche Forschungsgemeinschaft as well as the Hungarian Committee for Scientific and Technological Development.

The activity described in this work was also supported by the Hungarian Science Foundation (Project: OTKA T029049).

References

- Arfa-Kaboodvand K., Groten E., 1998: Einsatz des Wavelet-Transforms zur Untersuchung der kurzperiodischen Variation der Polbewegung. Zeitschrift für Vermessungswesen, 123, 8, 259-265
- Arfa-Kaboodvand K., Groten E., Zavoti J., Varga P., 1999: Stochastische und deterministische Analyse sowie Modellierung der Erdrotation mit Schwerpunkt: Polschwankung und ΔUT_1 (LOD), basierend auf GPS-Daten.. Mittelilungen des Bundesamtes für Kartographie und Geodäsie, 5, 126-133
- Barnes R.T.H., Hide R., White A.A., Wilson C.A., 1983: Atmospheric angular momentum fluctuations, length of day changes and polar motion. Proc. R. Astron. Soc., A387, 31-73

- Chao B.F., Gross R.S., 1995: Changes in the Earth's rotational energy induced by earthquakes. *Geophysical Journal International*, 122, 776-783
- Chao B.F., Merriam J.B., Tamura Y., 1995: Geophysical analysis of zonal tidal signals in length of day. *Geophysical Journal International*, 122, 765-775
- Chao B.F., Naito I., 1995: Wavelet analysis provides a new tool for studying Earth's rotation. *EOS*, 76, 161-165
- Chao B.F., Ray R.D., Egbert G.D., 1995: Diurnal/semidiurnal oceanic tidal angular momentum: Topex/Poseidon models in comparison with Earth's rotation rate. *Geophys. Res. Letters*, 22, 1993-1996
- Dickey J.O., Marcus S.L., Hide R., 1994: Angular momentum exchange among the solid Earth, atmosphere and oceans: A case study of the 1982-1983 El Nino event. *Journal of Geophysical Research*, 99, B 12, 23921-23937
- Eubanks T.M., Steppe J.A., Dickey J.O., Rosen R.D., Salstein D.A., 1988: Cause of rapid motions of the Earth pole, *Nature*, 334, B 178, 115-119
- Gambis D., 1992: Wavelet transform analysis of the length of day and the El-Nino/Southern Oscillation variations at interseasonal and interannual time scales. *Annales Geophysicae*, 10, 429-437
- Gilbert D., Holschneider M., LeMouél J.L., 1998: Wavelet analysis of the Chandler Wobble. *Journal of Geoph. Res.*, 103, B.11, 27069-27089
- Graffarend E., Engels J., Varga P., 1997: The spacetime gravitational field of a deformable body. *Journal of Geodesy*, 72, 11-30
- Gross R.S., 1993: The effect of ocean tides on the earth's rotation as predicted by the results of an ocean tide model. *Geophysical Research Letters*, 20, 4, 293-296
- Hide R., Dickey J.O., 1991: Earth variable rotation, *Science*, 253, 629-637
- Hobson E.W., 1995: The theory of spherical and ellipsoidal harmonics. Shlesha Publishing Company, New York
- Jentzsch G., 1997: Earth tides and ocean tidal loading in: *Tidal Phenomena*, Eds.: Wilhelm H., Zürn W., Wenzel H.-G. *Lectures Notes in Earth Sciences*, Springer, 145-172
- Kolaczek B., 1995: Short period variations of Earth rotation. *Proc. Journées 1995 Systèmes de Référence, Spatio-Temporales*, Warsaw, Poland, Publ. by the Space, Ras. Centre, PAS, 147-154
- Kosek W., 1995: Time variable bandpass filter spectra of real and complex-valued polar motion series. *Artificial Satellites. Planetary Geodesy*, 24, vol. 30, 1, 27-43
- Manshina L., Smylie D.E., 1967: Effect of earthquakes on the Chandler wobble and the secular polar shift. *Journal of Geophysical Research*, 72, 18, 4731-4743
- Melchior P., 1981: The tides of the planet Earth, Pergamon, 1-609
- Neilan R.E. (editor) 1998: International GPS service; IGS Central Bureau, JPL
- Pavel F., Uhink W., 1935: *Astronomisches Nachrichten*, 257, 365
- Pertzev B.P., Ivanova M.V., 1991: Indirect effect of oceanic tides in results of strainmeter observations. *Physics of the Earth*, 2, 84-88 (in Russian)
- Popinski N., Kosek W., 1994: Wavelet transform and its application for short period earth rotation analysis. *Artificial Satellites, Planetary Geodesy*, 22, 29, 75-88
- Rothacher M., Beutler G., Weber J., Hefty J., 2000: High frequency Earth rotation variations from the years of Global Positioning System data, *Yournal of Geophysical Research (Submitted)*
- Runcorn S.K., 1970: A possible cause of the correlation between earthquakes and polar motions. In: L. Manshina et al. (eds.), *Earth-quakes displacement fields and the rotation of the Earth*. D. Reidel Publishing Company, 181-187

- Smylie D.E., Manshina L., 1971: The elasticity theory of dislocations in real Earth models and changes in the rotation of the Earth. *Geophysical Journal of Royal Astronomical Society*, 23, 329-354
- Sprenger T.A., Beutler G., Rothacher M., 1999: Improving the orbit estimates of GPS satellites. *Journal of Geodesy*, 73, 147-157
- Varga P., 1988: Influence of the elastic stress accumulation on the Earth's polar position. *Proceedings of the International Symposium "Figure and Dynamics of the Earth, Moon and Planets.*
- Weber R., 1999: The ability of the GPS to monitor Earth rotation variation, *Acta Geodaetica et Geophysica Hungarica*, 34, 4, 457-473
- Zharov V.E., Gambis D., 1996: Atmospheric tides and rotation of the Earth. *Journal of Geodesy*, 70, 321-326

THE SHORT PERIOD NUTATIONS OF THE EARTH

Souchay Jean (1) and Marta Folgueira (2)

(1) Observatoire de Paris, Paris, France

(2) Instituto de Astronomia y Geodesia (UCM-CSIC),

Facultad de Ciencias Matematicas, Universidad Complutense de Madrid,
28040 Madrid, Spain

ABSTRACT

Facing the drastic improvements of VLBI and GPS observations which lead to a very high accuracy in the determination of the EOP (Earth Orientation Parameters), it was necessary to develop further the theoretical calculations of nutation coefficients, notably by lowering the truncation threshold of the amplitude of these coefficients. Thus, we show that at the microarsecond level, a significant amount of coefficients of nutation with sub-diurnal period are present. After describing their origin from the non-zonal harmonics of the geopotential, we explain their global effect on the modelization of the pole direction in space, discussing also the influence of the model of Earth chosen (rigid or non-rigid).

1. THE ORIGIN OF THE SHORT PERIOD NUTATIONS.

The non-rigid Earth nutation series adopted by the IAU (International Astronomical Union) in 1980 are based on the works of Kinoshita (1977) and Wahr (1979). In the first one, the rigid Earth nutation series were calculated by the application of the Hamiltonian canonical equations to the rotation of the rigid and elliptical Earth. In the second one, the transfer function for the nutations of an elliptical, elastic and oceanless Earth with fluid outer core and a solid inner core was obtained. The non-rigid Earth nutation coefficients were derived from the convolution between Wahr's transfer function and Kinoshita's rigid Earth nutation series.

The improvement in the accuracy of the techniques as Very Long Baseline Interferometry (VLBI), Lunar Laser Ranging (LLR) and Global Positioning System (GPS) have led in this decade to the extension of Kinoshita's theory and more precise determination of Wahr's transfer function.

The new transfer function are based on new models for Earth's interior and takes into account other geophysical effects as changes in the boundary shapes due to the non-hydrostatic equilibrium, changes in the density, the inelasticity of the mantle, etc. (Dehant and Defraigne, 1997), (Mathews et al., 1998), (Dehant et al., 1999).

In Kinoshita's work, the coefficients of nutation up to 0.1 *mas* (milliarcsecond) have been taken into account. The extension of this work was principally due to the better precision reached by the observations. Such extension has been carried out in several steps:

- $0.1 \text{ mas} \rightarrow 0.005 \text{ mas}$

This step made necessary the introduction of the direct and indirect planetary effects, of the influence of the second-order parts of the potential and some improvements due to an extension of the theory at the second order as the coupling effect between the rotational motion of the Earth and the orbital motion of the Moon: (Kinoshita and Souchay, 1990).

- $0.005 \text{ mas} \rightarrow 0.1 \mu\text{as}$ (microarcsecond)

In this step, the calculations of the planetary tilt-effect, the second order effects due to crossed-nutations and spin-orbit coupling and the influence of non-zonal harmonics of third and fourth degree was carried out: (Souchay and Kinoshita, 1996; 1997), (Folgueira et al., 1998a;b), (Souchay et al., 1999).

The short period nutations have their origin in the non-zonal harmonic coefficients of the geopotential. That is, they come from the harmonics C_{nm} and S_{nm} (with $m \neq 0$). Kinoshita (1977) studied theoretically the influence due to the Earth is not an axially symmetrical body (originated by C_{22} and S_{22} coefficients) and also proved numerically that such harmonics had no appreciable effect on the rotational motion of the Earth, at a level of 0.1 mas . The new level of truncation for the coefficients of nutation considered by Kinoshita and Souchay (1990) provided 7 terms in longitude and 3 terms in obliquity above 0.005 mas due to the triaxiality of the Earth. The new tables REN-2000 of the nutation for a rigid Earth model have included all the quasi-diurnal and sub-diurnal nutations above $0.1 \mu\text{as}$. The number of short period nutations considered is 252 terms in longitude and 190 in obliquity. This appreciable amount of new coefficients comes from the harmonics $C_{22}, C_{31}, C_{32}, C_{33}, C_{41}, S_{22}, S_{31}, S_{32}, S_{33}$ and S_{41} .

In the last years, new rigid Earth nutation series, calculated using different analytical methods, have come forth. These are SMART97, Bretagnon et al.'s series, and RDAN97, Roosbeek and Dehant's series (Bretagnon et al., 1997;1998), (Roosbeek and Dehant, 1998). In the next section, we evaluate the differences between these two series and REN-2000.

2. TEMPORAL EVOLUTION OF REN-2000 SHORT PERIOD NUTATIONS. COMPARISON WITH OTHER SERIES.

The figures 1 and 2 show the temporal evolution for 1 century of REN-2000 short period nutations for $\Delta\psi \sin \epsilon$ and $\Delta\epsilon$. As we can see, these contributions vary between $-60 \mu\text{as}$ and $+50 \mu\text{as}$ for longitude component and between $-50 \mu\text{as}$ and $+50 \mu\text{as}$ for obliquity component. The figures 3 and 4 present the temporal evolution for 1 century of the differences between SMART97 and REN-2000, for longitude and obliquity quasi-diurnal and sub-diurnal nutations. Finally, in the figures 5 and 6, we show the time domain comparison between RDAN97 and REN-2000, for longitude and obliquity components, when considering a 100 years time span.

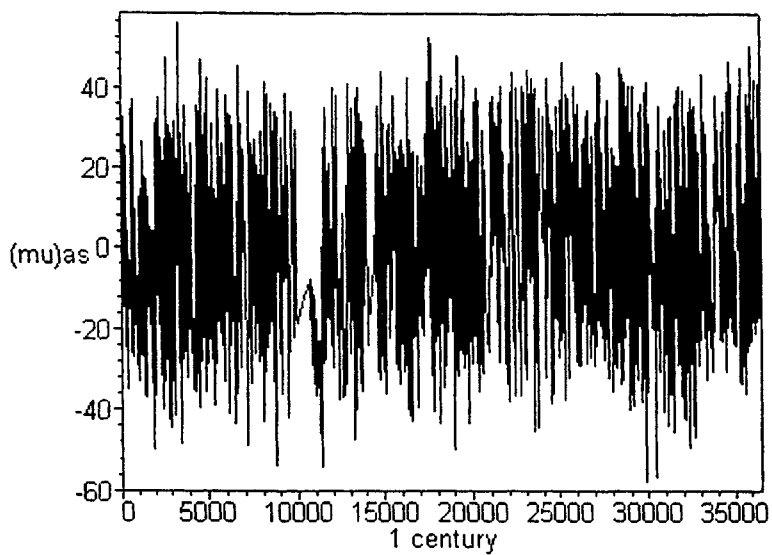


Figure 1: REN-2000 short period nutations in longitude.

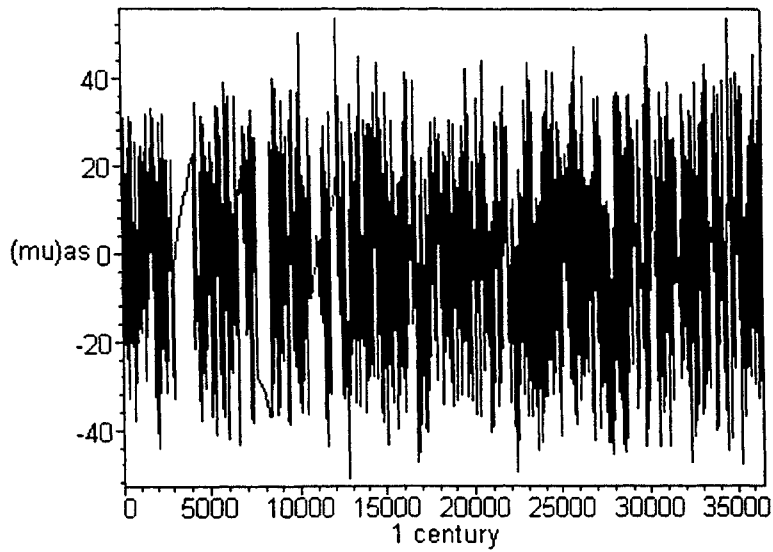


Figure 2: REN-2000 short period nutations in obliquity.

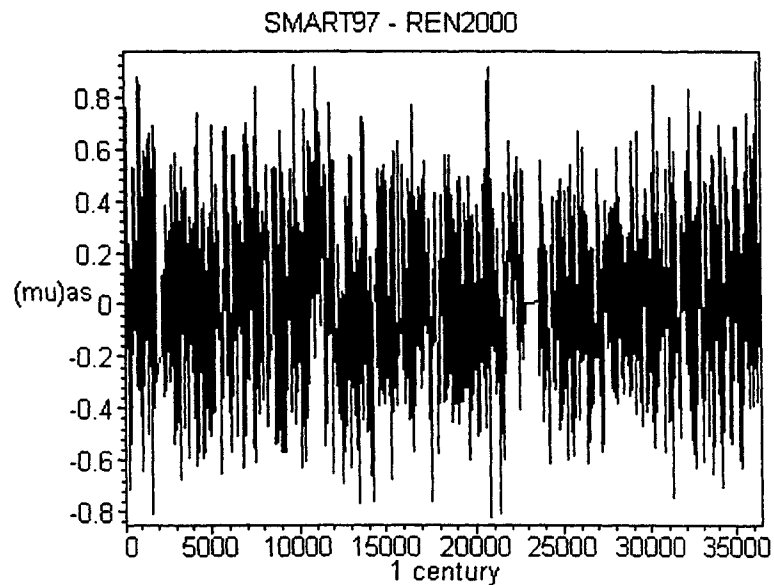


Figure 3: Time domain comparison between SMART97 and REN-2000, longitude part.

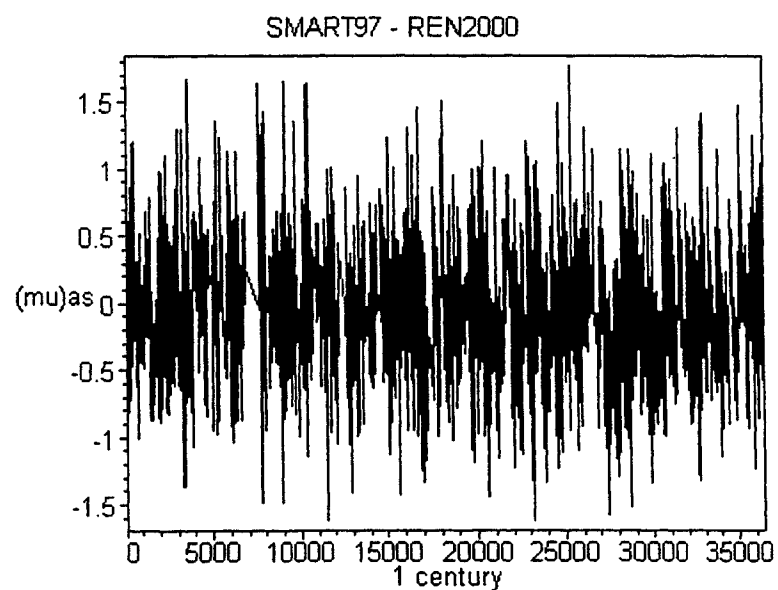


Figure 4: Time domain comparison between SMART97 and REN-2000, obliquity part.

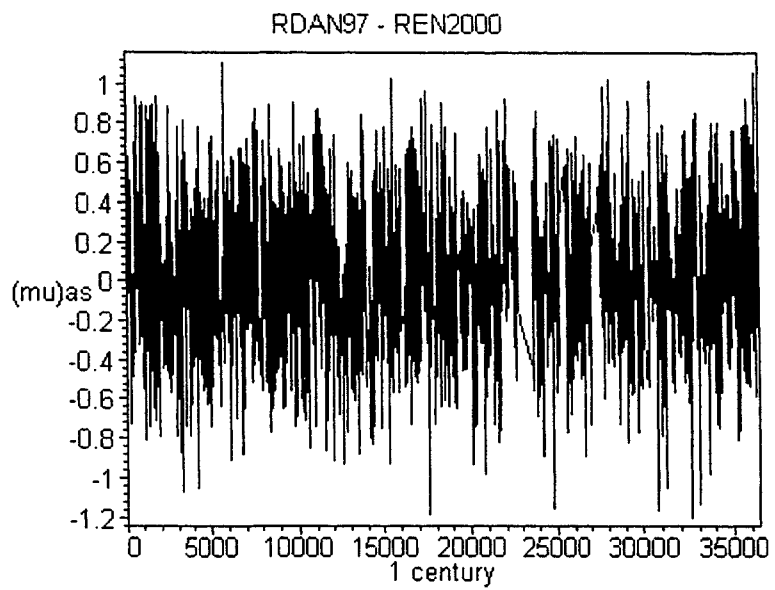


Figure 5: Time domain comparison between RDAN97 and REN-2000, longitude part.

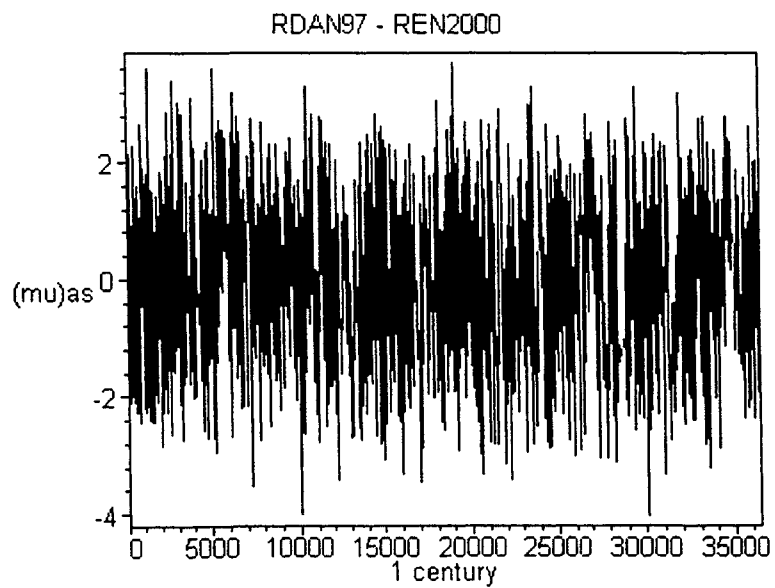


Figure 6: Time domain comparison between RDAN97 and REN-2000, obliquity part.

3. REFERENCES.

- P. Bretagnon, P. Rocher and J.L. Simon: 1997, "Theory of the rotation of the rigid Earth". *Astronomy and Astrophysics* **319**, pp. 305-317.
- P. Bretagnon, G. Francou, P. Rocher and J.L. Simon: 1998, "SMART97: A new solution for the rotation of the rigid Earth". *Astronomy and Astrophysics* **329**, pp. 329-338.
- V. Dehant and P. Defraigne: 1997, "New transfer functions for nutations of a non-rigid Earth". *J. Geophys. Res.* **102**.
- V. Dehant, F. Arias, Ch. Bizouard, P. Bretagnon, A. Brzezinski, B. Buffett, N. Capitaine, P. Defraigne P., O. de Viron, M. Feissel, H. Fliegel, A. Forte, D. Gambis, J. Getino, R. Gross, T. Herring, H. Kinoshita, S. Klioner, P.M. Mathews, D. McCarthy, X. Moisson, S. Petrov, R.M. Ponte, F. Roosbeek, D. Salstein, H. Schuh, K. Seidelmann, M. Soffel, J. Souchay, J. Vondrak, J.M. Wahr, P. Wallace, R. Weber, J. Williams, Y. Yatskiv, V. Zharov, S.Y. Zhu: 1998, "Considerations concerning the non-rigid Earth nutation theory". *Celestial Mechanics and Dynamical Astronomy* **72** (4): pp. 245-309.
- M. Folgueira: 1998, "Series solución del movimiento de rotación de la Tierra obtenidas por métodos analíticos". PhD Thesis, Universidad Complutense de Madrid.
- M. Folgueira, J. Souchay and H. Kinoshita: 1998a, "Effects on the nutation of the non zonal harmonics of third degree". *Celestial Mechanics and Dynamical Astronomy* **69** (4), pp. 373-402.
- M. Folgueira, J. Souchay and H. Kinoshita: 1998b, "Effects on the nutation of C_{4m} and S_{4m} harmonics". *Celestial Mechanics and Dynamical Astronomy* **70** (3), pp. 147-157.
- M. Folgueira and J. Souchay: 1999, "The diurnal and sub-diurnal nutations calculated by different theories of rigid Earth rotation". Journées 1998 Systemes de référence Spatio-temporels: Conceptual, convencional and practical studies related to Earth rotation. Pp. 178-179.
- H. Kinoshita: 1977, "Theory of the rotation of the rigid Earth". *Celestial Mechanics* **15**, pp. 277-326.
- H. Kinoshita and J. Souchay: 1990, "Theory of the nutation for the rigid Earth model at the second order". *Celestial Mechanics* **48**, pp. 187-265.
- P.M. Mathews, B.A. Buffet and T.A. Herring: 1998, "The magnetic coupling contribution to nutation". Journées 1998 Systemes de référence Spatio-temporels: Conceptual, convencional and practical studies related to Earth rotation.
- J. Souchay and H. Kinoshita: 1996, "Corrections and new developments in rigid Earth nutation theory: I. Lunisolar influence including indirect planetary effects". *Astronomy and Astrophysics* **312**, pp. 1017-1030.
- J. Souchay and H. Kinoshita: 1997, "Corrections and new developments in rigid Earth nutation theory: II. Influence of second-order geopotential and direct planetary effect". *Astronomy and Astrophysics* **318**, pp. 639-652.
- J. Souchay, B. Loysel, H. Kinoshita and M. Folgueira: 1999, "Corrections and new developments in rigid Earth nutation theory: III. Final tables "REN-2000" including crossed-nutation and spin-orbit coupling effects". *Astronomy and Astrophysics Supplement Series* **135**, pp. 111-131.
- F. Roosbeek and V. Dehant: 1998, "RDAN97: An analytical development of rigid Earth nutation series using the torque approach". *Celestial Mechanics and Dynamical Astronomy* **70**, pp. 215-253.
- J.M. Wahr: 1979, "The tidal motions of a rotating, elliptical, elastic and oceanless Earth". PhD Thesis, University of Colorado.

SHORT PERIODS IN EARTH ROTATION SEEN IN VLBI DATA ANALYSED BY THE LEAST-SQUARES COLLOCATION METHOD

Titov Oleg (1) and Harald Schuh (2)

(1) Saint-Petersburg University, Russia, Bibliotechnaya sq., 2, Petrodvorets, Saint-Petersburg, 198904, Russia - olegtitov@mail.ru

(2) Institut für Geodäsie und Geophysik, Technische Universität Wien, Austria
hschuh@luna.tuwien.ac.at

ABSTRACT

The least-squares collocation method (LSCM) is briefly explained. It requires the design of the a-priori correlation matrix for which examples are given. The LSCM applied on Very Long Baseline Interferometry (VLBI) data analysis allows the determination of the Earth rotation parameters with a very high temporal resolution. The results of parallel VLBI sessions which took place since 1998 using two independent VLBI networks were analyzed in the subdiurnal period range and compared by computing the wavelet cross-scalograms, the covariance spectrum and the normed coherency. Periods between 5 and 7 hours can be seen in many of the UT1-UTC data sets besides the well-known diurnal and semidiurnal periods. However, it is still questionable whether these short-period variations really exist, i.e. are due to geophysical excitation.

INTRODUCTION

Today, the Earth Rotation Parameters (ERPs) are usually estimated and published with a daily resolution. However, it is possible by VLBI to determine UT1-UTC and polar motion with a temporal resolution of as short as 3-7 minutes. This paper concentrates on ERP variations with periods shorter than 24 hours. Highly resolved ERPs monitored by VLBI were recently analyzed by Schuh and Titov (1999), Titov (2000), Schuh and Schmitz-Hübsch (2000). It is known that the strongest short-period signals are caused by oceanic tidal effects. 41 tides for UT1-UTC and 57 tides for polar motion most of them in the diurnal and semidiurnal period range were estimated from VLBI (Gipson, 1996) and from GPS observations (Rothacher et al., 2000).

Nevertheless, ERP measurements with high temporal resolution seem to reveal signals outside the semidiurnal and diurnal periods, too. These variations are supposed to be due to resonances with modes of the Earth or caused by high-frequency atmospheric oscillations. Transient and irregular variations could also be excited by episodic phenomena like strong earthquakes or typhoons.

All time series which were analyzed within the work presented in this publication were purely obtained by VLBI measurements. The eminent importance of VLBI in

geodesy and geophysics is due to its connection with an inertial reference frame formed by compact extragalactic radio sources. VLBI is unique in its ability to monitor without hypotheses all components of Earth orientation.

OBSERVATION OF EARTH ROTATION BY VLBI

For more than 20 years the technique of geodetic VLBI has been applied to measure the rotation of the Earth. The geodetic and geophysical interest in VLBI is based on the use of an inertial reference frame formed by a set of compact extragalactic radio sources. VLBI measures very accurately the angles between the Earth-fixed baseline vectors and the space-fixed radio sources. Thus, even the most subtle changes of the baseline lengths and changes of the baseline directions with respect to the inertial reference frame can be detected. Geodynamical phenomena such as polar motion, Universal Time 1 (UT1) variations, precession and nutation, Earth tides, ocean tidal response, and tectonic plate motions can be monitored with highest accuracy. The fundamentals of the VLBI technique, the main elements of a VLBI system and the most important geodetic results were described in many publications, e.g. by Schuh and Campbell (1994), Sovers et al. (1998). Schuh and Schmitz-Hübsch (2000) give an overview about the abilities of VLBI to monitor the ERPs and publish recent results on subseasonal time scales.

It is necessary to separate high-frequency variations of the ERPs from site dependent effects as rapid variations of the troposphere or unmodelled deformations due to oceanic or atmospheric loading. Subdiurnal variations of site dependent parameters could cause apparent subdiurnal variations of the ERPs estimated by the whole network. Fortunately, since 1998 parallel 24-hour sessions on the NEOS-A and CORE-A networks provide a good opportunity to compare the independent ERPs variations for the same epochs as will be shown later in this article.

APPLICATION OF THE LEAST-SQUARES COLLOCATION METHOD TO VLBI DATA

There are several approaches for VLBI data adjustment. All of them imply that the observables are not correlated. Thus, for VLBI data analysis usually a diagonal a-priori variance-covariance matrix is applied in the least-squares fit. But it is obvious that different reasons cause correlations between the observables: systematic errors, the stochastic nature of some parameters, etc. It was shown that an application of the full variance-covariance matrix improves the repeatability of geodetic parameter estimates (baseline lengths and station coordinates) (Schuh and Tesmer, 2000). Nevertheless, the construction of a full a-priori variance-covariance matrix is not simple because it is an iterative procedure and requires information about a-posteriori correlations.

Conventional least-squares estimation follows the formula

$$\hat{x} = (A^T Q_w^{-1} A)^{-1} A^T Q_w^{-1} l \quad (1)$$

where

Q_w - diagonal covariance matrix of observations,
 A - matrix of partial derivatives,
 l - vector of observables.

The least-squares collocation method (LSCM) (Titov, 2000) as an alternative approach for VLBI data adjustment provides

- a procedure for the construction of the full variance-covariance matrix,
- an approach for the use of this matrix.

The LSCM applies the following formula for the estimation of vector \hat{x}

$$\hat{x} = (A^T Q_0^{-1} A)^{-1} A^T Q_0^{-1} l, \quad (2)$$

with matrix

$$Q_0 = C Q_z C^T + Q_w, \quad (3)$$

where the matrix Q_z can be calculated based on information about covariance functions of the stochastic parameters (see below). The matrix C contains the partial derivatives of the stochastic parameters.

Correlation functions of wet tropospheric delay and of clock offset were applied for our analysis to take into account the variability of the corresponding parameters within 24 hours. The correlation functions of stochastic parameters are approximated using eq. (4) (Gubanov, Surkis, Titov, 1997).

$$q(\tau) = \frac{1}{\cos \varphi} \exp(-\alpha \tau) \cos(\beta \tau + \varphi), \quad (4)$$

where τ is a time lag (in part of days) with $0 \leq \tau \leq 1$; the following sets of parameters for the clock offset ($\alpha = 2.64 \text{ day}^{-1}$, $\beta = 8.64 \text{ day}^{-1}$, $\varphi = 0.33 \text{ radian}$) and for the wet tropospheric delay ($\alpha = 6.24 \text{ day}^{-1}$, $\beta = 6.48 \text{ day}^{-1}$, $\varphi = 0.82 \text{ radian}$) were used. Figure 1 and figure 2 represent plots of the correlation functions.

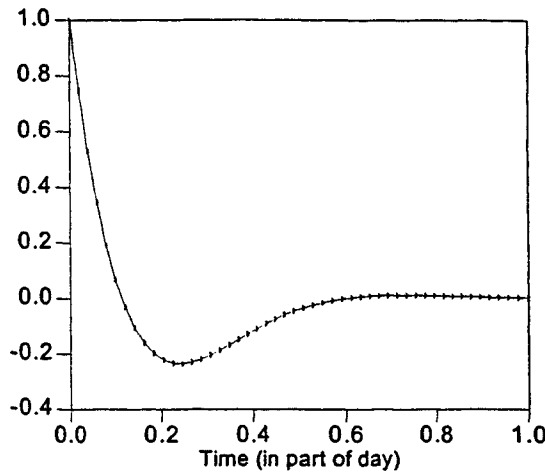


Fig. 1: Correlation function for clock offset

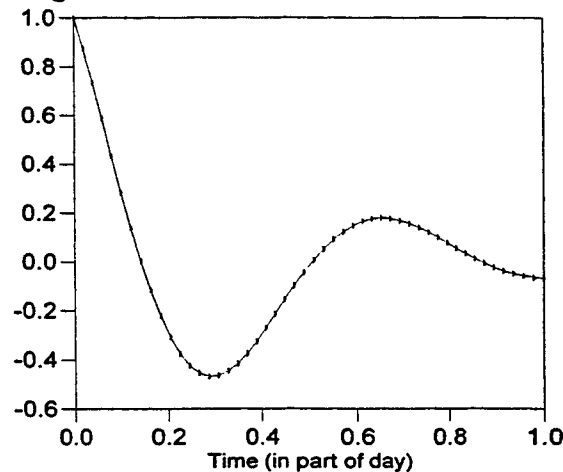


Fig. 2: Correlation function for wet tropospheric delay

FULL CORRELATION MATRIX ANALYSIS

The resulting variance-covariance matrix Q_0 eq. (3) is a full one. Non-diagonal elements of the matrix describe a mutual correlation between the observed delays. They depend on the time difference between the observations as well as on the geometry of the VLBI network. The table demonstrates the correlation coefficients between five delay observables taken on five baselines at the first epoch ($\tau = 0$) during NEOS-A session (23-Feb-1999). The VLBI sites Ny-Ålesund, NRAO20, Kokee and Fortaleza were considered.

	Fortaleza-Kokee	Fortaleza-NRAO20	Kokee-NRAO20	NRAO20-Ny-Ålesund	Kokee-Ny-Ålesund
Fortaleza - Kokee	1.000	0.740	-0.505	0	-0.447
Fortaleza - NRAO20		1.000	0.185	-0.211	0

Kokee - NRAO20			1.000	-0.274	0.661
NRAO20 - Ny-Ålesund				1.000	0.520
Kokee - Ny-Ålesund					1.000

Table: Correlations between observations on different baselines for the first epoch of the NEOS-A session on Feb. 23rd, 1999.

A zero element means that both baselines are made up by independent stations. A negative element means that the first station of the one baseline is the second station of the other baseline (e.g. the combination Fortaleza – Kokee and Kokee – NRAO20 in the table). Then, the elements of the partial derivatives matrix for the clock offset are equal to +1 and -1, correspondingly.

The dependence of the correlation coefficients on the time difference between the first epoch observation and the other observations on the baseline Fortaleza - Kokee is shown in fig. 3.

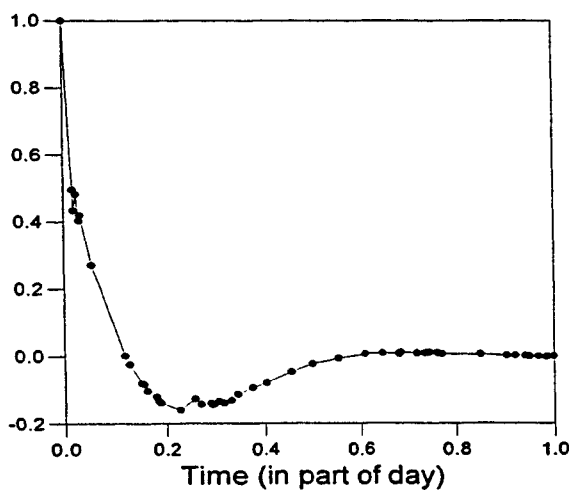


Fig. 3: Correlation function for baseline Fortaleza – Kokee (see text)

The application of the LSCM provides a way for increasing the repeatability of geodetic parameters such as baseline lengths or station coordinates. By the LSCM approach we can obtain global parameters, too (see paper "Estimation of subdiurnal tidal terms in UT1–UTC from VLBI data analysis" by Titov this volume).

DIURNAL AND SUBDIURNAL VARIATIONS OF EARTH ROTATION PARAMETERS

Very high temporal resolution of the Earth rotation parameters can be achieved by VLBI using the least-squares collocation method (LSCM) described in the previous paragraphs. Almost 400 VLBI experiments (NEOS-A from 1993 till 1999, CONT'96, CORE) each of them covering 24h (NEOS-A and CORE) or 120h (CONT)

were analyzed by Titov (2000) using the OCCAM VLBI software (Titov and Zaraoa, 1997) yielding time series of UT1-UTC and of polar motion with a resolution of 3-7 minutes. In this paragraph some examples for UT1-UTC will be given.

First, the main diurnal and semidiurnal variations due to the ocean tides were removed using the IERS Conventions (1996) correction model. The residuals, i.e. after correction of oceanic tidal terms and subtraction of a constant bias, were submitted to the wavelet transform (e.g. Schmidt, 2000; Schmidt and Schuh, 2000; both in this volume). Although ocean tidal influences had been corrected already according to the model recommended in the IERS Conventions (1996), many of the wavelet scalograms of the UT1-UTC series show residual energy in the diurnal and semidiurnal period range. Additionally, most of the data sets revealed irregular quasi-periodic fluctuations which are non-diurnal and non-semidiurnal. From the 120h CONT sessions very often (but not always) periods at 20 hours and 40 hours, around 8 hours and between 5 and 7 hours were found which are above the error level of the individual UT1-UTC parameters of better than $\pm 10\text{-}15$ microseconds of time. For more details see Schuh (1999).

Parallel sessions on different VLBI networks which took place since 1998 offer the opportunity for independent observations of the Earth rotation and hence the corresponding wavelet scalograms should show similar variations of the Earth rotation parameters. In figure 4 the UT1-UTC results obtained simultaneously by the VLBI NEOS-A network (Green Bank - Fortaleza - Kokee - Ny Alesund - Wettzell) and the CORE-A network (Fairbanks - Hartebeesthoek - Hobart - Matera - Westford - Algonquin Park) are plotted; both started from July, 28th, 1998, 18.00 to observe simultaneously for 24h (NEOS-A274 and CORE-A041). It should be noted that the two networks form two completely different VLBI ‘observing systems’, i.e. different radio sources were observed by different stations. As we are mainly interested in the short-period variations a comparison in the frequency domain was carried out. The two upper plots of figure 5 show the wavelet scalograms of the UT1-UTC series obtained by the two VLBI sessions. Both are quite similar: a dominant variation around 5-6 hours can be seen in the NEOS-A session results and in the CORE-A session results. The correspondence between the two scalograms is confirmed by the squared wavelet cross-scalogram (fig. 5, bottom). Additional information can be obtained from the normed coherencies and the covariances. The normed coherency function (fig. 5, bottom, right side) shows the generally good agreement between the two time series (NEOS-A and CORE-A) for the period range from 5-8 hours whereas the covariance function (fig. 5, bottom, left side) leads to the conclusion that the period around 5-6 hours is the most prominent one in the squared wavelet cross-scalogram. Both time series obviously contain also small variations around 3 hours.

UT1–UTC observed by VLBI, NEOS-A274 and CORE-A041 (28./29.07.1998)
bias and oceanic tidal removed

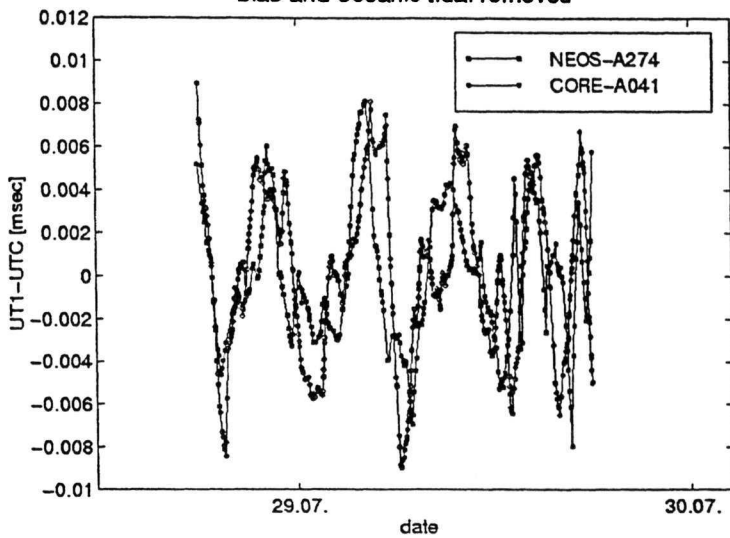


Fig.4: UT1-UTC parameters with high temporal resolution determined by two simultaneous VLBI sessions (NEOS-A274, CORE-A041) starting on July 28th, 1998 with a duration of 24 hours; a bias and ocean tidal terms were removed from the observations using the IERS Conventions (1996) model.

Morlet wavelet spectra of UT1–UTC
observed by VLBI

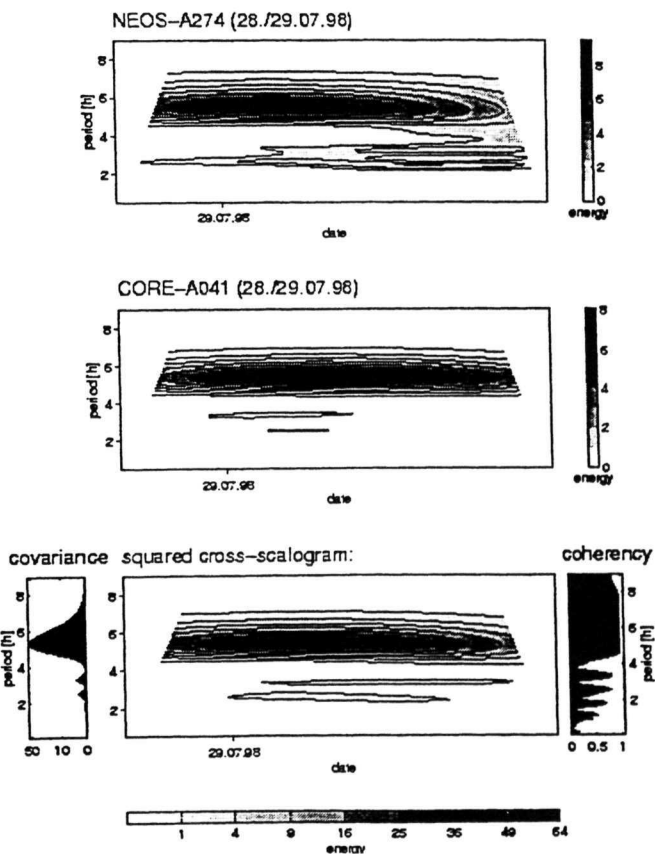


Fig. 5: Wavelet scalograms for periods shorter than 12 hours of two time series shown in figure 4, the squared wavelet cross-scalogram, the covariance (left) and the normed coherency (right).

Comparisons of a dozen simultaneous VLBI sessions observed in 1998 and 1999 by the NEOS-A and the CORE-A networks have been done. Not for all of them the agreement of the high-resolution Earth rotation time series is sufficiently good neither in time domain nor in frequency domain. Some of the parallel sessions give results which – even after subtraction of a constant bias – differ by more than two or three times the formal errors. This could be due to strong local atmospheric variations at one or some of the stations of a VLBI network what could influence the determination of the Earth rotation parameters by the whole VLBI network and hence cause apparent variations of the ERPs obtained by the LSCM. Indeed, wavelet analyses of highly-resolved tropospheric zenith delay parameters determined for the VLBI sites showed strong temporal and sometimes high frequency variations at some of the stations. However, a clear picture, i.e. correlation between tropospheric parameters and the ERPs estimated during a VLBI session could not be obtained.

CONCLUSIONS

Highly-resolved Earth rotation parameters were obtained by application of the LSCM on VLBI data. Irregular quasi-periodic variations of UT1-UTC can be seen in the wavelet scalograms besides the well-known diurnal and semidiurnal periods caused by the ocean tides. Although the tiny subdaily variations which could be seen in the VLBI results are above the error level of the observations and are statistically significant further careful tests have to be done to check whether they are real, i.e. caused by geophysical excitation.

REFERENCES

- Gipson, J.M.: 1996, Very long baseline interferometry determination of neglected tidal terms in high-frequency Earth orientation variation, *Journ. of Geophys. Res.*, 101(B12), 28051-28064.
- Gubanov, V., I. Surkis and O. Titov: 1997, 'Interday troposphere path length fluctuations', *Communications of IAA*, 103, Saint-Petersburg.
- MacMillan D.S., W.E. Hinrich, C.C. Thomas, N.R. Vandenberg, J.M. Bosworth, B. Chao, T.A. Clark and C. Ma: 1999, 'CORE: 1999, Continuos, High-Accuracy Earth Orientation Measurements', *Proceedings of the 13th Working Meeting on European VLBI for Geodesy and Astrometry*, Viechtach, Feb. 12-13, 1999, ed. by W. Schlüter and H. Hase, Bundesamt für Kartographie und Geodäsie, Wettzell, 166-171.
- Rothacher M., G. Beutler, R. Weber and J. Hefty: 2000, 'High-Frequency Earth Rotation Variations From Three Years of Global Positioning System Data', subm. to *Journal of Geophysical Research*.

- Schmidt M.: 2000, 'Wavelet Analysis of Stochastic Signals', IERS Technical Note No 28, (this volume).
- Schmidt, M. and H. Schuh: 2000, 'Abilities of Wavelet Analysis for Investigating Short-Period Variations of Earth Rotation', IERS Technical Note No 28, (this volume).
- Schuh, H.: 1999, 'The Rotation of the Earth Observed by VLBI', *Acta Geod. Geoph. Hung.*, 34(4), 421-432.
- Schuh, H. and J. Campbell: 1994, 'VLBI in geodynamical investigations', *Acta Geod. Geophys. Hung.*, 29 (3-4), 397-420.
- Schuh, H. and O. Titov: 1999, 'Short-period variations of the Earth rotation parameters as seen by VLBI', Proc. of the 13th Working Meeting on European VLBI for Geodesy and Astrometry, Viechtach, Feb. 1999, ed. by W. Schlüter and H. Hase, 172-177.
- Schuh, H. and H. Schmitz-Hübsch: 2000, 'Short Periods in Earth Rotation as seen by VLBI', submitted to *Surveys in Geophysics*.
- Schuh, H. and V. Tesmer: 2000, 'Considering A-Priori Correlations in VLBI Data Analysis', IVS 2000 General Meeting Proceedings ed. by N.R. Vandenberg and K.D. Baver, NASA/CP-2000-209893, 237-242.
- Sovers, O.J., J.L. Fanselow and C.S. Jacobs: 1998, 'Astrometry and geodesy with radio interferometry: experiments, models, results', *Rev. of Modern Physics*, 70, No. 4, 1393-1454.
- Titov, O.: 2000, 'Estimation of the subdiurnal UT1-UTC variations by least squares collocation method', *Astronomical and Astrophysical Transactions*, V. 19, 113-126.
- Titov, O. and N. Zarraoa: 1997, 'OCCAM 3.4 User's Guide', Communications of the Institute for Applied Astronomy (IAA), St. Petersburg, No. 69.
- ... IERS Conventions (1996): 1996, ed. by D. D. McCarthy, IERS Technical Note 21, Observatoire de Paris.

CONTRIBUTION OF THE GPS TO MONITOR EARTH ORIENTATION PARAMETERS

Weber Robert (1), Rothacher M. (2), Beutler G. (3)

(1) Institute of Geodesy and Geophysics, TU-Vienna

(2) Research Facility of Satellite Geodesy, TU-Munich

(3) Astronomical Institute, University of Berne

Abstract

In February 1994 CODE, one of the seven analysis centers of the IGS, started to derive nutation rates in addition to the routinely estimated polar motion and UT1-UTC rates. In 1999, a set of nutation amplitude corrections for 34 periods with respect to the IERS96 model as well as to the IAU80 model was presented in (*Rothacher et al., 1999*) based on 3.5 years of data. It has been demonstrated that GPS is especially sensitive to periods up to about 20 days. This paper deals with an update of the published amplitude corrections by taking into account the most recent observation data.

Additionally the quality of currently available subdaily polar motion series as well as the consequences of changes in processing and orbit modeling, which may impair the consistency of the series over time, will be discussed briefly.

Introduction

GPS data has proven to be a valuable source for the computation of accurate polar motion (PM) series. The series are of high quality mainly because of the uninterrupted coverage with observation data and the more or less regular distribution of the active IGS tracking sites (*Neilan, 1998*). In this context (*Kouba et al., 1999*) give a comprehensive description of IGS combined and contributed daily ERP solutions, considering in special AAM/ERP correlation studies and comparisons of combined OAM and AAM with excess PM rates.

Since 1995 the CODE Analysis Center produces besides the regular daily submissions PM- and LOD-estimates with a two hour time resolution. This sub-daily series, calculated from the same IGS observational data as the time series with one day resolution, are extremely suitable for studying half-daily and daily tidal signals. Based on about 3 years of data (*Rothacher et al., 2000*) have determined 57 tidal terms in PM and 41 in UT1 with an internal consistency of the estimated amplitudes in the order of $1\mu\text{s}$ in UT1 and $10\mu\text{as}$ in PM. The agreement of the GPS results with ocean tide models derived from altimeter data is at the same level. The chapter Subdaily Polar Motion below will focus on aspects related to the consistency of these series over the past years.

Nutation

In contrast to polar motion the estimation of corrections to the apriori nutation model ($\delta\Delta\varepsilon$, $\delta\Delta\psi$) was uniquely reserved to VLBI in the past. Satellite techniques used to determine UT1-UTC rates (LOD) at the most. (*Rothacher et al., 1999*) have shown, that there is no reason to discriminate between the estimation of the former and the latter quantities. Offsets in UT1-

UTC and in nutation are correlated with the orbital elements and unmodeled orbit perturbations lead to systematic errors in the rate estimates of both parameter types.

$$\begin{aligned}\Delta(UT1-UTC) &= -(\Delta\Omega + \cos i \cdot \Delta u_o) / k \\ \delta\Delta\varepsilon &= \cos\Omega \cdot \Delta i + \sin i \cdot \sin\Omega \cdot \Delta u_o \\ \delta\Delta\psi \cdot \sin\varepsilon_o &= -\sin\Omega \cdot \Delta i + \sin i \cdot \cos\Omega \cdot \Delta u_o\end{aligned}\quad (1)$$

(Ω ...right ascension of the ascending node, u_o ...argument of latitude at the osculation epoch, i ... inclination of the orbit, k ...ratio of universal time to sidereal time)

We may parameterize corrections in nutation, e.g. in obliquity, with respect to the reference model as piece-wise linear functions

$$\delta\Delta\varepsilon = \delta\Delta\varepsilon_0 + \dot{\delta\Delta\varepsilon}(t - t_0) \quad (2)$$

enforcing continuity at the interval boundaries. Due to equations (1) $\delta\Delta\varepsilon_0$ has to be constrained to the reference model (IAU 1980, IERS96), but $\dot{\delta\Delta\varepsilon}$ may be freely estimated. To obtain corrections in the nutation amplitudes $A_{ij}^\varepsilon, A_{oj}^\varepsilon$, the quantity $\delta\Delta\varepsilon$ can be represented as

$$\delta\Delta\varepsilon(t) = \sum_{j=1}^n A_{ij}^\varepsilon \cos\theta_j(t) + \sum_{j=1}^n A_{oj}^\varepsilon \sin\theta_j(t) \quad (3)$$

and the first derivative as

$$\dot{\delta\Delta\varepsilon}(t) = -\sum_{j=1}^n A_{ij}^\varepsilon \sin\theta_j(t) \frac{\partial\theta_j}{\partial t} + \sum_{j=1}^n A_{oj}^\varepsilon \cos\theta_j(t) \frac{\partial\theta_j}{\partial t} \quad (4a)$$

For the nutation in longitude, of course, a similar relation holds

$$\dot{\delta\Delta\psi}(t) = -\sum_{j=1}^n A_{oj}^\psi \sin\theta_j(t) \frac{\partial\theta_j}{\partial t} + \sum_{j=1}^n A_{ij}^\psi \cos\theta_j(t) \frac{\partial\theta_j}{\partial t} \quad (4b)$$

The θ_j denote a linear combination of the Delaunay variables and n the number of waves in consideration. The A_i, A_o are usually called in-phase and out-of-phase components. Advantageously these numbers may be converted to prograde and retrograde circular amplitudes. For details see (*Defraigne et al., 1995*).

The results given below are based on 1765 daily trend-reduced nutation rate estimates covering the period from April 1994 till March 1999. The formal errors of these nutation rates were about $25\mu\text{as}/d$ ($\dot{\Delta\varepsilon}, \dot{\Delta\psi} \sin\varepsilon_o$). The orbit models in use during this time span characterize the satellite motion (3-day arcs) by a set of initial conditions, one set of radiation pressure coefficients and by pseudo-stochastic pulses once per revolution in radial and along track direction.

Till the end of 1996 solar radiation pressure has been parametrized only by a direct radiation pressure coefficient and the y-bias. Afterwards three constant terms (direct, y-bias, x-bias) and periodic terms in x-direction were included in the estimation process. (Springer *et al.*, 1998) have shown, that the selection of such a parameter-subset optimizes the orbit quality and the quality of the UT1-UTC rate estimates. Tentatively we may deduce, that the effects of mismodeled radiation pressure parameters on the orbital elements are either short periodic perturbations ($f(u_o)$; revolution period) or long term variations with annual and semi-annual character. These variations are not critical for monitoring nutation terms with periods below 30 days, but the former may be critical for LOD.

Due to the fact, that retrograde diurnal PM is geometrically equivalent to nutation, it is impossible to solve for both simultaneously. Thus, to overcome the singularity, amplitudes of PM terms within this frequency range were constrained to zero.

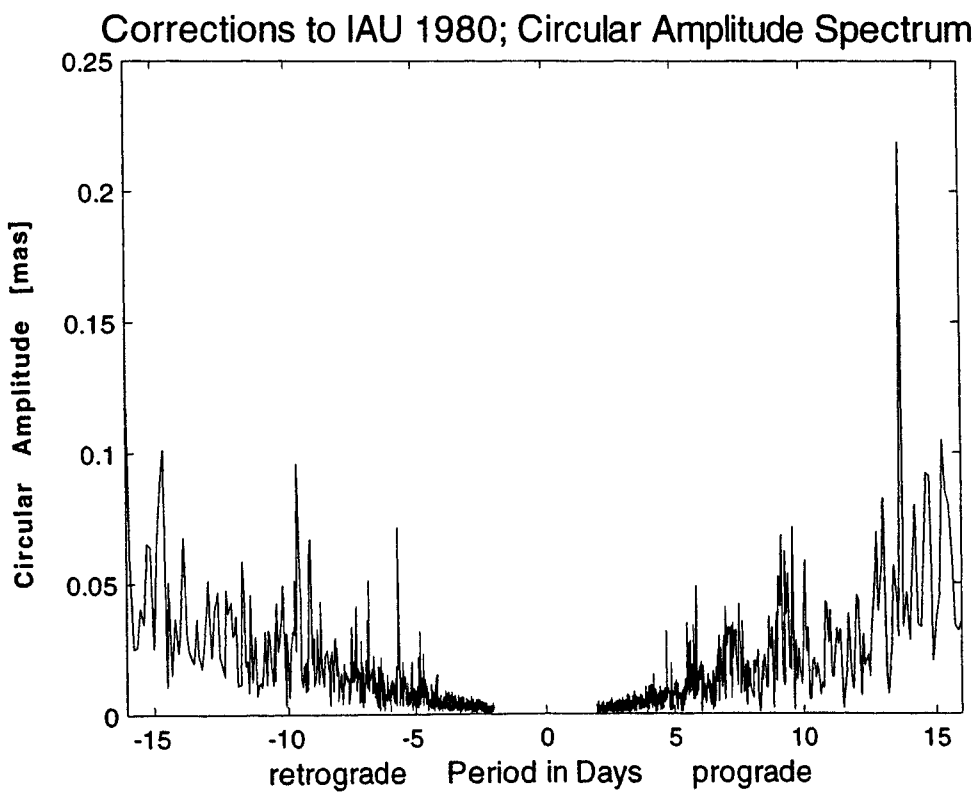


Figure 1

Figure 1 shows the spectrum of circular nutation amplitude corrections with respect to the IAU 1980 model obtained from the rate amplitude spectrum by using the conversion factor $1/\omega_j = T_j / 2\pi$. Afterwards, amplitude corrections were determined by a least square algorithm for 20 periods and listed in Tables 1a,b below (label CODE99). The weighted rms of the resulting post-fit residuals of the nutation rate corrections ($\Delta\dot{\alpha} \doteq \Delta\dot{\epsilon}; \Delta\dot{\psi}\sin\epsilon$) of $\sigma_{\Delta\dot{\alpha}} = 0.3 \text{ mas/d}$ indicates that the formal errors of the GPS estimation (see above) are not really representative.

For comparison the IERS96 model and CODE98 solution are given as well. CODE98 refers to (Rothacher *et al.*, 1999) who presented amplitude corrections both in obliquity and in longitude for 34 terms based on 3.5 years of data.

Table 1a: Nutation Amplitude Corrections in $\Delta\epsilon$ relative to the IAU 1980 Model
 (units: 0.001 mas)

Argument	Period days	CODE99		CODE98		IERS 96
		cos / sin	stdev	cos / sin	stdev	cos / sin
2 0 2 2 2	4.68	+31/ *	8	+34/ 0	8	+47/ 0
0 0 2 4 2	4.79	+24/ *	8	+28/ 0	8	+29/ 0
3 0 2 0 1	5.49	*/ *	9	+21/ 0	9	+24/ 0
1 0 2 2 2	5.64	+49/ *	9	+14/ 0	10	+25/ 0
1 -1 2 2 2	5.73	+28/ *	10	+27/ 0	10	+25/ 0
-1 0 2 4 2	5.80	-27/ *	10	-10/ 0	10	-34/ 0
0 0 2 2 2	7.10	+21/ *	12	+62/ 0	12	+43/ 0
-2 0 2 4 2	7.35	-44/ *	12	-31/ 0	13	-48/ 0
3 0 2 -2 2	8.75	-46/ *	15	-48/+18	15	-40/ 0
-1 0 4 0 2	9.06	-23/ *	16	-34/+19	16	-49/ 0
1 0 2 0 1	9.12	-85/ *	16	n.e.		-65/+8
1 0 2 0 2	9.13**	0 / +35	16	+20/+34	16	0 / +35
-1 0 2 2 2	9.56	-41/ +18	16	-36/+20	17	-46/+7
1 0 0 2 1	9.63	+73/+28	17	+32/+27	17	+49/ 0
0 0 2 0 1	13.63	+89/+33	34	n.e.		+76/+32
0 0 2 0 2	13.66**	+164/+136	27	+125/+115	24	+164/+136
0 -1 2 0 2	14.19	-34/ +67	24	0 / +60	25	0 / 0
-2 0 2 2 2	14.63	+65/ -62	25	+52/ -39	26	+40/ 0
0 0 0 2 2	14.77	+94/ *	25	+80/ *	26	+75/ 0*

Table 1b: Nutation Amplitude Corrections in $\Delta\psi$ relative to the IAU 1980 Model
 (units: 0.001 mas)

Argument	Period days	CODE99		CODE98		IERS 96
		sin / cos	stdev	sin / cos	stdev	sin / cos
0 0 2 4 2	4.79	+49/*	14	+42/+25	20	+ 29/ 0
3 0 2 0 1	5.49	-31/ *	15	-31/ *	23	+ 24/ 0
1 0 2 2 2	5.64	+89/*	17	+67/ *	24	+ 32/ 0
1 -1 2 2 2	5.73	-52/+31	18	-49/+38	25	- 59/ 0
-1 0 2 4 2	5.80	+75/*	18	+27/ *	25	+ 49/ 0
2 1 2 0 2	6.73	+22/+29	21	* / *	29	+ 40/ 0
0 1 2 2 2	6.96	+41/+29	21	+44/ *	30	+ 54/ 0
0 0 2 2 2	7.10	-69/ *	22	-83/ *	31	- 54/ 0
0 -1 2 2 1	7.23	-40/ *	22	n.e.		- 44/ 0
1 0 2 0 1	9.12**	-65/*		n.e.		- 65/ 0
1 0 2 0 2	9.13	-26/+58	38	-31/+51	40	- 37/+77
-1 0 2 2 2	9.56	-60/ *	29	-61/ *	42	- 65/ 0
0 1 2 0 2	13.17	+97/*	40	+66/ *	57	+ 57/ 0
0 0 2 0 1	13.63	-171/+48	50	n.e.		-152/+37
0 0 2 0 2	13.66**	-320/+269		-284/+272	61	-320/+269
-2 0 2 2 2	14.63	+70/-162	45	+223/-124	65	+ 39/ 0

* ... estimates below one sigma uncertainty

n.e. ... not estimated

** ... constrained to IERS 1996 value

Discussion

We find no drastic differences in the amplitudes of the CODE solutions (except in the 14.63 term in $\Delta\psi$, which is still unsatisfactory). This implies that the solution becomes more and more stable due to the extended time interval. The formal errors of the coefficients in Tables 1a and 1b basically follow the rule

$$\sigma_G = \sigma_{\Delta\dot{\alpha}} \cdot \sqrt{\frac{2}{m}} \cdot \frac{1}{\omega_j} \quad (5)$$

$\sigma_{\Delta\dot{\alpha}}$... rms of post-fit residuals of the nutation rate corrections

m ... number of nutation rate estimates

With $m=1765$ and $\sigma_{\Delta\dot{\alpha}} = 0.3 \text{ mas/d}$ we find $\sigma_G = 0.0016 \cdot T_j \text{ mas}$. In contrast to equation (5) the formal errors of amplitude corrections computed from VLBI data (σ_V) do not show this dependence on the frequency (see Figure 2).

$$\sigma_V = \sigma_{\Delta\dot{\alpha}} \cdot \sqrt{\frac{2}{m}} \quad (6)$$

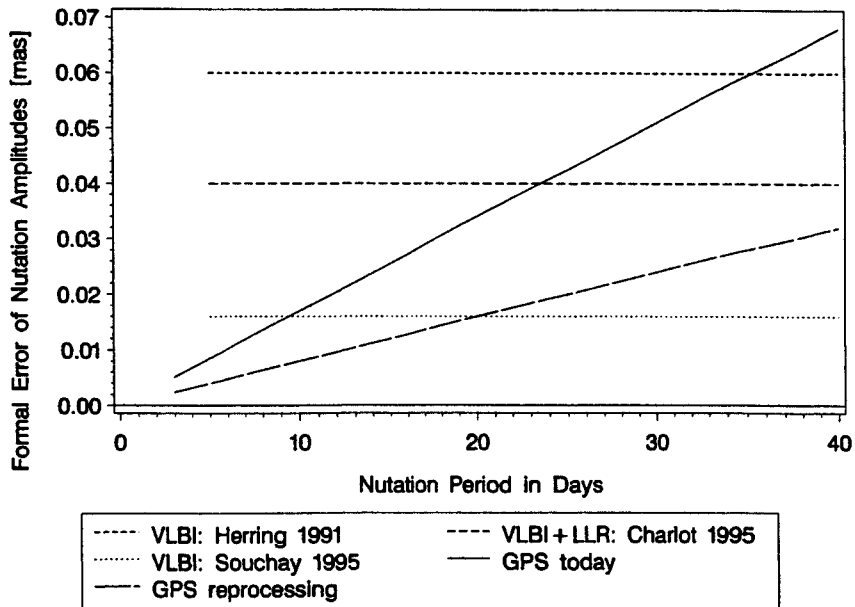


Figure 2

Thus assuming again for instance $m=1765$, $\sigma_{\Delta\dot{\alpha}} = 0.6 \text{ mas}$ (Herring et al., 1991) results in $\sigma_V = 0.020 \text{ mas}$. More recent publications (Souchay et al., 1995, Charlot et al., 1995) show smaller numbers, indicating further improvements in modeling.

The comparison of (5) and (6) immediately leads to the conclusion that GPS is able to deliver unique contributions to the nutation spectrum in the high frequency range (up to 14 days). Moreover, amplitude corrections for terms with periods ranging from 14 to 28 days may be

used in comparisons as independent determinations (although they are less accurate than the VLBI estimates). Both techniques are still improving in terms of data modelling as well as in data acquisition, which will decrease the error bars of the observed nutation series significantly in the future.

Subdaily Polar Motion

Due to ongoing attempts aiming to improve the processing strategy, the resulting series sometimes suffer from inhomogeneity and are subsequently difficult to interpret (see e.g. Rothacher *et al.*, 1999). At the CODE Analysis Center, for example, several model changes concerning the force field, the weighting of the observations (elevation dependence), the time resolution of the estimates or the realization of the reference frame can be reported between 1993 and 1998. Thus, the homogeneous recalculation of ERP-series with the most recent (and best available) strategy promises a remarkable reduction of inherent systematic errors. Test calculations were carried out, focusing on the period from Sept. 1, 1996 till Dec. 31 the same year. Data sets and models basically differ from the original computation due to the inclusion of more low-elevation data, the consideration of ocean loading effects, an improved modeling of solar radiation pressure and last but not least due to an increased time resolution of the ERPs of one hour.

The series were computed with respect to the model by Ray (Ray, 1996). Because of the well-known effect, that satellite techniques are restricted to estimate UT-rates, the difference UT-UTC has to be recovered by integration. Nutation offset drift parameters were constrained to reflect the IERS 1996 empirical model given in (Mc Carthy, 1996).

A short look at the residual 'amplitude spectrum' in PM shows us large, still remaining differences in the prograde diurnal band (Figure 3a). Due to the short series a more detailed assignment to special waves is not possible at the moment. But it might be assumed, that the differences stem from tides with periods very close to 24 hours ($S1, \psi 1$) and therefore within the 2:1 resonance of the orbit period and the sidereal day.

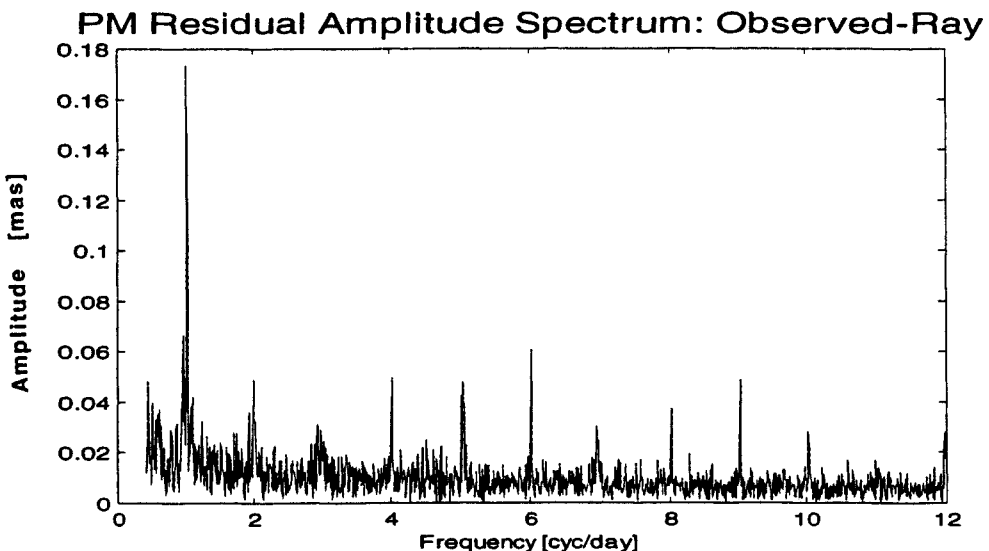


Figure 3a: Prograde Polar Motion

Similar to the UT-series there are small peaks at the higher harmonics of one cycle/day, which have to be investigated in the near future. Figure 3b shows the corresponding retrograde spectrum (same scale) giving evidence that terms at the nutation frequency have been suppressed successfully. Moreover, both plots tell us that GPS results and the Ray-Model correspond fairly good in the semidiurnal band. Compared to the original series the 'new' series show a more smooth behaviour. Remaining differences are dominated by a 14-days period both in PM and in UT1.

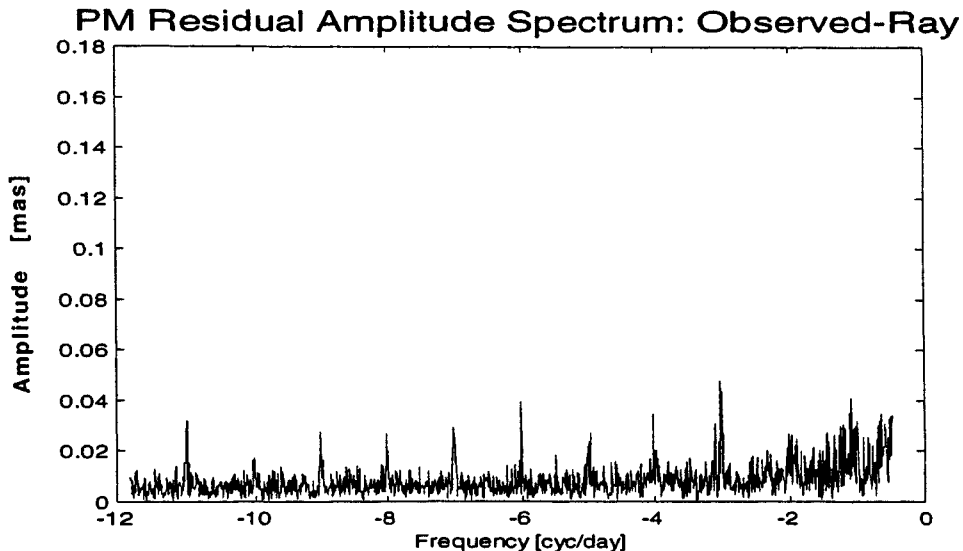


Figure 3b: Retrograde Polar Motion

Summary

GPS is able to determine a number of coefficients in the nutation series with a precision of about +/-15 micro-arcseconds growing linearly with the associated period. As expected, the contributions concentrate in the first place on terms with short periods (up to 14 days). Nevertheless, there is some residual power at periods up to a month or more. Due to correlations of the orbit force parameters with other parameter types, improving the orbit model can cause inconsistencies in the nutation rate series. Therefore reprocessing efforts and correlation studies are encouraged.

The nutation amplitude corrections computed from the GPS series provide a significant contribution to the comparison of analytic and semi-empirical nutation models. In future the combined analysis of VLBI, LLR and GPS series in order to estimate nutation amplitudes will be a worthwhile undertaking.

In terms of PM and LOD the processing of the remaining 1993-1996 GPS data is still under way and the results will be used to replace the corresponding parts of the elder series, e.g. in order to evaluate an improved set of ocean tide coefficients.

References

- Beutler G., R. Weber, E. Brockmann, M. Rothacher, St. Schaer, A. Verdun, 1998,
The GPS as a Tool in Global Geodynamics,
 in 'GPS for Geodesy', Teunissen, Kleusberg (eds.)
 pp. 569-598, Springer-Verlag, Berlin/Heidelberg.
- Beutler G., J. Kouba, M. Rothacher, R. Weber, 1999,
Polar Motion with Daily and Subdaily Time Resolution,
 Proceedings of the IAU Colloquium No.178, Cagliari.
- Brzezinski A., 1994,
Atmospheric Excitation of Nutation estimated from the 4-times daily Effective Angular Momentum Data,
 Paper presented at the 22nd General Assembly of the IAU , The Hague.
- Charlot P., O.J. Sovers, J.G. Williams, X.X. Newhall, 1995,
Precession and Nutation from joint analysis of radio interferometric and lunar laser ranging observations, Astron.J., 109(1), pp. 418-427.
- Defraigne P., V. Dehant, 1995,
Towards new non-rigid Earth Nutations,
 Proceedings to the Journees 1995, pp. 45-52, Space Research Centre Warsaw, Poland.
- Defraigne P., V. Dehant, P. Paquet, 1995,
Link between the retrograde-prograde nutations and nutations in obliquity and longitude,
 in 'Celestial Mechanics and Dynamical Astronomy', Vol. 62, pp. 363-375.
- Herring T.A., B.A. Buffett, P.M. Mathews and I.I. Shapiro, 1991,
Forced Nutations of the Earth: Influence of Inner Core Dynamics; 3. Very Long Interferometry Data Analysis,
 Journal of Geophysical Research, Vol. 96, No. B5, pp. 8259-8273.
- Kouba J., G. Beutler, M. Rothacher, 1999,
IGS Combined and Contributed ERP Solutions,
 Proceedings of the IAU Colloquium No.178, Cagliari.
- McCarthy D.D. (editor), 1996,
IERS Conventions,
 IERS Technical Note 21, Observatoire de Paris.
- Neilan, R.E. (editor), 1998,
International GPS Service; IGS Directory,
 IGS Central Bureau, JPL.
- Ray R.D., 1996,
Tidal Variations in the Earth's Rotation,
 in 'IERS Conventions', McCarthy D.D. (editor)
 IERS Technical Note 21, pp. 76-77, Observatoire de Paris.

Rothacher M., G. Beutler, T.A. Herring, R. Weber, 1999,
Estimation of Nutation Using the Global Positioning System,
Journal of Geophysical Research (JGR), Vol. 104, No. B3, pp. 4835-4859.

Rothacher M., G. Beutler, R. Weber, J. Hefty, 2000,
High Frequency Earth Rotation Variations from three Years of Global Positioning System Data,
Submitted to the Journal of Geophysical Research.

Souchay J., M. Feissel, C. Bizouard, N. Capitaine and M. Bougard, 1995,
Precession and Nutation for a Non-Rigid Earth; Comparison between Theory and VLBI Observations, Astronomy and Astrophysics, Vol. 299, pp. 277-287.

Springer T., G. Beutler, M. Rothacher, 1998,
A new Radiation Pressure Model for the GPS Satellites, in Proceedings of the IGS 1998 Analysis Center Workshop, edited by J.Dow, J.Kouba and T. Springer, pp. 89-106, ESOC, Darmstadt.

Weber R., 1996,
Monitoring Earth Orientation Variations at the Center for Orbit Determination in Europe
ÖZf Vermessung & Geoinformation; Heft 3/1996 ; pp. 269-275, Vienna.

Weber R., 1999,
The Ability of the GPS to Monitor Earth Rotation Variation
in 'Acta Geodaetica et Geophysica Hungarica',
Volume 34, Number 4, pp. 457 – 473, Akademiai Kiado, Budapest.

HIGH FREQUENCY ATMOSPHERIC EXCITATION OF EARTH ROTATION

Brzezinski Aleksander (1)- Petrov Sergei D. (2)

(1) Space Research Centre, Polish Acad. Of Sciences, Warsaw, Poland

(2) Institute of Applied Astronomy, St. Petersburg, Russia

1. INTRODUCTION

Recent determinations of the Earth orientation parameters by the space geodetic measurements revealed rapid variations in Earth rotation. These variations are at least partly driven by the fluctuations of the atmospheric angular momentum. Two types of atmospheric excitations are observed at short periods extending from several days down to 12 hours. First type is a set of tidal waves, principally of thermal origin, appearing at diurnal and semidiurnal frequencies. Second group comprises pseudoharmonic variations due to the free modes in global atmospheric circulation, such as Rossby-Haurwitz waves ψ_3^1 and ψ_1^1 with periods of about 10 and 1.2 days. The corresponding variations in Earth rotation are much smaller than the seasonal effects of atmospheric origin, nevertheless are important when taking into account the current accuracy level of monitoring changes in Earth rotation.

In this paper which is an extension of our earlier study (Petrov *et al.*, 1998), we investigate such excitations from the point of view of both theoretical modeling and observational evidence based on the available time series of the *atmospheric angular momentum* (AAM). We give a general description of the atmospheric excitation of Earth rotation and review main features of the high frequency AAM variations. Then we perform spectral analysis of the homogeneous 4-times daily AAM series based on the recent reanalysis data. Finally we estimate from the AAM data the high frequency atmospheric influences on polar motion and on the length of day variation.

2. GENERAL DESCRIPTION

Perturbations in Earth rotation are conventionally split up into the equatorial component, *polar motion*, and the axial component which is expressed either as changes in the *length of day* (l.o.d.) or as the *universal time* UT1 variation. Atmospheric excitation appears in all 3 components of the Earth's rotation vector. It has been proven that the atmosphere is a dominating driving agent at periods from weeks up to about 2 years, with a particularly strong seasonal signal; see (Eubanks, 1993) for review. At diurnal and semidiurnal periods the atmospheric excitation is in most cases much weaker than the corresponding oceanic excitation, nevertheless is non-negligible in view of the current observational accuracy and the expected future requirements.

There are two different methods of modeling atmospheric influences on Earth rotation. The first one, commonly referred to as the torque approach, consists in computation of the atmospheric torque upon the solid Earth, while the second one, the angular momentum approach, is based on the angular momentum balance between the solid Earth and the overlying atmosphere; see e.g. (Wahr, 1982) for theoretical background. These two approaches are equivalent from the first principles therefore, when properly implemented in computations, should give similar results. This is in fact the case at low frequencies, but there are still significant differences, up to one order of magnitude, at diurnal retrograde frequencies corresponding to nutation; compare e.g. recent estimates by Bizouard *et al.* (1998) and Gegout *et al.* (1998).

In the angular momentum approach, which is applied in this paper, the excitation is expressed by the AAM function $\tilde{\chi}$ introduced by Barnes *et al.* (1983), which has been initially corrected for the elastic rotational and loading deformations of the Earth. The AAM consists of the matter (pressure) term $\tilde{\chi}^p$ which can be estimated from the routine surface pressure observations, and the motion (wind) term $\tilde{\chi}^w$ depending on the wind velocities at various heights above the surface of the Earth. The excitation by the pressure term is additionally modified by the oceanic response to the atmospheric forcing. At periods longer than weeks the simple so-called *inverted barometer* (IB) approximation for the ocean response seems to be appropriate (Wahr, 1982), but at shorter periods the oceanic response becomes highly non-equilibrium and no adequate dynamical models are available so far.

Atmospheric excitation of polar motion can be expressed by the following “broad band” Liouville equation derived by Brzeziński (1994)

$$(\partial_t - i\sigma_c)(\partial_t - i\sigma_f) p = -i\sigma_c[(\partial_t - i\sigma_f)(\chi^p + \chi^w) + (\partial_t - i\sigma_c)(a_p \chi^p + a_w \chi^w)] \quad (1)$$

in which ∂_t denotes the time derivative operator, $i = \sqrt{-1}$ is imaginary unit, $p = x - iy$ stands for polar motion expressed as complex quantity and $\chi = \chi_1 + i\chi_2$ is the corresponding equatorial AAM function, σ_c, σ_f are the *Chandler wobble* (CW) and the *free core nutation* (FCN) angular frequencies of resonance, and $a_p = 9.2 \times 10^{-2}, a_w = 5.5 \times 10^{-4}$ are dimensionless constants.

The transfer function of eq.(1) is rather complicated due to the presence of 2 sharp peaks expressing the CW and FCN resonances and 1 notch resulting from the coupling between these resonances (see (Brzeziński, 1994, p. 164) for discussion), therefore comparisons between geodetic and geophysical estimates is difficult, particularly in the time domain. A simplified version of this equation is obtained after neglecting the FCN resonance, which is equivalent to the assumption $a_p = a_w = 0$:

$$(\partial_t - i\sigma_c) p = -i\sigma_c(\chi^p + \chi^w). \quad (2)$$

This is the classical low-frequency approximation of the polar motion equation (Brzeziński, 1992), but it can also be applied at high frequencies with exception of the nutation (that means diurnal retrograde) band; see (Brzeziński, 1994) and (Petrov, 1998) for argumentation. Note that in eq.(2) χ^p, χ^w are equivalent driving agents of polar motion, but this is no longer the case in the vicinity of the FCN resonance, as expressed by the last term of eq.(1).

Atmospheric excitation of the axial component of Earth rotation is expressed by the following equation

$$\delta\lambda/\lambda_o = -\chi_3, \quad (3)$$

in which $\delta\lambda$ denotes increment of l.o.d. from its mean value $\lambda_o = 2\pi/\Omega$, and Ω is the mean angular velocity of diurnal sidereal rotation. This equation is considerably simpler than the equation of polar motion, eq.(1) or eq.(2), because the transfer function is constant therefore the comparisons between geodetic and geophysical estimates are very simple both in the time domain and in the frequency domain.

3. AAM VARIATIONS: MAIN FEATURES

The equatorial component of the high frequency atmospheric excitation comprises two groups, namely a set of the tidal waves appearing at diurnal and semidiurnal periods, and a number of the broad band oscillations associated with the atmospheric normal modes. Atmospheric tides are principally of thermal origin but the gravitational contributions are probably non-negligible. The diurnal retrograde (that means migrating clockwise, from the East to the West) tidal waves in the equatorial AAM contributing to the precession/nutation, were investigated extensively in our recent paper (Bizouard *et al.*, 1998). It is commonly believed that diurnal/semidiurnal atmospheric excitations are weaker than the corresponding oceanic effect,

with the only one exclusion, namely the Sun-fixed S_1 tide contributing to the annual prograde nutation.

Two sets of the atmospheric normal modes which are important for Earth rotation are the retrograde rotational waves ψ_n^m , the Rossby-Haurwitz waves (toroidal modes), and the retrograde and prograde gravity modes ξ_n^m (spheroidal modes). Among them only ψ_1^1 , ψ_3^1 and ξ_2^1 modes will couple with polar motion and only ξ_2^0 will couple with the l.o.d. changes (Eubanks, 1991). The ψ_3^1 mode with retrograde period of about 10 days was first detected in the AAM data by Brzeziński (1987) and also observed in the polar motion data with the amplitude of the order of 1 mas (Eubanks *et al.*, 1988). The ψ_1^1 mode with retrograde period of about 1.2 days has been detected in the AAM data and should cause polar motion of the order of 30 μ as (Eubanks, 1991). The ξ_2^1 mode with predicted period of 0.61 days (*ibid.*), has not received observational evidence so far.

As concern the axial component of excitation, the atmospheric effects within the frequency range of interest, i.e. between 1 cycle in several days and one cycle in 12 hours, are confined to the diurnal and semidiurnal tidal waves which are expected to be much weaker than the corresponding oceanic influences.

4. AAM VARIATIONS: DATA ANALYSIS

In the computations reported here we used a 40-years homogeneous series of the 4-times daily AAM estimates (Salstein and Rosen, 1997) computed on the basis of results of the U.S. National Center for Environmental Prediction (NCEP) / U.S. National Center for Atmospheric Research (NCAR) reanalysis project (Kalnay *et al.*, 1996), spanning the period from 1958.0 to 1997.7. The input data contains 2 versions of the pressure term, the one which is not corrected for the ocean response, designated below χ^p , and the other one with the inverted barometer correction, designated $\chi^p + \text{IB}$.

We started the analysis from estimating the overall power spectra of the input AAM series by the maximum entropy method (Brzeziński, 1995). Then we extracted diurnal/semidiurnal components of the AAM by the so-called complex demodulation procedure (see e.g. (Bizouard *et al.*, 1998) for description) and studied them in details. Finally, the corresponding amplitudes in polar motion and l.o.d. were estimated by convolving the integrated AAM power spectrum with the theoretical transfer function, and then compared to the corresponding oceanic contributions taken from the IERS Conventions (McCarthy, 1996).

From the inspection of the overall AAM power spectra shown in Fig. 1 we can conclude what follows.

Equatorial component. These are mixed power spectra with sharp peaks at seasonal, diurnal and semidiurnal frequencies superimposed on the background continuous spectra. Power spectrum of the pressure term is approximately symmetrical with respect to zero frequency, while the wind term is mostly retrograde: from the integration we estimate that 95% of its power is at retrograde frequencies and as much as 80% of the power is concentrated within the diurnal retrograde band alone. For periods shorter than about 3 days, the wind term has similar power as the pressure term at prograde frequencies and much higher power at retrograde frequencies; for longer periods the pressure term is prevailing. The IB correction reduce significantly the continuous power spectrum of the pressure term and introduce new features, such as a broad peak at the frequency ± 1.3 cycles/day. All the expected normal modes, ψ_1^1 , ψ_3^1 and ξ_2^1 , are clearly visible in the equatorial AAM functions. An interesting common feature of the 3 spectra is a sharp peak at the retrograde O_1 frequency, which provides important verification of the AAM functions; see (Petrov, 1998) for explanation.

Axial component. Similarly as for the equatorial component, we have mixed power spectra with sharp peaks at seasonal, diurnal and semidiurnal frequencies superimposed on the background

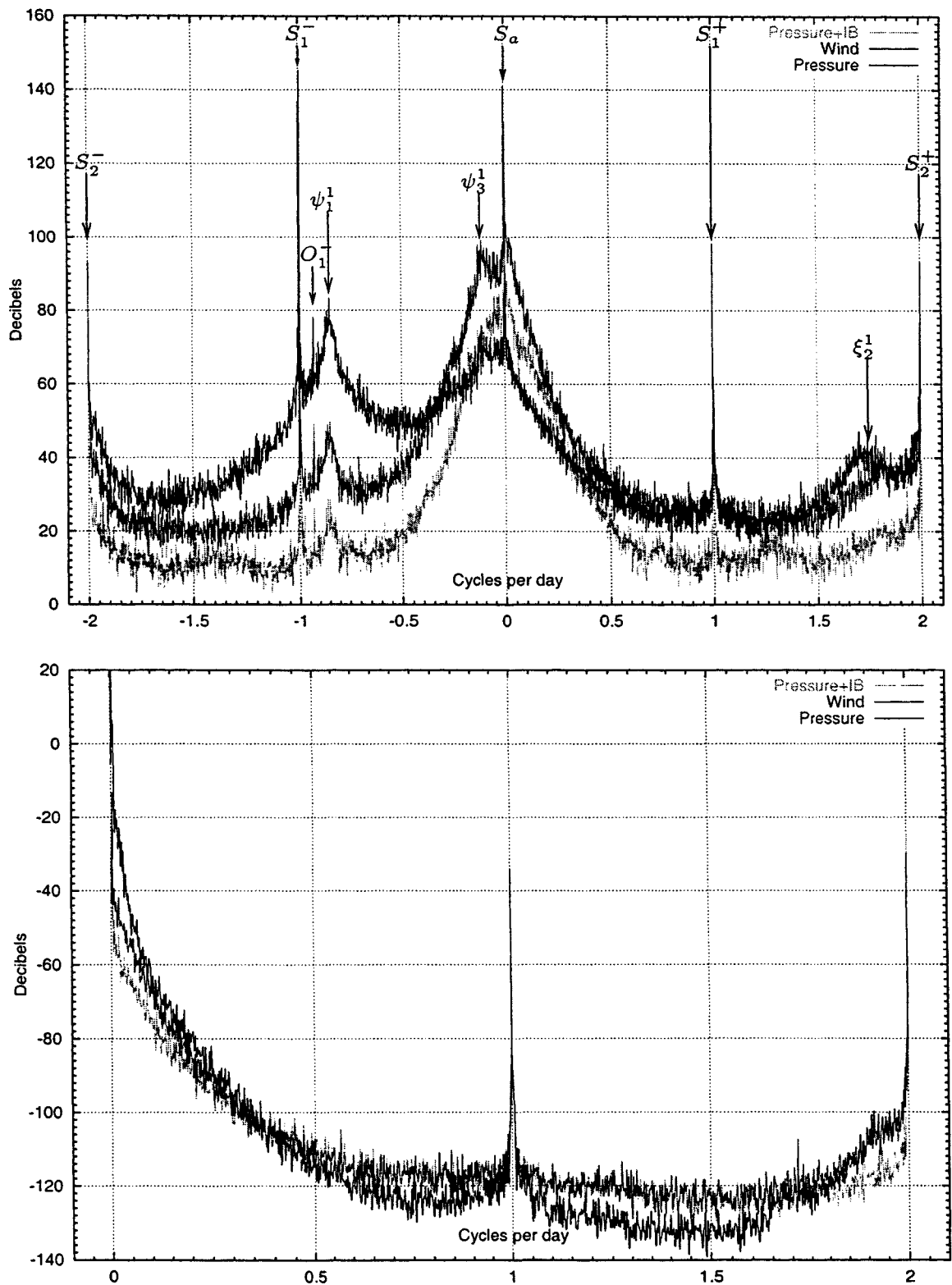


Figure 1: Overall maximum entropy method power spectra of the NCEP/NCAR reanalysis AAM series, equatorial component (upper diagram) and axial component (lower diagram).

Table 1.

Diurnal/semidiurnal atmospheric tides in polar motion, μas

Prograde		Retrograde	
in phase	out of phase	in phase	out of phase
S_1	-5.2	4.9	-16.6
P_1	0.6	-1.2	-2.0
K_1	1.4	0.7	51.2
ψ_1	-0.5	0.5	108.7
S_2	-2.8	0.6	2.8
			-0.6

Diurnal/semidiurnal atmospheric tides in LOD, μs

LOD		UT1-UTC	
in phase	out of phase	in phase	out of phase
S_1	1.2	-3.1	-0.5
S_2	0.0	-6.0	-0.5
			0.0

NOTE: Diurnal retrograde component of polar motion corresponds to nutation. The ‘in phase’/‘out of phase’ convention is the same as described in details by Bizouard *et al.* (1998).

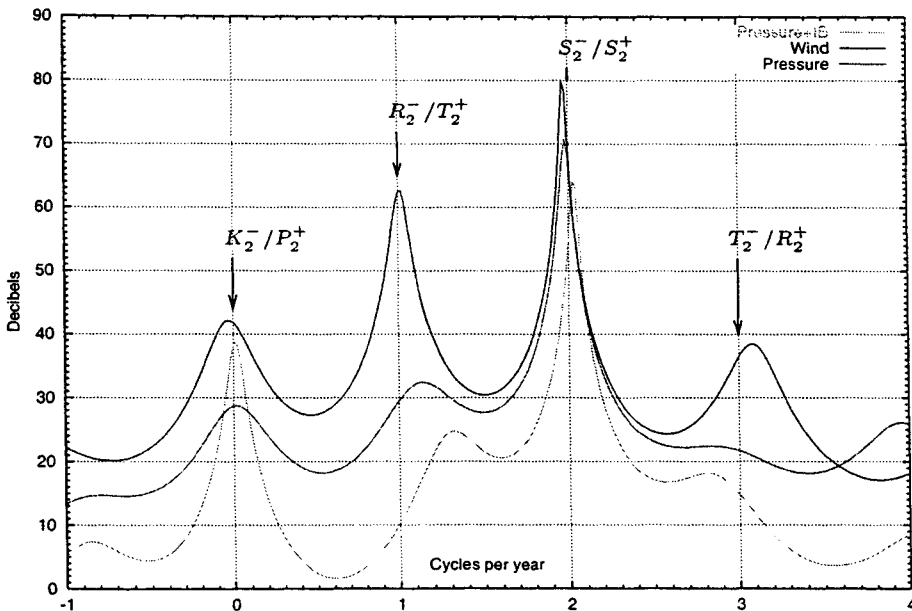


Figure 2: Power spectra of equatorial AAM series in semidiurnal retrograde band (frequency 0 corresponds to -2 cycles per day in Fig. 1).

continuous spectra. It can be observed a strong increase of power towards zero frequency, the 40-50 day peak can only be seen in the wind term. At periods shorter than about 1 week, the wind and pressure terms have similar power; at longer periods the wind term is prevailing.

Let us now investigate in a more detailed way different terms of the equatorial component of the AAM function.

Semidiurnal variations (Fig. 2, Tab. 1). Detailed spectral analysis is not possible with the 6-hourly estimates because the Nyquist limits are just inside this band, in particular such analysis cannot discriminate between prograde and retrograde oscillations (that is the reason why only the retrograde component is shown in Fig. 2). The estimated total atmospheric effect in polar motion is only about 3 μas , that is 2 orders lower than the oceanic effect; cf. Table 8.4 of the IERS Conventions (McCarthy, 1996).

Diurnal retrograde variations (Tab. 1; for the plot of the power spectra see Fig. 1 of Bizouard *et al.* (1998)). This spectral band corresponding to nutation has been investigated in details by Bizouard *et al.* (1998), therefore we recall here only briefly some important conclusions. To

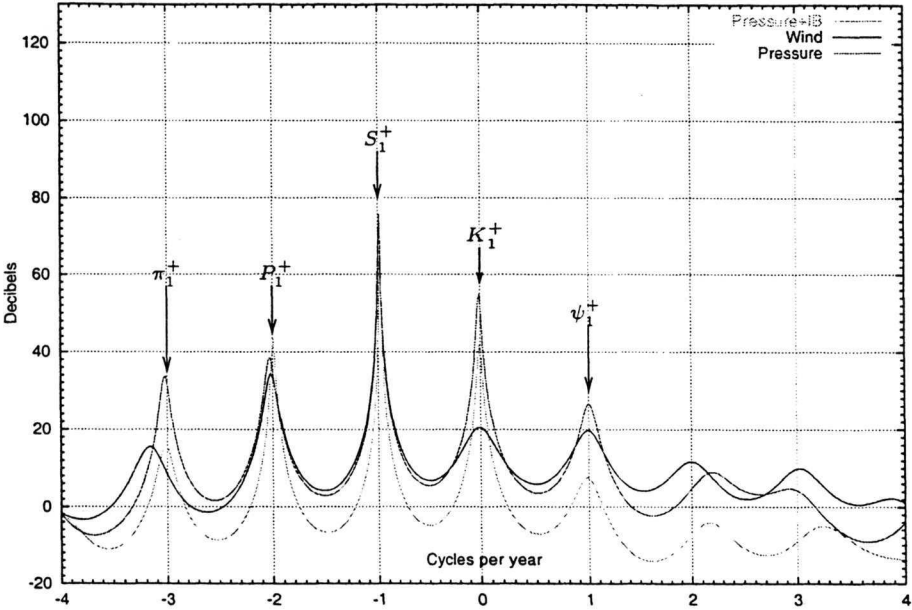


Figure 3: Power spectra of equatorial AAM series in diurnal prograde band (frequency 0 corresponds to 1 cycle per day in Fig. 1).

the observable level, atmosphere contributes to the nutation constituents with periods +1 yr ($77 \mu\text{as}$), -1 yr ($53 \mu\text{as}$), $+1/2 \text{ yr}$ ($45 \mu\text{as}$) and constant offset of the celestial pole ($\delta\psi \sin \epsilon_o = -86 \mu\text{as}$, $\delta\epsilon = 77 \mu\text{as}$), corresponding to the atmospheric tides S_1 , ψ_1 , P_1 and K_1 , respectively. Dominating contribution is from the pressure variations; only the $1/2 \text{ yr}$ prograde nutation is driven mostly by the wind term. Striking correlation between the variability of the VLBI nutation amplitudes and the atmospheric contribution provides a strong indication that the estimated effect is real. Observed degradation of correlation with VLBI data when the IB correction is applied confirms earlier claims that this correction is not adequate at nearly diurnal frequencies.

Diurnal prograde variations (Fig. 3, Tab. 1). Power spectrum of the pressure term has similar shape as in the nutation band (cf. Fig. 1 of Bizouard *et al.* (1998)), but the corresponding polar motion has an amplitude of about $7 \mu\text{as}$ only. The power of the wind term is about 40 decibels below that at diurnal retrograde frequencies (cf. *ibid.*), as could be expected from general considerations.

Atmospheric normal modes (Fig. 1, Tab. 2). The ψ_1^1 retrograde mode is similar in all 3 time series, but the strongest peak is in the wind term χ^w . The ψ_3^1 mode is similar in χ^p and χ^w , though much stronger in the first case; the IB correction seems to smooth it out to a certain extent and move some power to the prograde frequencies. The ξ_2^1 mode is manifested as a broad peak at prograde period of 0.6 days only slightly arising from the continuous background, nevertheless is visible in all spectra; the strongest one is in the wind term χ^w . We modeled all the 3 atmospheric normal modes as pseudoharmonic oscillations and estimated their parameters: central periods T , the quality factors Q and the mean amplitude of the corresponding polar motion (Tab. 2). Numerical experiment described by Petrov and Brzeziński (1996) demonstrated that when taking into account the model of the ψ_3^1 oscillation in processing polar motion data, the residuals became less correlated which results in improving the whole estimation.

Let us now discuss briefly the axial component of the AAM function. The detailed power spectra in the diurnal and semidiurnal frequency bands show similar features as in the case of the equatorial component presented so far, therefore will be not shown here. The main

Table 2.

Atmospheric normal modes in polar motion

	Period, d	Mean amplitude, μas			Quality factor
		Press.	Press.+IB	Wind	
ψ_3^1	8.3	537	199	147	5
ψ_1^1	1.2	2	1	30	10
ξ_2^1	0.6	2	1	2	-

atmospheric contribution (Tab. 1) is from the S_1 tide: $3.3 \mu\text{s}$ in LOD and $0.5 \mu\text{s}$ in UT1, and from the S_2 tide: $6.0 \mu\text{s}$ in LOD and $0.5 \mu\text{s}$ in UT1. These effects are significantly smaller than diurnal and semidiurnal oceanic contributions given in Table 8.3 of the IERS Conventions (McCarthy, 1996).

5. SUMMARY AND DISCUSSION

Diurnal and semidiurnal atmospheric tides contribute below $10 \mu\text{as}$ to polar motion and below $1 \mu\text{s}$ to UT1, that is by about 2 orders of magnitude less than the corresponding oceanic influence. A more significant and well observable atmospheric effect on nutation is of the order of $100 \mu\text{as}$. Atmospheric normal modes ψ_1^1 , ψ_3^1 and ξ_2^1 are clearly visible in all power spectra of the equatorial AAM data. Their contributions to polar motion are of the order of 1 mas, $30 \mu\text{as}$ and $3 \mu\text{as}$, respectively. The ξ_2^1 gravity mode which has not been observed so far, has only prograde component. Simple numerical experiment demonstrated that including atmospheric normal modes in modeling polar motion can improve the estimation procedure. Finally we like to caution that the estimated high frequency atmospheric effects on Earth rotation remain uncertain as long as we have no adequate dynamical model of the ocean response to the atmospheric forcing.

Acknowledgments: This research has been supported by the Polish National Committee for Scientific Research (KBN) under grant No. 9 T12E 013 15.

REFERENCES

- Barnes R. T. H., Hide R., White A. A., and Wilson C. A. (1983). Atmospheric angular momentum fluctuations, length-of-day changes and polar motion, *Proc. R. Soc. London*, **A387**, 31–73.
- Bizouard Ch., Brzeziński A. and Petrov S. (1998). Diurnal atmospheric forcing and temporal variations of the nutation amplitudes, *Journal of Geodesy*, **72**, 561–577.
- Brzeziński A. (1987). Statistical investigations on atmospheric angular momentum functions and on their effects on polar motion, *manuscripta geodaetica*, **12**, 268–281.
- Brzeziński A. (1992). Polar motion excitation by variations of the effective angular momentum function: considerations concerning deconvolution problem, *manuscripta geodaetica*, **17**, 3–20.
- Brzeziński A. (1994). Polar motion excitation by variations of the effective angular momentum function, II: extended model, *manuscripta geodaetica*, **19**, 157–171.
- Brzeziński A. (1995). On the interpretation of maximum entropy power spectrum and cross-power spectrum in earth rotation investigations, *manuscripta geodaetica*, **20**, 248–264.
- Eubanks T. M. (1991). Fluid normal modes and rapid variations in the rotation of the Earth, *unpublished manuscript*.
- Eubanks T. M. (1993). Variations in the orientation of the Earth, in. D. E. Smith and D. L. Turcotte (eds.), *Contributions of Space Geodesy to Geodynamics: Earth Dynamics, Geodynamics Series*, Vol.24, American Geophysical Union, Washington, D.C., 1–54.
- Eubanks T. M., Steppe J. A., Dickey J. O., Rosen R. D. and Salstein D. A. (1988). Causes of rapid motions of the Earth's pole, *Nature*, **334**, 115–119.

- Gegout P., Hinderer J., Legros H., Greff M. and Dehant V. (1998). Influence of atmospheric pressure on the Free Core Nutation, precession and some forced nutational motions of the Earth, *Phys. Earth Planet. Interiors*, **106**, 337–351.
- Kalnay E., Kanamitsu M., Kistler R., Collins W., Deaven D., Gandin L., Iredell M., Saha S., White G., Woollen J., Zhu Y., Chelliah M., Ebisuzaki W., Higgins W., Janowiak J., Mo K. C., Ropelewski C., Wang J., Leetmaa A., Reynolds R., Jenne R. and Joseph D. (1996). The NMC/NCAR 40-year reanalysis project, *Bull. Amer. Met. Soc.*, **77**, No.3, 437–471.
- McCarthy D. D. (ed.) (1996). IERS Conventions 1996, *IERS Technical Note 21*, Observatoire de Paris.
- Petrov S. D. (1998). *Modeling geophysical excitation of Earth rotation: stochastic and nonlinear approaches*, Ph.d. Thesis, Space Research Centre of the Polish Acad. of Sciences, Warsaw, Poland.
- Petrov S. D., Brzeziński A. (1996). On the contribution of the atmospheric normal modes to the polar motion excitation, *Proceedings of the Russian Conference “Modern Problems and Methods of Astrometry and Geodynamics”*, 23–28 September 1996, St. Petersburg, 308–313.
- Petrov S. D., Brzeziński A. and Bizouard Ch. (1998). Diurnal and semidiurnal variations of the atmospheric angular momentum and Earth orientation parameters, *Trudy IPA RAN, wyp.3 “Astrometria i geodinamika”*, St. Petersburg, 24–35, in Russian.
- Salstein D. A. and Rosen D. (1997). Global momentum and energy signals from reanalysis systems, in: *Proc. 7th Conference on Climate Variations*, 2–7 February 1997, Long Beach, California, 344–348.
- Wahr J. M. (1982). The effects of the atmosphere and oceans on the earth's wobble – I. Theory, *Geophys. J. R. Astr. Soc.*, **70**, 349–372.

IRREGULAR SHORT PERIOD VARIATIONS IN EARTH ROTATION

Kosek Wiesław - Space Research Centre, Polish Academy of Sciences Bartycka 18A,
00-716 Warsaw, Poland

ABSTRACT

Irregular variations in Earth Rotation Parameters (ERP) were detected by the autocovariance and autoregressive prediction methods applied in the forward and backward directions of time. Time variable Fourier Transform Band Pass Filter (FTBPF) spectra of the unpredictable variations of the ERP reveal that pole coordinates data are mostly disturbed in the spectral range from about 50 to 250 days while length of day (LOD) data are mostly disturbed in the spectral range from about 20 to 110 days. The most energetic irregular variations in the ERP occurred in the beginning of 1988 and 1995 years.

ANALYSIS

Irregular variations are such variations that cannot be predicted by any linear prediction method. They are caused by irregular changes of amplitudes and/or phases of oscillations. To detect irregular variations in the ERP data (x, y pole coordinates data and LOD data) the autocovariance (Kosek 1993, 1997; Kosek et al. 1998) and autoregressive (Priestley 1981) prediction methods together with time variable FTBPF (Kosek 1995; Popiński and Kosek 1995) spectral analysis were applied. In these both prediction methods the first prediction point in the future and in the past is computed and added at the end or at the beginning of data, respectively, so the next prediction point can be computed. The difference between the prediction and data in the future or in the past computed at different starting prediction epochs reveals unpredictable or irregular variations of the ERP.

The ERP (x, y and LOD) IERS C04 (IERS 1998) with the sampling interval of 1 day were used to detect their irregular variations. LOD data were converted to LODR data by removing tidal model of the IERS Conventions (McCarthy 1996). The ERP data were filtered by the Butterworth high pass filter (HPF) (Otnes and Enochson 1972) with the 270-day cutoff period to remove longer period oscillations. To detect irregular variations the autocovariance and autoregressive prediction methods were applied to compute predictions in forward and backward directions of time. The number of data used for prediction computation was equal to N=3000. This data span was sliding in forward or backward directions along the whole data interval of 1962-1999.3 with a time step equal to 1 day to compute the prediction points in 14th and 21st day in the future and in the past, respectively. The irregular variation time series are computed as the differences between short period ERP data and their predictions. These prediction errors in 14th day in the future and in the past do not exceed the value of 20 mas in case of pole coordinates data and 0.8 ms in case of LOD data as it was shown previously by Kosek et al. (1995, 1998). Usually, the prediction error in y is smaller than in x pole coordinate data. To see better the time moments of irregular variations as well as the agreement between the two prediction methods the absolute values of the differences in 14th

and 21st day in the future and in the past were smoothed with a boxcar window with the half a year time length. These smoothed irregular variations are shown in Figure 1.

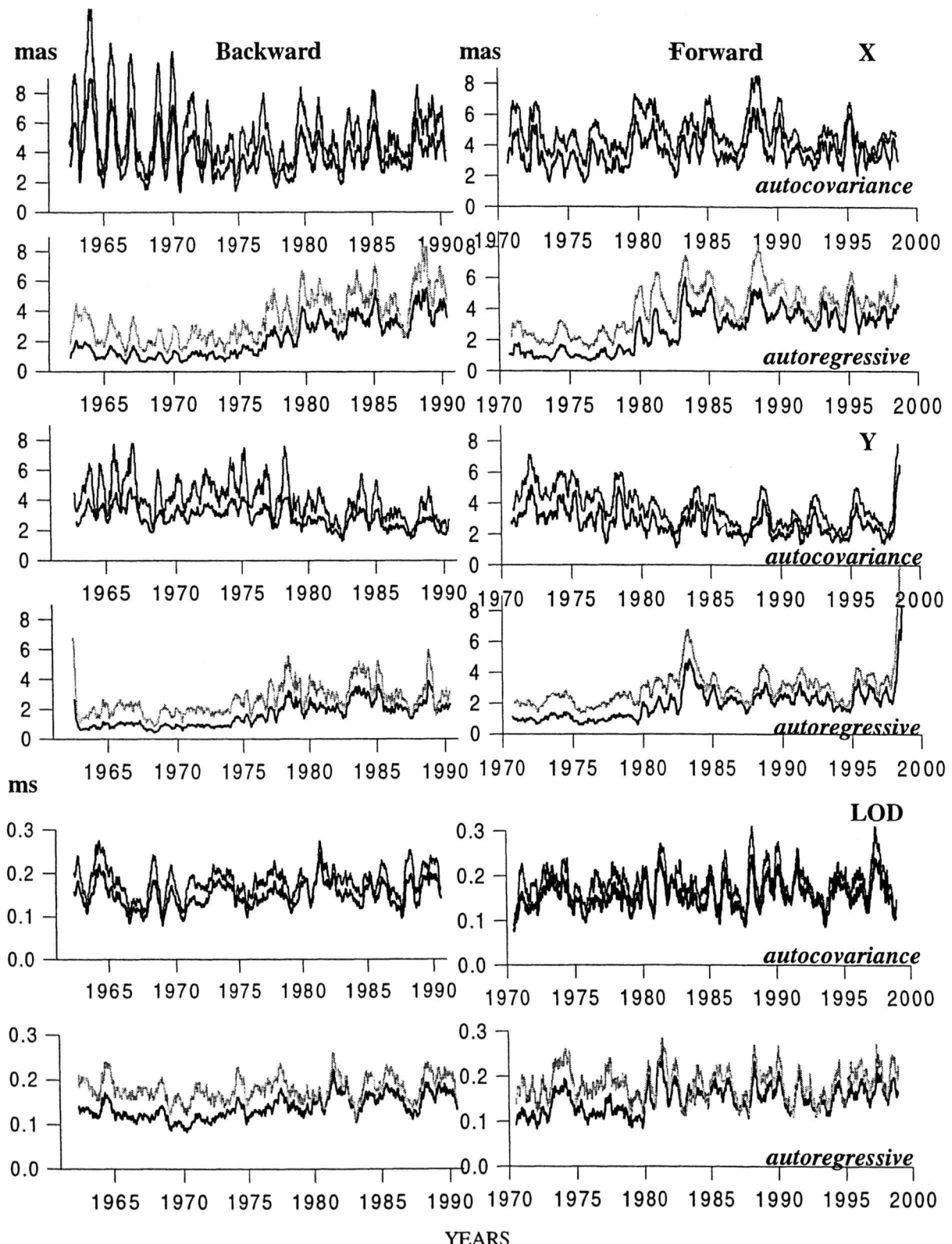


Fig. 1. Half a year mean of the absolute value of the difference between short period IERS C04 ERP data and their forward and backward autocovariance and autoregressive predictions in 14th (lower line) and 21st (upper line) day in the future and the past.

These differences for forward and backward autocovariance and autoregressive prediction methods are of the same order and they reveal unpredictable variations in the short period ERP data. The mean differences in 14th and 21st day in the future are very similar in case of both prediction methods as well as forward and backward directions though their values at 21st day are greater than in the 14th day as expected. These is also a good agreement between the mean irregular variations computed by the two prediction methods after 1980 year. Before 1980 the amplitudes of irregular variations computed by the autoregressive prediction method are smaller than those computed by the autocovariance prediction method.

To see in what frequency range short period oscillations are disturbed by irregular variations the FTBPF was applied to compute the time variable spectra of the difference between short period ERP data and their forward autocovariance prediction in 14th day in the future. It can be noticed that the time variable spectra are very similar in the case of x, y and LOD data what shows that in the particular time moments these ERP data cannot be predicted with a high precision (Fig. 2). In x and y pole coordinates data the oscillations with periods from about 50 to 250 days are mostly disturbed by irregular variations while in LOD data the oscillations with periods from about 30 to 100 days are mostly disturbed.

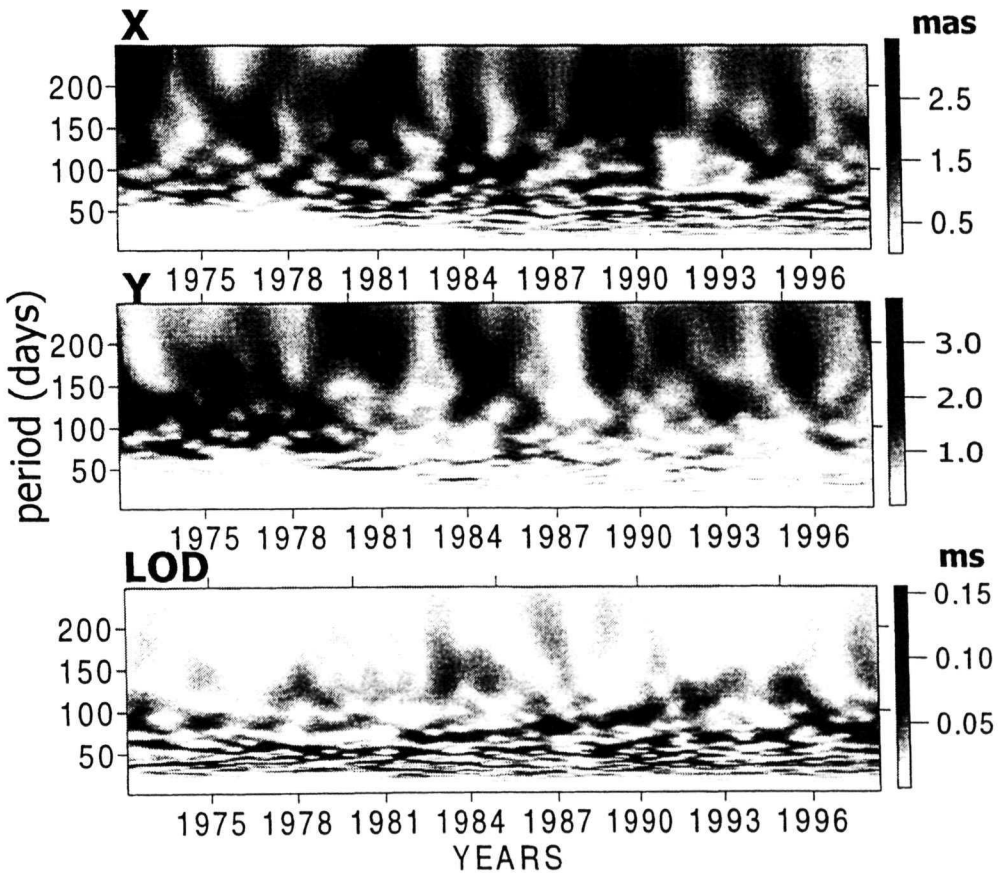


Fig. 2. The FTBPF amplitude spectra ($\lambda=0.002$) of the difference between short period ERP data and their forward autocovariance prediction in 14th day in the future.

CONCLUSIONS

The forward and backward autocovariance and autoregressive prediction methods reveal the existence of irregular variations in short period ERP data. The most energetic irregular variations occurred in the beginning of the following epochs:

X	1980-1981	1984	1985	1988	1990	1995	1997.5
Y		1981	1984	1985	1988.5	1992.5	1995
LOD	1980	1981.5	1985	1986	1988	1990	1992
						1994-1996	1998

The prediction accuracy of the autoregressive and autocovariance prediction methods are of the same order for LOD data for x, y pole coordinates data after 1980 year. Time variable amplitude spectra of irregular variations in x, y pole coordinates data are very similar after 1980.

Acknowledgements. This paper was supported by the Grant No 51/T12/97/1 of Polish Committee of Scientific Research under leadership of Prof. B. Kołaczek.

REFERENCES

- IERS 1998, Annual Report, Observatoire de Paris, France,
- Kosek 1993. The Autocovariance Prediction of the Earth Rotation Parameters. *Proc. 7th International Symposium "Geodesy and Physics of the Earth" IAG Symposium No. 112*, Potsdam, Germany, Oct. 5-10, 1992. H. Montag and Ch. Reigber (eds.), Springer Verlag, pp. 443-446.
- Kosek W., 1997. Autocovariance Prediction of Short Period Earth Rotation Parameters, *Artificial Satellites, Journal of Planetary Geodesy*, Vol. 32, No. 2, 75-85.
- Kosek W. 1995, Time Variable Band Pass Filter Spectra of Real and Complex-Valued Polar Motion Series, *Artificial Satellites, Planetary Geodesy*, No 24, Vol. 30 No 1, 27-43.
- Kosek W., Kołaczek B., 1995. Irregular Short Period Variations of Polar Motion. *Proc. Journees 1995 "Systemes de Reference Spatio-Temporels"*, Warsaw, Poland, Sep. 18-20, 1995. pp 117-120.
- Kosek W., McCarthy D.D., Luzum B. 1998, Possible Improvement of Earth Orientation Forecast Using Autocovariance Prediction Procedures, *Journal of Geodesy* 72, 189-199.
- McCarthy D.D. (ed.) 1996. IERS Conventions (1996)., *IERS Technical Note 21*. Paris. France.
- Otnes R.K., Enochson L. 1972, *Digital Time Series Analysis*, John Wiley and Sons Publishing Company, New York.
- Popiński W., Kosek W. 1995, The Fourier Transform Band Pass Filter and its Application to Polar Motion Analysis, *Artificial Satellites*, Vol. 30, No 1, 9-25.
- Priestley M.B. 1981, *Spectral Analysis and Time Series*, Academic Press, London.

WAVELET ANALYSIS OF STOCHASTIC SIGNALS

Michael Schmidt - Deutsches Geodätisches Forschungsinstitut, (DGFI)
 Marstallplatz 8 - D-80539 München, Germany
 E-mail: schmidt@dgfi.badw.de

1 INTRODUCTION

In the last years the wavelet transform has become a very appropriate tool for analysing geodetic observations. In opposite to the classical Fourier transform the most important feature of the wavelet transform is the detection of time-varying amplitudes and/or frequencies. The wavelet theory is described by many authors; see e.g. (CHUI 1994) or (LOUIS ET AL. 1998). Generally observed time series like the nutation values obtained by Very Long Baseline Interferometry (SCHMIDT AND SCHUH 1999) are stochastic signals. Thus, the theory of stochastic signals or processes has to be combined with wavelet theory. From this point of view some important foundations of the wavelet analysis of stochastic signals are presented in this paper. Especially two aspects, namely the variance distribution and the interpretation of the cross-covariance function, will be described in more detail and will be discussed in the last section. A numerical example of the procedure derived in this article is presented in the paper "Abilities of wavelet analysis for investigating short-period variations of Earth rotation" by SCHMIDT AND SCHUH (2000), also published in this volume.

2 FOURIER ANALYSIS

The most important component of Fourier analysis is the classical *Fourier transform*, defined by

$$X(j\omega) = \int_{\mathbb{R}} x(t) e^{-j\omega t} dt \quad \text{with } j = \sqrt{-1}, \quad (2.1)$$

which transforms a continuous signal $x(t)$ with $x \in \mathbb{C}$ and $t \in \mathbb{R}$ from the time domain into the frequency domain represented by the angular frequency $\omega \in \mathbb{R}$. The Fourier transform may be modified by some kind of filtering and re-transformed into the time domain by the *inverse Fourier transform*

$$x(t) = \frac{1}{2\pi} \int_{\mathbb{R}} X(j\omega) e^{j\omega t} d\omega. \quad (2.2)$$

We assume that $x(t)$ is both element of the space $L^1(\mathbb{R})$ of the absolute integrable functions and element of the space $L^2(\mathbb{R})$ of the square integrable functions. Thus, the condition

$$\int_{\mathbb{R}} |x(t)|^2 dt = \int_{\mathbb{R}} x^*(t) x(t) dt < \infty \quad (2.3)$$

holds, where $x^*(t)$ denotes the conjugate complex function of $x(t)$. Applying Parseval's formula to equation (2.3) and substituting $x^*(t) y(t)$ for $x^*(t) x(t)$, we obtain the relation

$$\int_{\mathbb{R}} x^*(t) y(t) dt = \frac{1}{2\pi} \int_{\mathbb{R}} X^*(j\omega) Y(j\omega) d\omega \quad (2.4)$$

(PAPOULIS 1984, p.279). By analogy with (2.1) $Y(j\omega)$ denotes the Fourier transform of the signal $y(t)$.

In the next step we assume that the signal $x(t)$ represents a time series or *stochastic process*. Generally a *stationary* stochastic process is characterized by the feature that the statistical properties do not change with time (PRIESTLEY 1981, p.104). The process $x(t)$ is called *wide-sense stationary* if the *expected value function*

$$\mu_x(t) = E[x(t)] = \mu_x \quad (2.5)$$

is a constant and the *autocovariance function*

$$C_x(t_1, t_2) = E[(x^*(t_1) - \mu_x^*(t_1))(x(t_2) - \mu_x(t_2))] = C_x(\tau) \quad (2.6)$$

depends only on the time difference $\tau = t_2 - t_1$. In the statistical usage the expected value function denotes the *first moment function* and the autocovariance function the *second central moment function* of the stochastic signal (KOCH AND SCHMIDT 1994, p.164). In the following the term "stationary" will mean "wide-sense stationary". Because of (2.3) and (2.5) the Fourier transform of a stationary stochastic process does not exist in general. Thus, according to the theorem of Wiener-Khintchine the frequency content is determined by the Fourier transform of the autocovariance function (2.6)

$$S_x(\omega) = \int_{\mathbb{R}} C_x(\tau) e^{-j\omega\tau} d\tau. \quad (2.7)$$

Since the relation $C_x(\tau) = C_x^*(-\tau)$ holds the *Fourier spectrum* $S_x(\omega)$ is a real-valued function. Without loss of generality we assume that the expected value function (2.5) is equal to zero

$$\mu_x = 0. \quad (2.8)$$

Frequently the autocovariance function (2.6) is not known. To derive a suitable estimation of the autocovariance function we suppose that the time series $x(t)$ is observed within a certain time interval $T = t_2 - t_1$ with $t_1 \leq t \leq t_2$. Hence, the realisation

$$x_T(t) = \begin{cases} x(t) & \text{for } t \in T \\ 0 & \text{for } t \notin T \end{cases} \quad (2.9)$$

fulfills the condition (2.3) and the Fourier transform reads

$$X_T(j\omega) = \int_{\mathbb{R}} x_T(t) e^{-j\omega t} dt = \int_T x(t) e^{-j\omega t} dt. \quad (2.10)$$

If we suppose that the process $x_T(t)$ is *ergodic*, estimates of the expected value function and the autocovariance function are calculable from one single realisation (PRIESTLEY 1981, p.340).

Hence, a suitable but biased estimation of the autocovariance function $C_x(\tau)$ is given by the well-known formula

$$\tilde{C}_x(\tau) = \frac{1}{T} \int_{t_1}^{t_2-\tau} x^*(t) x(t+\tau) dt \quad (2.11)$$

with $\tilde{C}_x(-\tau) = \tilde{C}_x^*(\tau)$ for $0 \leq \tau \leq T$ (PRIESTLEY 1981, p.721). Substituting $\tilde{C}_x(\tau)$ for the autocovariance function $C_x(\tau)$ in equation (2.7) we obtain the estimation

$$\tilde{S}_x(\omega) = \int_{-T}^T \tilde{C}_x(\tau) e^{-j\omega\tau} d\tau \quad (2.12)$$

of the Fourier spectrum $S_x(\omega)$. Without going into details the Fourier spectrum may be calculated by means of the Fourier transform (2.10)

$$\tilde{S}_x(\omega) = \frac{1}{T} |X_T(j\omega)|^2 \quad (2.13)$$

(KOCH AND SCHMIDT 1994, p.220). According to (2.2) we compute the inverse Fourier transform of equation (2.12) and set $\tau = 0$. Thus, comparing this result with equation (2.11) we obtain the relations

$$E_{x_T} = T \tilde{\sigma}_x^2 = \int_T |x(t)|^2 dt = \frac{T}{2\pi} \int_{\mathbb{R}} \tilde{S}_x(\omega) d\omega \quad (2.14)$$

for the total energy E_{x_T} of the stochastic process $x_T(t)$ defined in (2.9). The quantity $\tilde{\sigma}_x^2$ stands for the estimation of the *variance function* $\sigma_x^2 = C_x(0)$. It has to be mentioned that (2.14) is only valid if the assumption $\mu_x = 0$ is applied to the expected value function. Otherwise we have to substitute the second moment function of the signal for the second central moment function (KOCH UND SCHMIDT 1994, p.164). However, we recognize from equation (2.14) that with $\mu_x = 0$ the estimated variance $\tilde{\sigma}_x^2$ is a measure of the average power of the stochastic signal $x_T(t)$.

Analogously to (2.9) we introduce the realisation $y_T(t)$ of a stationary and ergodic process $y(t)$ with the expected value function $\mu_y = 0$ and the autocovariance function $C_y(\tau) = E[y^*(t)y(t+\tau)]$. According to (2.12) and (2.13) an estimation $\tilde{S}_{x,y}(j\omega)$ of the *Fourier cross-spectrum* $S_{x,y}(j\omega)$ is given by

$$\tilde{S}_{x,y}(j\omega) = \int_{-T}^T \tilde{C}_{x,y}(\tau) e^{-j\omega\tau} d\tau = \frac{1}{T} X_T^*(j\omega) Y_T(j\omega), \quad (2.15)$$

where the function

$$\tilde{C}_{x,y}(\tau) = \frac{1}{T} \int_{t_1}^{t_2-\tau} x^*(t) y(t+\tau) dt \quad (2.16)$$

with $\tilde{C}_{x,y}(-\tau) = \tilde{C}_{y,x}^*(\tau)$ and $0 \leq \tau \leq T$ is a biased estimation of the *cross-covariance function* $C_{x,y}(\tau)$. According to (2.10) $Y_T(j\omega)$ denotes the Fourier transform of the process $y_T(t)$. Generally the estimation $\tilde{S}_{x,y}(j\omega)$ is a complex-valued function with $\tilde{S}_{x,y}(j\omega) = \tilde{S}_{y,x}^*(j\omega)$. The function

$$\Gamma_{x,y}(j\omega) = \frac{S_{x,y}(j\omega)}{(S_x(\omega) S_y(\omega))^{1/2}} \quad (2.17)$$

with $0 \leq |\Gamma_{x,y}(j\omega)| \leq 1$ is a measure for the similarity of the two processes $x_T(t)$ and $y_T(t)$ in dependence on the angular frequency ω . Whereas the so-called *coherency* $\Gamma_{x,y}(j\omega)$ may be interpreted as a correlation function in the frequency domain, the *cross-correlation function*

$$\rho_{x,y}(\tau) = \frac{C_{x,y}(\tau)}{\sigma_x \sigma_y} \quad (2.18)$$

with $0 \leq |\rho_{x,y}(\tau)| \leq 1$ describes the correlation structure between the two processes $x_T(t)$ and $y_T(t)$ in the time domain. Estimates for the variances $\sigma_x^2 = C_x(0)$ and $\sigma_y^2 = C_y(0)$ are computed from equation (2.11) setting $\tau = 0$ as mentioned above. The square of equation (2.17) is called *normed coherency* (MEIER AND KELLER 1990, p.68).

3 WAVELET ANALYSIS

The main disadvantage of the classical Fourier transform (2.1) is the fact that it determines the frequency content of the signal $x(t)$ without any information about the location of the frequencies in the time domain. The *continuous wavelet transform*

$$X(b, a) = \int_{\mathbb{R}} x(t) \psi_{a,b}^*(t) dt \quad (3.1)$$

analyses the signal $x(t)$ in the two-dimensional *phase space* spanned by the *shift parameter* $b \in \mathbb{R}$ and the *scale parameter* $a \in \mathbb{R} \setminus \{0\}$ (CHUI 1992, p.5). Thus, the functions

$$\psi_{a,b}(t) = |a|^{-1/2} \psi\left(\frac{t-b}{a}\right), \quad (3.2)$$

which are generally localized both in the time domain and the frequency domain, are substituted for the complex oscillations $e^{j\omega t}$ of infinite length of the Fourier transform (2.1). The Fourier transform

$$\Psi(j\omega) = \int_{\mathbb{R}} \psi(t) e^{-j\omega t} dt \quad (3.3)$$

of the *wavelet function* $\psi(t)$ satisfies the so-called *admissibility condition*

$$C_\psi = \int_{\mathbb{R}} \frac{|\Psi(j\omega)|^2}{|\omega|} d\omega < \infty \quad (3.4)$$

which may be rewritten into the equivalent form

$$\int_{\mathbb{R}} \psi(t) dt = 0. \quad (3.5)$$

The Fourier transform of the function $\psi_{a,b}(t)$ from equation (3.2) is given by

$$\Psi_{a,b}(j\omega) = |a|^{1/2} \Psi(jaw) e^{-j\omega b}. \quad (3.6)$$

Thus, applying Parseval's formula (2.4) to equation (3.1) we obtain the wavelet transform with respect to the frequency domain

$$X(b, a) = \frac{|a|^{1/2}}{2\pi} \int_{\mathbb{R}} X(j\omega) \Psi^*(jaw) e^{j\omega b} d\omega, \quad (3.7)$$

if the Fourier transform $X(j\omega)$ of the signal $x(t)$ exists. An example for a wavelet function often used in geodetic and geophysical applications is the *Morlet function*; see e.g. (SCHMIDT AND SCHUH 1999) or (SCHMIDT AND SCHUH 2000).

The main advantage of the wavelet transform is given by the fact that the signal is analysed in an adaptive time-frequency window. Thus, the width of the window is narrow for the high-frequency components and wide for the low-frequency parts of the signal. However, the width and the height of the window are restricted to the uncertainty principle, which means that the

area of the resolution cell remains independent of the location in the phase space.

Again we assume that the signal $x(t)$ is stationary and ergodic. Since the condition (3.5) holds for the wavelet function $\psi(t)$ the expected value function $E[X(b, a)] = \mu_X$ of the wavelet transform (3.1) of a stationary signal is always equal to zero. To derive the autocovariance function $E[X^*(b_1, a) X(b_2, a)] = C_X(b_1, b_2, a)$ of the wavelet transform we first evaluate the product $X^*(b_1, a) X(b_2, a)$. After inserting the wavelet transform (3.1) once for $b = b_1$ and once again for $b = b_2$ and considering equation (3.2) the expression

$$\begin{aligned} X^*(b_1, a) X(b_2, a) &= |a|^{-1} \left(\int_{\mathbb{R}} x^*(t_1) \psi\left(\frac{t_1 - b_1}{a}\right) dt_1 \right) \left(\int_{\mathbb{R}} x(t_2) \psi^*\left(\frac{t_2 - b_2}{a}\right) dt_2 \right) \\ &= |a|^{-1} \int_{\mathbb{R}} \int_{\mathbb{R}} \psi\left(\frac{t_1 - b_1}{a}\right) \psi^*\left(\frac{t_2 - b_2}{a}\right) x^*(t_1) x(t_2) dt_1 dt_2 \end{aligned}$$

follows. Setting $t_2 = t_1 + \tau$ we recognize that the autocovariance function

$$C_X(b_1, b_2, a) = \int_{\mathbb{R}} C_x(\tau) \int_{\mathbb{R}} \psi_{a,s}^*(\tau) \psi_{-a,\beta}(s) ds d\tau = C_X(\beta, a) \quad (3.8)$$

of the wavelet transform only depends on the scale parameter a and the difference $\beta = b_2 - b_1$ between the two values b_1 and b_2 for the shift parameter b . Hence, the wavelet transform (3.1) of a stationary signal is stationary, too. Now we define the family of so-called *zeta-functions*

$$\zeta_{a,\beta}(\tau) = \int_{\mathbb{R}} \psi_{a,s}(\tau) \psi_{-a,\beta}^*(s) ds = \int_{\mathbb{R}} \psi_{a,\beta}(t) \psi_{a,\tau}^*(t) dt = \zeta\left(\frac{\tau - \beta}{a}\right) \quad (3.9)$$

and rewrite equation (3.8)

$$C_X(\beta, a) = \int_{\mathbb{R}} C_x(\tau) \zeta_{a,\beta}^*(\tau) d\tau. \quad (3.10)$$

Since the function $\zeta(\tau)$ from (3.9) satisfies the condition (3.5), we conclude from equation (3.10) that the autocovariance function $C_X(\beta, a)$ of the wavelet transform (3.1) results from a wavelet transform of the autocovariance function $C_x(\tau)$ by means of the wavelet function $\zeta(\tau)$. Applying Parseval's formula (2.4) to equation (3.10) we finally obtain

$$C_X(\beta, a) = \frac{|a|}{2\pi} \int_{\mathbb{R}} S_x(\omega) |\Psi(ja\omega)|^2 e^{j\omega\beta} d\omega. \quad (3.11)$$

Hence, in the frequency domain the autocovariance function $C_X(\beta, a)$ is calculated from the integration of the weighted Fourier spectrum $S_x(\omega)$. The weight function $|a| |\Psi(ja\omega)|^2$ only depends on the scale parameter a .

After substituting the estimation (2.13) for the Fourier spectrum $S_x(\omega)$ into equation (3.11) the expression

$$\tilde{C}_X(\beta, a) = \frac{1}{2\pi T} \int_{\mathbb{R}} \left(|a|^{1/2} X_T^*(j\omega) \Psi(ja\omega) \right) \left(|a|^{1/2} X_T(j\omega) \Psi^*(ja\omega) e^{j\omega\beta} \right) d\omega \quad (3.12)$$

follows. Applying Parseval's formula (2.4) again and considering equation (3.7) the estimated autocovariance function reads

$$\tilde{C}_X(\beta, a) = \frac{1}{T} \int_{\mathbb{R}} X_T^*(b, a) X_T(b + \beta, a) db, \quad (3.13)$$

where

$$X_T(b, a) = \int_{\mathbb{R}} x_T(t) \psi_{a,b}^*(t) dt = \int_T x(t) \psi_{a,b}^*(t) dt \quad (3.14)$$

denotes the wavelet transform (3.1) of the stochastic signal $x_T(t)$ defined in (2.9). A suitable alternative to the computation of the autocovariance function by means of equation (3.13) is given by equation (3.10) after inserting the estimation (2.11) of the autocovariance function $C_x(\tau)$

$$\tilde{C}_X(\beta, a) = \int_{-T}^T \tilde{C}_x(\tau) \zeta_{a,\beta}^*(\tau) d\tau. \quad (3.15)$$

Setting $\beta = 0$ in the equations (3.11) and (3.13) we obtain the relations

$$\tilde{\sigma}_X^2(a) = \frac{|a|}{2\pi} \int_{\mathbb{R}} \tilde{S}_x(\omega) |\Psi(ja\omega)|^2 d\omega = \frac{1}{T} \int_{\mathbb{R}} |X_T(b, a)|^2 db, \quad (3.16)$$

for the estimation $\tilde{\sigma}_X^2(a)$ of the scale-dependent *variance function* $\sigma_X^2(a) = C_X(0, a)$ of the wavelet transform (3.14). From the integration of equation (3.16) over the scale domain we derive the expressions

$$E_{x_T} = \frac{T}{C_\psi} \int_{\mathbb{R}} \tilde{\sigma}_X^2(a) \frac{da}{a^2} = \frac{1}{C_\psi} \int_{\mathbb{R}} \int_{\mathbb{R}} |X_T(b, a)|^2 db \frac{da}{a^2} \quad (3.17)$$

for the total energy E_{x_T} of the signal $x_T(t)$ considering the admissibility condition (3.4) and the definition (2.14) (KUMAR AND FOUFOULA-GEORGIOU 1994, p.13). Thus, the *wavelet scalogram*

$$W_x(b, a) = |X_T(b, a)|^2 \quad (3.18)$$

may be interpreted as the *energy density function* depending on the shift parameter b and the scale parameter a . Equating (2.14) and (3.17) we finally obtain the relation

$$\tilde{\sigma}_x^2 = \frac{1}{C_\psi} \int_{\mathbb{R}} \tilde{\sigma}_X^2(a) \frac{da}{a^2} \quad (3.19)$$

between the estimated values of the total variance σ_x^2 of the signal and the scale-dependent variances $\sigma_X^2(a)$ of the wavelet transform.

Again we introduce the realisation $y_T(t)$ of the stochastic signal $y(t)$ and define corresponding to the equations (3.13) and (3.15) the estimation

$$\tilde{C}_{X,Y}(\beta, a) = \int_{-T}^T \tilde{C}_{x,y}(\tau) \zeta_{a,\beta}^*(\tau) d\tau = \frac{1}{T} \int_{\mathbb{R}} X_T^*(b, a) Y_T(b + \beta, a) db \quad (3.20)$$

of the *cross-covariance function* $C_{X,Y}(\beta, a)$. According to (3.14) $Y_T(b, a)$ denotes the wavelet transform of the process $y_T(t)$. The estimation

$$\tilde{\sigma}_{X,Y}(a) = \frac{1}{T} \int_{\mathbb{R}} W_{x,y}(b, a) db \quad (3.21)$$

of the scale-dependent wavelet *covariance function* $\sigma_{X,Y}(a) = C_{X,Y}(0, a)$ is computed from (3.20) setting $\beta = 0$. By analogy with (3.18) the complex-valued function

$$W_{x,y}(b, a) = X_T^*(b, a) Y_T(b, a) \quad (3.22)$$

is called the *wavelet cross-scalogram*. Finally we define the *cross-correlation function*

$$\rho_{X,Y}(\beta, a) = \frac{C_{X,Y}(\beta, a)}{\sigma_X(a) \sigma_Y(a)} \quad (3.23)$$

with $0 \leq |\rho_{X,Y}(\beta, a)| \leq 1$ depending on the difference $\beta = b_2 - b_1$ and the scale parameter a . Estimates for the cross-covariance function $C_{X,Y}(\beta, a)$ and the variances $\sigma_X^2(a)$ and $\sigma_Y^2(a)$ are calculated from the equations (3.20) and (3.16), respectively. For $\beta = 0$ we call the function $|\Gamma_{X,Y}(a)|^2$ with $\rho_{X,Y}(0, a) = \Gamma_{X,Y}(a)$ the *normed coherency* of the wavelet transform.

4 CONCLUSIONS

The main objective of this article is to combine the theory of stochastic signals or processes with the wavelet theory. Generally, a stochastic signal or time series is characterized by its moment functions, namely the expected value function and the autocovariance function. Based on the autocovariance function of a stationary and ergodic signal and the cross-covariance function of two stochastic signals of the same kind, the following two aspects are the most important results derived in the previous section:

- According to equation (3.19) the estimated value $\tilde{\sigma}_x^2$ of the total variance σ_x^2 of the stationary stochastic signal $x_T(t)$, defined in (2.9) is decomposed into the scale-dependent variance components $\tilde{\sigma}_X^2(a)$, defined in equation (3.16). As mentioned in the context of equation (2.14) the value of the total variance is equal to the average power of a signal with zero mean. Thus, the dominant structures of the signal are detected by means of the wavelet scalogram (3.18), which represents the energy density function. Because of the fact that the angular frequency ω is related to the scale parameter a of the wavelet transform, the wavelet analysis determines time-dependent frequencies of stochastic signals.
- The cross-covariance function $C_{x,y}(\tau)$ determines the time lag between similar structures of two signals $x(t)$ and $y(t)$. By means of the wavelet transform (3.10) a scale-dependent time lag function is derived. Since the scale parameter a is related to the angular frequency ω , the described procedure allows the introduction of frequency-dependent time lags in the excitation functions for modelling polar motion and length of day variations.

An example for the application of the procedure derived in this article is presented in the paper "Abilities of wavelet analysis for investigating short-period variations of Earth rotation" by SCHMIDT AND SCHUH (2000, this volume).

REFERENCES

- CHUI, C.K. (1994) An Introduction to Wavelets. Academic Press, Boston
- KOCH, K.R. and M. SCHMIDT (1994) Deterministische und stochastische Signale. Dümmler, Bonn
- KUMAR, P. and E. FOUFOULA-GEORGIOU (1994) Wavelet Analysis in Geophysics: An Introduction. In: FOUFOULA-GEORGIOU, E. and P. KUMAR (ed.) Wavelets in Geophysics. Academic Press, San Diego
- LOUIS, A.K., MAASS, P. and A. RIEDER (1998) Wavelets. Teubner, Stuttgart
- MEIER, S. and W. KELLER (1990) Geostatistik. Springer, Wien
- PAPOULIS, A. (1984) Signal Analysis. Mc-Graw-Hill, Auckland
- PRIESTLEY, M.B. (1981) Spectral Analysis and Time Series. Academic Press, London
- SCHMIDT, M. and H. SCHUH (1999) Wavelet-Analyse der mit VLBI beobachteten Nutationsreihen. Z Vermessungswesen 124:24-30
- SCHMIDT, M. and H. SCHUH (2000) Abilities of wavelet analysis for investigating short-period variations of Earth rotation. IERS Technical Note No 28

ABILITIES OF WAVELET ANALYSIS FOR INVESTIGATING SHORT-PERIOD VARIATIONS OF EARTH ROTATION

Michael Schmidt, Harald Schuh - Deutsches Geodätisches Forschungsinstitut, (DGFI)
 Marstallplatz 8 - D-80539 München, Germany
 E-mail: schmidt@dgfi.badw.de

1 INTRODUCTION

In the last decade the sub-seasonal variations of polar motion and length of day containing oscillations with periods shorter than half a year have been investigated and their time variations have been found. Correlations in the time domain between sub-seasonal variations of Earth rotation and sub-seasonal variations of effective atmospheric angular momentum functions were determined and studied. A comprehensive list of references is given by KOLACZEK et al. (2000).

Today, besides the standard Fourier analysis of which the foundations will be given in the second section of this paper, the wavelet analysis is a very powerful method for analysing time series such as Earth rotation data. In the main part of the paper the wavelet cross-covariance function, the wavelet cross-scalogram, the wavelet cross-correlation function and the normed coherency will be defined. These are excellent tools for the comparison of polar motion and length of day (LOD) time series with atmospheric angular momentum (AAM) time series. Examples will be given for the short-period range, i.e. for periods between 5 and 150 days (for LOD) and between 5 and 60 days (for polar motion).

2 FOURIER ANALYSIS

First we assume that a wide sense stationary and ergodic time series or stochastic signal $x(t)$ is observed within the time intervall $T = t_2 - t_1$ with $t_1 \leq t \leq t_2$. Generally, a process is called *stationary* if the mean or *expected value function* $E[x(t)] = \mu_x$ is a constant and the *autocovariance function* $E[(x^*(t_1) - \mu_x^*)(x(t_2) - \mu_x)] = C_x(\tau)$ depends only on the time difference $\tau = t_2 - t_1$. Without loss of generality we assume that the signal $x(t)$ is of zero mean. Thus, the *Fourier transform* reads

$$X_T(j\omega) = \int_T x(t) e^{-j\omega t} dt . \quad (2.1)$$

Estimations $\tilde{C}_x(\tau)$ and $\tilde{S}_x(\omega)$ of the autocovariance function $C_x(\tau)$ and the *Fourier spectrum* $S_x(\omega)$ are given by

$$\tilde{C}_x(\tau) = \frac{1}{T} \int_{t_1}^{t_2-\tau} x^*(t) x(t+\tau) dt , \quad (2.2)$$

$$\tilde{S}_x(\omega) = \frac{1}{T} |X_T(j\omega)|^2 \quad (2.3)$$

with $\tilde{C}_x(-\tau) = \tilde{C}_x^*(\tau)$ for $0 \leq \tau \leq T$. $x^*(t)$ denotes the conjugate complex function of $x(t)$. Analogously to the time series $x(t)$ we introduce the stationary and ergodic signal $y(t)$ with the expected value function $\mu_y = 0$ and the autocovariance function $E[y^*(t)y(t+\tau)] = C_y(\tau)$. An estimation $\tilde{S}_{x,y}(j\omega)$ of the *Fourier cross-spectrum* $S_{x,y}(j\omega)$ is given by

$$\tilde{S}_{x,y}(j\omega) = \int_{-T}^T \tilde{C}_{x,y}(\tau) e^{-j\omega\tau} d\tau = \frac{1}{T} X_T^*(j\omega) Y_T(j\omega) , \quad (2.4)$$

where the function

$$\tilde{C}_{x,y}(\tau) = \frac{1}{T} \int_{t_1}^{t_2-\tau} x^*(t) y(t+\tau) dt \quad (2.5)$$

with $\tilde{C}_{x,y}(-\tau) = \tilde{C}_{y,x}^*(\tau)$ and $0 \leq \tau \leq T$ is an estimation of the *cross-covariance function* $C_{x,y}(\tau)$. The complex-valued function

$$\Gamma_{x,y}(j\omega) = \frac{S_{x,y}(j\omega)}{(S_x(\omega) S_y(\omega))^{1/2}} \quad (2.6)$$

with $0 \leq |\Gamma_{x,y}(j\omega)| \leq 1$ is a measure for the similarity of the two processes $x(t)$ and $y(t)$ in dependence on the angular frequency ω .

3 MORLET WAVELET ANALYSIS

The *continuous wavelet transform* of the stationary stochastic signal $x(t)$ - introduced in the last section - is defined by

$$X_T(b, a) = \int_T x(t) \psi_{a,b}^*(t) dt , \quad (3.1)$$

where a denotes the *scale parameter* and b the *shift parameter*. The functions

$$\psi_{a,b}(t) = |a|^{-1/2} \psi\left(\frac{t-b}{a}\right) \quad (3.2)$$

are computed from the wavelet function $\psi(t)$ which is restricted to the admissibility condition $\int_{\mathbb{R}} \psi(t) dt = 0$. In geodetic and geophysical applications the complex-valued *Morlet wavelet function*

$$\psi(t) = e^{j\omega_0 t} (e^{-t^2/2\sigma^2} - 2 e^{-\omega_0^2 \sigma^2/4} e^{-t^2/\sigma^2}) \quad (3.3)$$

is often used. If we choose $\omega_0 = 2\pi$ for the constant ω_0 the value of the scale parameter a is approximately equal to the period time $\frac{2\pi}{\omega}$; see e.g. (SCHMIDT 1996). The constant $\sigma \geq 1$ defines the shape of the envelope of the Morlet wavelet function. Because of the admissibility condition the expected value function of the wavelet transform of a stationary signal is always

equal zero. Thus, an estimation of the autocovariance function $E[X^*(b_1, a) X(b_2, a)] = C_X(\beta, a)$ of the wavelet transform is given by

$$\tilde{C}_X(\beta, a) = \int_{-T}^T \tilde{C}_x(\tau) \zeta_{a,\beta}^*(\tau) d\tau \quad (3.4)$$

where $\beta = b_2 - b_1$ is the difference between the two values b_1 and b_2 for the shift parameter b (SCHMIDT 2000). The so-called *zeta-functions*

$$\zeta_{a,\beta}(\tau) = \int_{\mathbb{R}} \psi_{a,\beta}(t) \psi_{a,\tau}^*(t) dt = \zeta\left(\frac{\tau - \beta}{a}\right) \quad (3.5)$$

are computed from the wavelet function $\psi(t)$. Because of the fact that the function $\zeta(\tau)$ satisfies the admissibility condition, we conclude from equation (3.4) that the autocovariance function $C_X(\beta, a)$ of the wavelet transform (3.1) is obtained by a wavelet transform of the autocovariance function $C_x(\tau)$ by means of the wavelet function $\zeta(\tau)$. In the case of the Morlet wavelet function (3.3) the zeta function reads approximately

$$\zeta(\tau) = \sqrt{\pi} \sigma e^{j\omega_0 \tau} e^{-\tau^2/4\sigma^2}. \quad (3.6)$$

Besides formula (3.4) a second representation of the estimated autocovariance function $\tilde{C}_X(\beta, a)$ is given by

$$\tilde{C}_X(\beta, a) = \frac{1}{T} \int_{\mathbb{R}} X_T^*(b, a) X_T(b + \beta, a) db \quad (3.7)$$

(SCHMIDT 2000). Thus, for $\beta = 0$ the *wavelet scalogram*

$$W_x(b, a) = |X_T(b, a)|^2 \quad (3.8)$$

may be interpreted as the *energy density function* depending on the shift parameter b and the scale parameter a ; see e.g. (KUMAR and FOUFOULA-GEORGIOU 1994, p.13).

Again we introduce a second stationary stochastic signal $y(t)$ and define - corresponding to the equations (3.4) and (3.7) - the estimation

$$\tilde{C}_{X,Y}(\beta, a) = \int_{-T}^T \tilde{C}_{x,y}(\tau) \zeta_{a,\beta}^*(\tau) d\tau = \frac{1}{T} \int_{\mathbb{R}} X_T^*(b, a) Y_T(b + \beta, a) db \quad (3.9)$$

of the *cross-covariance function* $C_{X,Y}(\beta, a)$. According to (3.1) $Y_T(b, a)$ denotes the wavelet transform of the process $y(t)$. Analogously to (3.8) the complex-valued function

$$W_{x,y}(b, a) = X_T^*(b, a) Y_T(b, a) \quad (3.10)$$

is called the *wavelet cross-scalogram*. Finally we define the *cross-correlation function*

$$\rho_{X,Y}(\beta, a) = \frac{C_{X,Y}(\beta, a)}{\sigma_X(a) \sigma_Y(a)} \quad (3.11)$$

with $0 \leq |\rho_{X,Y}(\beta, a)| \leq 1$ depending on the difference $\beta = b_2 - b_1$ and the scale parameter a . For $\beta = 0$ the square of the cross-correlation function $\rho_{X,Y}(0, a) = \Gamma_{X,Y}(a)$ is denoted as the *normed coherency* of the wavelet transform. Estimates for the cross-covariance function $C_{X,Y}(\beta, a)$ and the variances $C_X(0, a) = \sigma_X^2(a)$ and $C_Y(0, a) = \sigma_Y^2(a)$ are calculated from the equations (3.7) and (3.9), respectively.

4 NUMERICAL EXAMPLES

If the value of the square $|W_{x,y}(b, a)|^2 = W_x(b, a) W_y(b, a)$ of the wavelet cross-scalogram (3.10) is equal to zero, we cannot decide whether only one of the wavelet scalograms $W_x(b, a)$ and $W_y(b, a)$ is zero or both. Thus, the process of comparing two signals $x(t)$ and $y(t)$ includes the computation both the squared cross-scalogram and the normed coherency defined in the context of equation (3.11). This will be demonstrated by the following examples, which are based on the data sets of *length of day (LOD)*, *polar motion* and *atmospheric angular momentum (AAM)*. LOD and polar motion were taken from the IERS C04 series for the years 1980 till 1998. The corresponding AAM series derived from global meteorological data by NCEP (National Center for Environmental Prediction) was also provided by IERS (series aam.ncep.reanalysis.1958.1999).

In the first example we compare the LOD-data set with the χ_3 -data set of AAM. In the second example polar motion

$$x(t) = x_1(t) - j x_2(t) \quad (4.1)$$

is compared with the AAM-data sets of χ_1 and χ_2 combined to the complex function

$$y(t) = \chi_1(t) + j \chi_2(t). \quad (4.2)$$

$x_1(t)$ and $x_2(t)$ are the time series of the pole coordinates. The minus sign in (4.1) has to be considered because of the orientation of the coordinate system. The procedure is divided into three parts: First we compute the wavelet scalograms $W_x(b, a)$ and $W_y(b, a)$ of the two signals. In the next step we calculate the square of the wavelet cross-scalogram $W_{x,y}(b, a)$ as the product of the two scalograms. Finally, the normed coherency $|\Gamma_{X,Y}(a)|^2$ is computed. The results - calculated with $\omega_0 = 2\pi$ and $\sigma = 2$ for the constants in the Morlet wavelet function (3.3) and the zeta function (3.6) - are visualized in the figures 1 to 3 and can be summarized by:

1. Comparison of LOD with χ_3 -data set (fig. 1): There is obviously a very good agreement of the wavelet scalograms for periods longer than 35 days. The normed coherency amounts more than 0.9; further peaks are detected clearly at 20 days with a normed coherency of ~ 0.6 and at 10 days with a normed coherency of ~ 0.2 .
2. Comparison of polar motion with χ_1 -, χ_2 -data sets (fig. 2,3): The results are presented below in table 1.

prograde motions		retrograde motions	
period [d]	nor. coherency	period [d]	nor. coherency
48	~ 0.54	-58	~ 0.42
38	~ 0.52	-42	~ 0.43
29	~ 0.42	-20	~ 0.55
17	~ 0.35	-14	~ 0.44
9	~ 0.20	-8	~ 0.30

Table 1: Results of comparison between polar motion and AAM time series

5 CONCLUSIONS

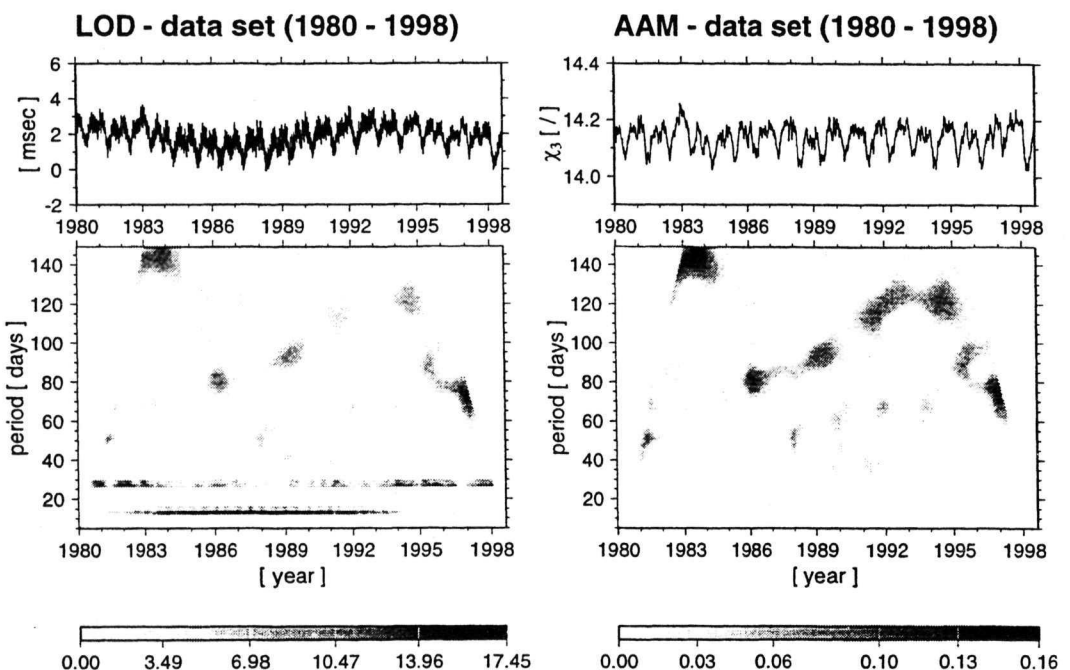
When interpreting the figures 1-3 the following conclusions can be drawn:

1. The irregular short-period variations of LOD between 35 days and 150 days are mainly caused by atmospheric excitations; the normed coherency is between 0.90 and 0.96 (see fig. 1).
2. Atmospheric influences with periods as short as 20 days and 10 days on LOD can be seen, which is demonstrated by a normed coherency of 0.6 and 0.2, respectively (see fig. 1).
3. The irregular short-period variations of polar motion are partially caused by atmospheric excitations (maxima at prograde periods of 48, 38, 29, 17 and 9 days and retrograde periods of -58, -42, -20, -14 and -8 days) with a normed coherency between 0.2 and 0.55 (see fig. 2,3).
4. The variations with very short periods (shorter than ± 25 days) are bigger in AAM than in polar motion (relative to long periods) (see fig. 2,3).
5. For the very short periods (shorter than ± 25 days) the retrograde polar motions are comparatively bigger than the prograde motions. This can be seen even better when those parts of the wavelet scalograms (fig. 2,3) i.e. for periods shorter than ± 25 days are plotted only (not shown here).
6. A considerable fraction of the very short retrograde polar motions is caused by atmospheric excitation which can be derived from the relatively high normed coherencies in the period range shorter than -25 days. According to table 1 the biggest value for the normed coherency between the polar motion and the AAM series is obtained for retrograde motions with a period of -20 days (normed coherency ~ 0.55).
7. In future we will consider scale-dependent time delays between the observed data sets and the excitation functions according to equation (3.9).

REFERENCES

- KOLACZEK, B., KOSEK, W. and H. SCHUH (2000) Short-period oscillations of Earth rotation. In: DICK, S. (ed.) Proc of the IAU Colloquium 178 Polar Motion: Historical and scientific problems, Cagliari, Sept. 1999, published by the Astronomical Society of the Pacific (in press)
- KUMAR, P. and E. FOUFOULA-GEORGIOU (1994) Wavelet Analysis in Geophysics: An Introduction. In: FOUFOULA-GEORGIOU, E. and P. KUMAR (ed.) Wavelets in Geophysics. Academic Press, San Diego
- SCHMIDT, M. (1996) Moderne Methoden der Signalanalyse. Z Vermessungswesen 121:315-325
- SCHMIDT, M. (2000) Wavelet analysis of stochastic signals. IERS Technical Note No 28

Wavelet scalograms



Square of cross-scalogram and normed coherency

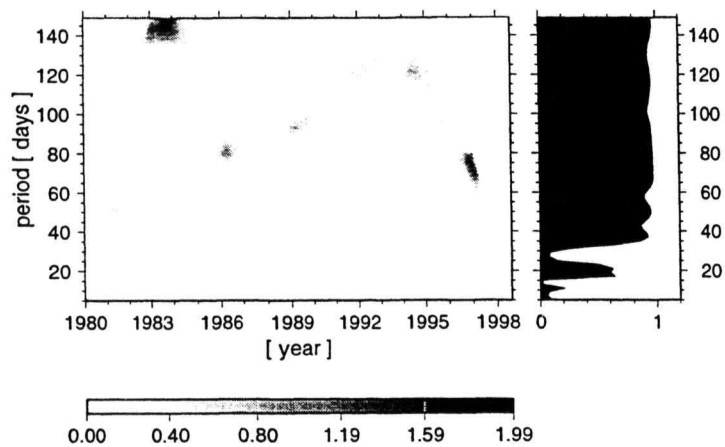
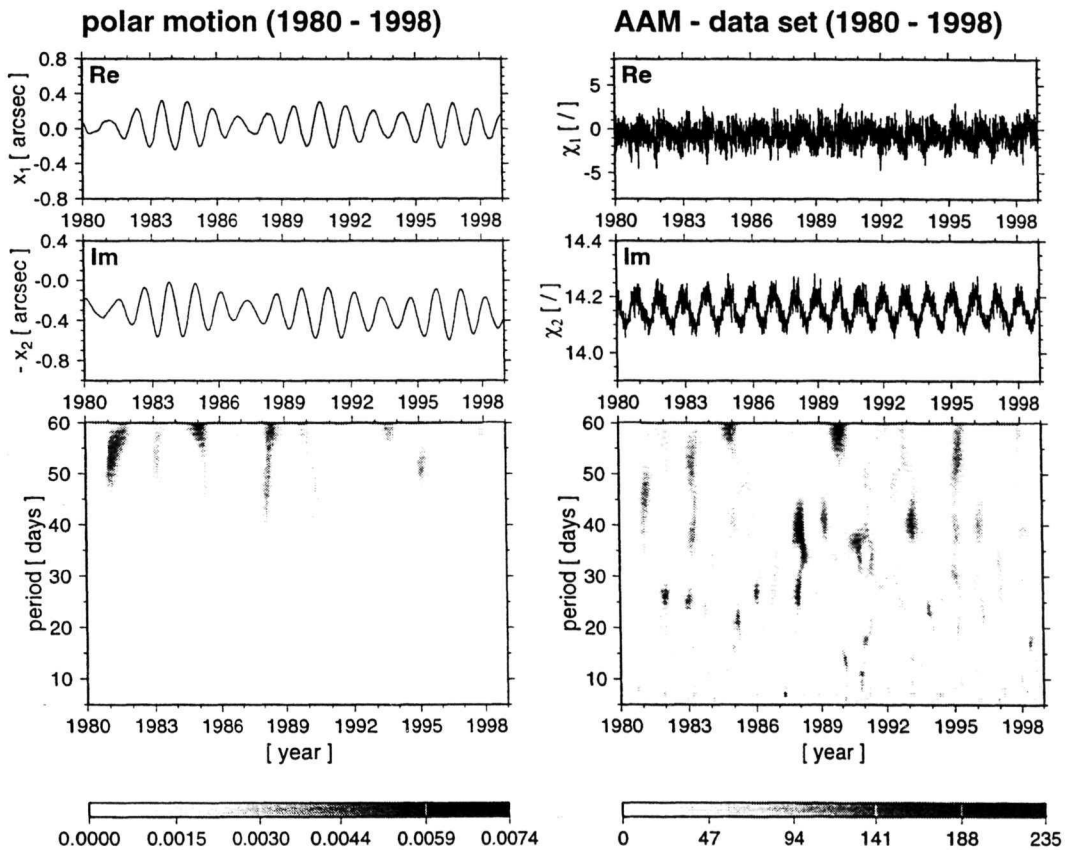


Figure 1: Comparison of LOD-data set with AAM χ_3 -data set

Wavelet scalograms (prograde)



Square of cross-scalogram and normed coherency

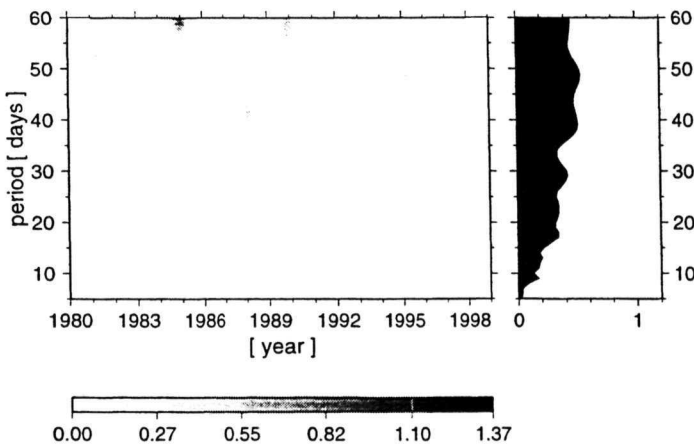
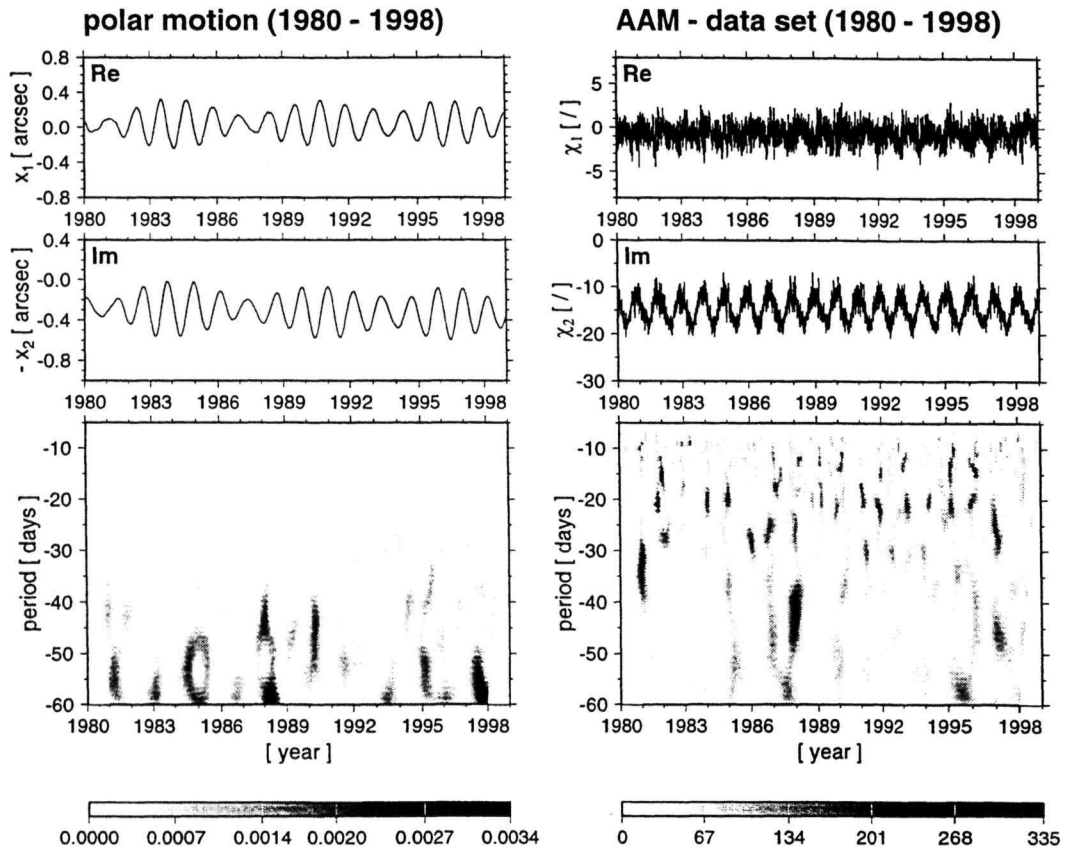


Figure 2: Comparison of polar motion with AAM χ_1 -, χ_2 -data sets (prograde)

Wavelet scalograms (retrograde)



Square of cross-scalogram and normed coherency

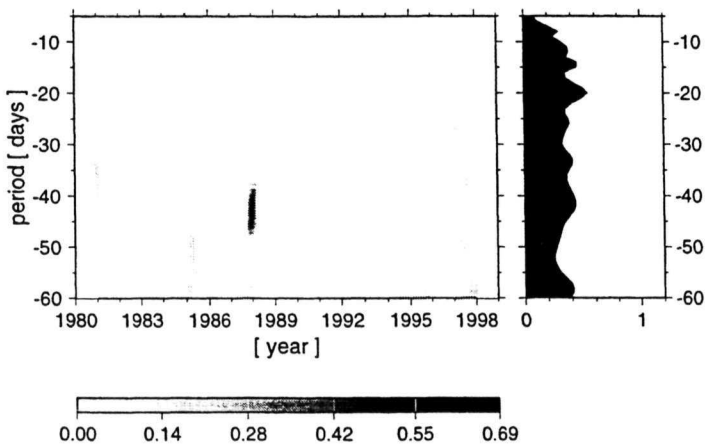


Figure 3: Comparison of polar motion with AAM χ_1 - χ_2 -data sets (retrograde)

COMPARISON BETWEEN THE FOURIER TRANSFORM BAND PASS FILTER AND THE WAVELET TRANSFORM SPECTRO-TEMPORAL ANALYSES ON THE EARTH ROTATION PARAMETERS AND THEIR ATMOSPHERIC EXCITATION FUNCTIONS

Kosek Wiesław.(1), Popiński Waldemar.(2)

(1) Space Research Centre, Polish Academy of Sciences Warsaw, Poland

(2) Department of Standards, Central Statistical Office, Warsaw, Poland

ABSTRACT

In this paper the three spectro-temporal analyses: the Fourier Transform Band Pass Filter (FTBPF), the Wavelet Transform (WT) and Harmonic Wavelet Transform (HWT) are compared on short period Earth Rotation Parameters (ERP) and the Atmospheric Angular Momentum (AAM) data. The computed time variable and time-frequency spectra of length of day (LOD) data reveal various effects of changing the time and frequency resolution in the FTBPF and frequency resolution in the HWT spectra.

TIME VARIABLE FTBPF AND TIME-FREQUENCY HWT/WT SPECTRA AND COHERENCE

Short period oscillations in the ERP data have variable amplitudes and corresponding spectra depend strongly on data time span. Thus, spectro-temporal analyses are necessary. In the WT the time series is transformed into time-frequency domain by computing convolution with a dilated analysing function e.g. Morlet wavelet, Mexican hat etc. (Chui 1992, Popiński and Kosek 1994). The WT moduli represent time-frequency spectra and are functions of instantaneous amplitudes of oscillations (Chui 1992). In the Morlet wavelet the σ parameter can be introduced which directly controls the time-frequency resolution of the relevant WT.

The FTBPF enables computation of time variable spectrum and coherence in which changing of time and frequency resolution is possible (Kosek 1995, Popiński and Kosek 1995a, 1995b, Kosek et al. 1998, Kosek and Popiński 1999). The square root of time variable FTBPF spectrum is proportional to the instantaneous amplitudes of oscillations.

In the HWT the frequency resolution can be changed by applying harmonic wavelets with localised spectral windows defined by the central frequency and the frequency bandwidth (Newland 1998). The HWT enables improving frequency resolution of a spectrum in comparison to the WT. In time-frequency analysis by the HWT the WT coefficient of a signal is defined by the convolution of this signal and the complex-valued harmonic wavelet function localised in frequency domain. In practice the FFT of a time series is multiplied by the FT of the harmonic wavelet function, which is of boxcar type possibly tapered by the gaussian window for better frequency resolution. Next, applying the inverse FFT, we estimate the magnitude of the wavelet transform coefficients representing time-frequency spectrum dependent on the two parameters: the window halfwidth λ and smoothing parameter σ (Newland 1998). The HWT time-frequency coherence estimates the correlation between the HWT coefficients of two time series (Kosek and Popiński 1999).

DATA AND THEIR ANALYSIS

In this paper the following time series were used:

- 1) The ERP (x, y pole coordinates and LOD) IERS C04 data in 1962.0 - 1999.3 years with 1-day sampling interval (IERS 1998),
- 2) the equatorial and axial components χ^{w+p+ib} of the atmospheric angular momentum (AAM) reanalysis data in 1958.0 - 1999.3, computed by the National Center for Environmental Prediction / National Center for Atmospheric Research (NCEP/NCAR), being the sum of the wind and pressure modified by inverted barometric correction (Salstein et al. 1993), the sampling interval is equal to 0.25 days.

From the LOD IERS C04 data tides were removed according to the IERS Conventions (McCarthy 1996) and next they were filtered by the Butterworth high pass filter (HPF) (Otnes and Enochson 1972) with the 270-day cutoff period to remove longer period oscillations. Next, the time variable and time-frequency spectra of such filtered LOD data were computed using the FTBPF, WT and HWT (Fig. 1).

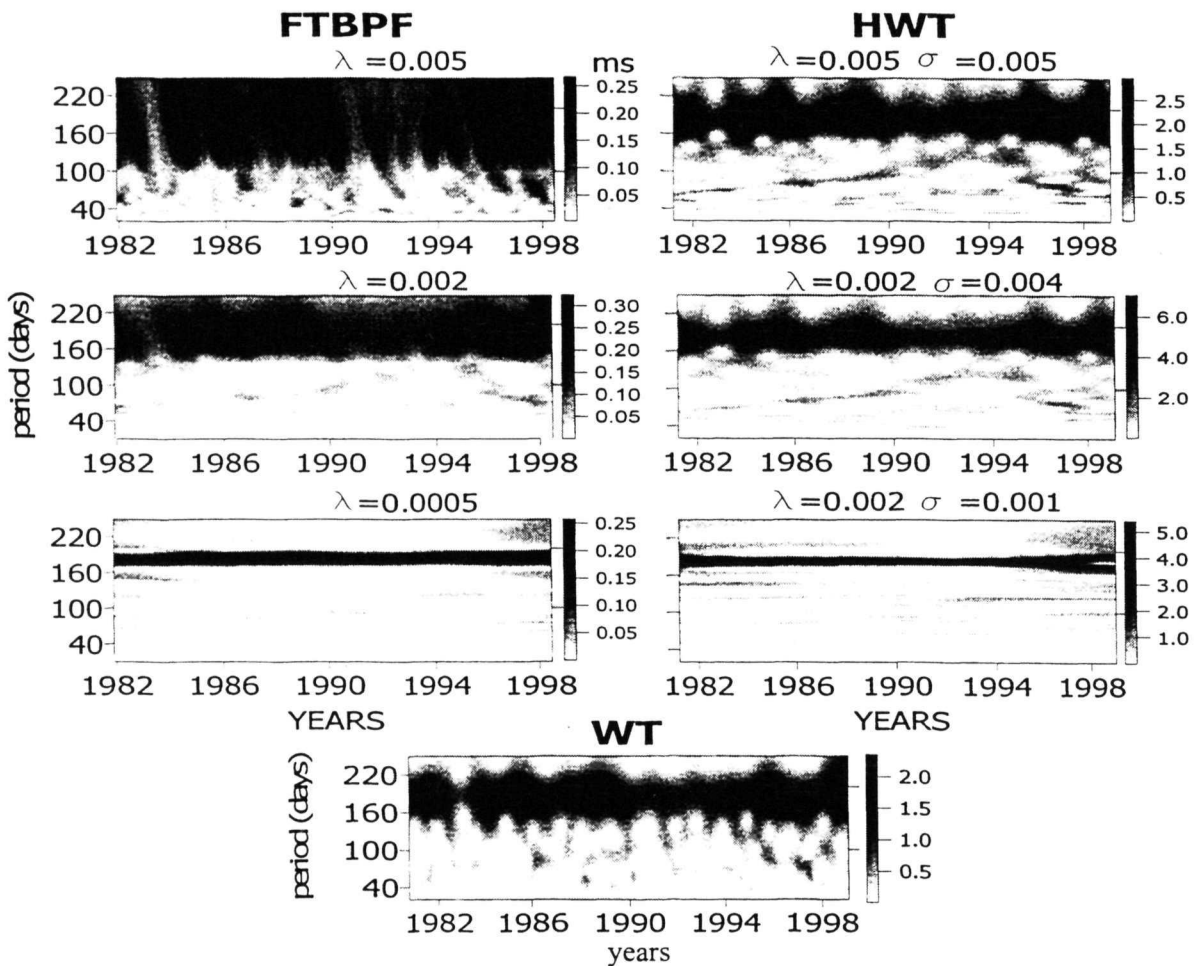


Fig. 1. Time variable FTBPF amplitude spectra, the HWT time-frequency spectra with different parameter values and the WT spectrum (Morlet wavelet) of the LOD IERS C04 data filtered by the Butterworth HPF with 270-day cutoff period.

In the FTBPF time variable and the HWT time-frequency analysis methods it is possible to increase the frequency resolution, however, in the case of the FTBPF it's also possible to increase the time resolution by increasing the λ parameter. It can be seen that decrease of the λ parameter in the FTBPF or λ and σ parameters in the HWT increases the frequency

resolution of time variable and time-frequency LOD spectra. Decrease of the λ parameter in computation of the FTBPF amplitude spectrum results in decreasing the computed amplitude values. The spectra reveal that in LOD data there is semi-annual oscillation of non-tidal origin with the amplitude of the order of 0.3 ms. Decrease of the λ parameter enabled resolving the semi-annual and semi-Chandler oscillations in polar motion data (Kosek and Popiński 1999).

The atmospheric influence on the ERP is described by the equatorial and axial components of the Effective AAM excitation function χ_1, χ_2, χ_3 (Barnes et al. 1983). This atmospheric excitation function can be compared with the geodetic excitation function ψ_1, ψ_2, ψ_3 which were computed from the IERS EOPC04 data (IERS 1998), where χ_1, χ_2 were computed by Wilson and Haubrich (1976) deconvolution formula and $\psi_3 = -LOD$. Comparison of the atmospheric and geodetic excitation functions can be performed by computing the coherence which shows the influence of the AAM excitation functions on the ERP as a function of a frequency or period. The coherences between $\chi_1 + i\chi_2$ and $\psi_1 + i\psi_2$ as well as χ_3 and ψ_3 were computed by the FTBPF with the parameter value $\lambda = 0.0015$ and the HWT with the parameter values $\lambda = 0.005, \sigma = 0.005$ (Fig. 2).

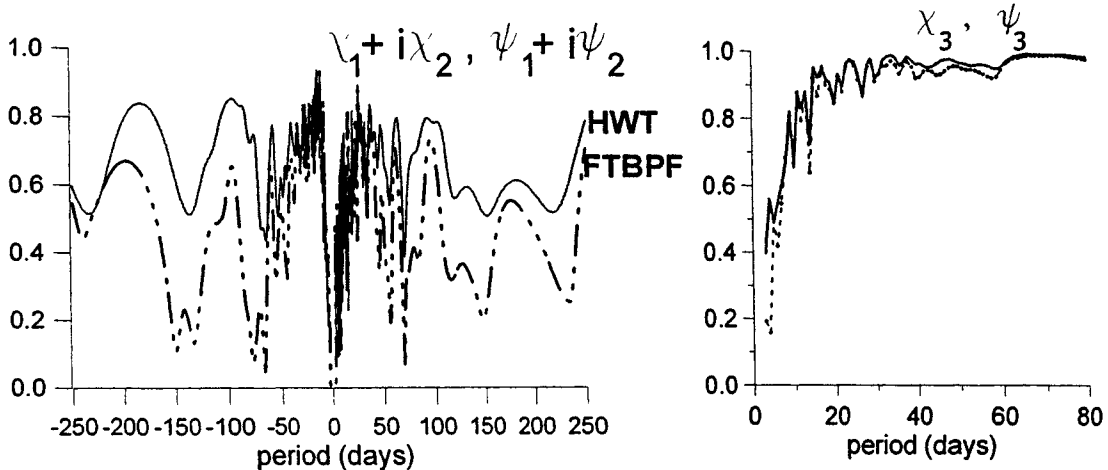


Fig. 2. The coherence between the atmospheric χ_1, χ_2, χ_3 and geodetic ψ_1, ψ_2, ψ_3 excitation functions computed by the FTBPF ($\lambda = 0.0015$) (dotted line) and the HWT ($\lambda = 0.005, \sigma = 0.005$) (solid line).

It can be noticed that the coherence between equatorial components of the atmospheric and geodetic excitation function is usually greater for the HWT than for the FTBPF and of the order of 0.6-0.8 for 182 and ~ 100 -day retrograde oscillations, 0.9 for ~ 10 -day retrograde oscillation and ~ 25 -day prograde oscillation. The coherence between the axial components of the atmospheric and geodetic excitation functions is very high for oscillations with periods greater than ~ 20 days. The coherence functions computed by the two methods vary similarly with a period change for the equatorial and axial components of the excitation functions. The time variable FTBPF and the HWT time-frequency coherences between the equatorial components of the atmospheric and geodetic excitation functions computed by Kosek and Popiński (1999) show also agreement in time variations for the two methods.

CONCLUSIONS

The HWT and FTBPF enable computation of time-frequency and time variable spectra of LOD data with a possibility of changing frequency resolution, however, the FTBPF enables improving time resolution too by increasing the λ parameter value. The coherences between the atmospheric and geodetic excitation functions computed by the FTBPF and HWT are very similar, though the FTBPF coherence between equatorial components of the atmospheric and geodetic excitation functions has usually smaller values than the HWT coherence. The coherence between axial components of the atmospheric and geodetic excitation functions drops for oscillations with periods less than ~20-days.

Acknowledgements. This paper was supported by the grant of the Polish Committee of Scientific Research No 52/T12/97/13 under the leadership of Prof. B. Kołaczek.

REFERENCES

- Barnes R.T.H., Hide R., White A.A., and Wilson C.A. 1983, Atmospheric Angular Momentum Fluctuations, length-of-day changes and polar motion, *Proc. R. Soc. London, A387*, 31-73.
- Chui C.K. 1992, An Introduction to Wavelets, *Wavelet Analysis and its Application Vol. 1*, Academic Press, Boston-San Diego.
- IERS 1998, Annual Report, Observatoire de Paris, France,
- Kosek W. 1995, Time Variable Band Pass Filter Spectra of Real and Complex-Valued Polar Motion Series, *Artificial Satellites, Planetary Geodesy*, No 24, Vol. 30, No 1, 27-43.
- Kosek W., McCarthy D.D., Luzum B. 1998, Possible Improvement of Earth Orientation Forecast Using Autocovariance Prediction Procedures, *Journal of Geodesy* 72, 189-199.
- Kosek W., Popiński W. 1999, Comparison of the spectro-temporal analysis methods on polar motion and its atmospheric excitation. *Artificial Satellites, Journal of Planetary Geodesy*, Vol. 34, No 2, 65-75.
- McCarthy D.D. (ed.) 1996, IERS Conventions (1996), *IERS Technical Note 21*, Paris, France.
- Newland D.E. 1998, Time-Frequency and Time-Scale Signal Analysis by Harmonic Wavelets, in *Signal Analysis and Prediction*, A. Prohazka, J. Uhlir, P.J. Rayner, N.G. Kingsbury (eds), Birkhauser, Boston.
- Otnes R.K., Enochson L. 1972, *Digital Time Series Analysis*, John Wiley and Sons Publishing Company, New York.
- Popiński W., Kosek W. 1994, Wavelet Transform and Its Application for Short Period Earth Rotation Analysis, *Artificial Satellites*, Vol. 29, No 2, 75-83.
- Popiński W., Kosek W. 1995a, Discrete Fourier and Wavelet Transforms in Analysis of Earth Rotation Parameters, in *Proc. Journees 1995 - Earth Rotation, Reference Systems in Geodynamics and Solar System*, 18-20 September, Warsaw, Poland, 121-124.
- Popiński W., Kosek W. 1995b, The Fourier Transform Band Pass Filter and its Application to Polar Motion Analysis, *Artificial Satellites*, Vol. 30, No 1, 9-25.
- Salstein, D.A., D.M. Kann, A.J. Miller, R.D. Rosen 1993, The Sub-bureau for Atmospheric Angular Momentum of the IERS: A Meteorological Data Center with Geodetic Applications., *Bull. Amer. Meteor. Soc.*, 74, 67-80.
- Wilson C.R. and Haubrich R.A. 1976, Meteorological Excitation of the Earth's Wobble, *Geophys. J. R. Astron. Soc.* 46, 707-743.

MODES OF VARIABILITY IN HIGH-FREQUENCY ATMOSPHERIC EXCITATION FOR MOLAR MOTION

Nastula Jolanta (1) and David A. Salstein (2)

(1) Space Research Centre Polish Academy of Sciences, Warsaw, Poland

(2) Atmospheric and Environmental Research, Inc. Cambridge, MA, USA

ABSTRACT Excitation of polar motion is related to the redistribution of atmospheric mass. Such a change is detected in atmospheric pressure, whose fluctuations are connected to observed climate patterns. Here we determine modes of the atmospheric excitation functions for polar motion by complex eigenvector analysis as a prelude to understanding a relation between atmospheric excitation and climate patterns. Examined are sub-seasonal variations of pressure, and of pressure as modified by the inverted barometer (IB) relationship, of atmospheric excitation for polar motion, computed in 108 geographic sectors for the period 1948-1999, from (NCEP/NCAR) reanalysis data. In the case of pressure the first two modes have maxima over the North Atlantic-Europe region, the North Pacific and the South Pacific. Applying the IB correction results in the dominance of the Eurasian landmass instead.

INTRODUCTION

Although the important role of atmospheric and oceanic signals for polar motion excitation has been well documented, it is clear, however, that even the combined atmospheric and oceanic forcing as determined from data currently available data do not explain all of the observed polar motion signals [see reviews by Eubanks, 1993; Ponte, 1998].

Studies of regional variability in the atmospheric excitation functions fields are necessary, as a way to understand the processes involved. To do so, we use a spatial decomposition of the atmospheric excitation functions spanning the globe. The regional variations of atmospheric excitation functions have already been computed in several papers. Salstein & Rosen [1989] used a set of two-dimensional sectors to determine that subseasonal fluctuations of atmospheric mass in such areas as the North Atlantic, North Pacific, and the whole southern oceans strongly influence the global excitation functions for polar motion. Using an 8-year data set, Nastula [1997] partly confirmed that result. Some of the regions identified by Salstein & Rosen were found to be important, but sub-seasonal variations of polar motion were strongly coherent only with the pressure over midlatitude land areas [Nastula 1997; Nastula et al., 1997]. When the inverted barometer (IB) relationship is included, spatial structure in the atmosphere over the oceans is eliminated and temporal variability is much reduced. Thus, applying the IB correction to the pressure leads to the dominance of Eurasia and America instead, with nearly all Southern Hemisphere contributions disappearing. Most recently Nastula & Salstein [1999] used a much longer and more reliable data set to expand upon the earlier results, isolating most clearly the Eurasian, North American and other regions as important for exciting high-frequency polar motion with Eurasia especially prominent in this regard.

Our goals are to confirm the important role of some regions for excitation of sub-seasonal polar motion and, more importantly, to examine if variations over the most important regions are associated with climate patterns. To do so we attempt to estimate modes of the atmospheric excitation functions by complex eigenvector analysis (Complex Empirical Orthogonal Functions Analysis). Techniques like this CEOF analysis are often used to derive patterns of climate variability.

ATMOSPHERIC DATA

A commonly used technique for comparing the polar motion excitation with atmospheric phenomena is through the determination of the so-called atmospheric excitation functions for polar motion, χ_1^A and χ_2^A , describing the

effective changes in the angular momentum components about two equatorial axes conventionally taken to point towards the Greenwich and 90° E meridians, respectively [Barnes et. al., 1983].

For this study we use two regional data sets of atmospheric excitation functions for polar motion, computed in 108 equal-area sectors by Nastula & Salstein [1999] from four-times daily gridded data produced by the U.S. National Centers for Environmental Prediction/National Center for Atmospheric Research (NCEP/NCAR) reanalyses system [Salstein et al. 1993]. The basic data include atmospheric surface pressure and the vertical distribution of the horizontal components of wind velocity on a 2.5° × 2.5° latitude-longitude grid. To produce equal-area sectors we divide the globe, placing meridional boundaries every 30° of longitude and zonal boundaries at 6.4, 19.5, 33.7, 51.1° and 90° north and south [see Figure 1 in Nastula & Salstein, 1999]. In this paper, we attempt a characterisation of patterns in excitations of subseasonal polar motion. So oscillations with periods longer than 150 days are removed from the time series in every sector by the use of a higher-order sine high-passed Butterworth filter [Otne & Enochson, 1972] and a cut-off period equal to 150 days. Additionally, because we are focused here on oscillations with periods longer than 20 days, the atmospheric time series at every sector were averaged over 10 days to decrease the number of points.

COMPLEX EMPIRICAL ORTHOGONAL FUNCTION ANALYSIS

The modes here are the eigenvectors of the covariance matrix formed from the data, and for each eigenvector one can derive a time series of coefficients by projecting the data onto the eigenvector. The product of the eigenvector and its associated time series, reproduces one portion of the original data, and summing up all such products will reconstruct the entire original data set.

To apply CEOF analysis to our data, we first formed the two-dimensional data matrix F with complex-valued elements f_{km} :

$$F = \begin{bmatrix} f_{11} & f_{1r} \\ f_{22} & + & f_{2r} \\ . & & . \\ . & & . \\ f_{n1} & & f_{nr} \end{bmatrix} \quad (1)$$

Here $f_{km} = \chi^A_{km} = (\chi^A_1 + i \chi^A_2)_{km}$ is complex-valued atmospheric excitation at 108 locations taken at times t_k from 1948 to 1999, and $m=1, 2 \dots r$ ($r = 108$ the number of sectors), and $k=1, 2 \dots n$ (the number of points for the period from 1948 to 1999). This way of ordering data into a matrix is referred to as S-mode analyses [Preisendorfer, 1988; Bjornsson & A. A. Venegas, 1997].

Next, by using singular value decomposition we decompose the data matrix F into the form [Marple, 1987]:

$$F = U \Gamma V^T \quad (2)$$

Then we form the covariance matrix R :

$$R = F^* T F = (U \Gamma V^T)^* T (U \Gamma V^T) = V \Gamma^{*T} \Gamma V^T = V \Lambda V^T \quad (3)$$

Λ is a diagonal matrix containing the eigenvalues λ_m ($m=1 \dots 108$) of covariance matrix R . The column vectors of the unitary matrix V are the eigenvectors $ceof_m$ for the R corresponding to the eigenvalues λ_m . The eigenvectors here are complex and can be expressed in term of magnitude and phase $|ceof_m| e^{i\theta_m}$. Unlike real EOF's where each mode represents a standing wave pattern, CEOF's can resolve propagating waves [Horel, 1984; Preisendorfer, 1988]. To see how eigenvectors evolve in time one can calculate time series of expansions coefficients associated with each eigenvector from the following relation:

$$c_{km} = \sum_{l=1}^{108} ceof_{lm} f_{kl} \quad (4)$$

The proportion of the total variance in the data explained by the m -th eigenvector is given by formula (5).

$$\nu_m = \lambda_m / \sum_{m=1}^{108} \lambda_m \quad (5)$$

The magnitude of ν_m can provide a measure of significance of each eigenvector. Figure 1 shows percent variability explained by ceof_m versus mode number. For the case of pressure with IB correction the first four modes explain nearly 50% of the variability, with the first four modes accounting for 19.2%, 13.9%, 11.1% and 6.4% of the total variance. The first four modes, however, for the case of pressure explains only 20% with 5.6%, 5.2%, 4.6%, 4.5% of the total variance respectively.

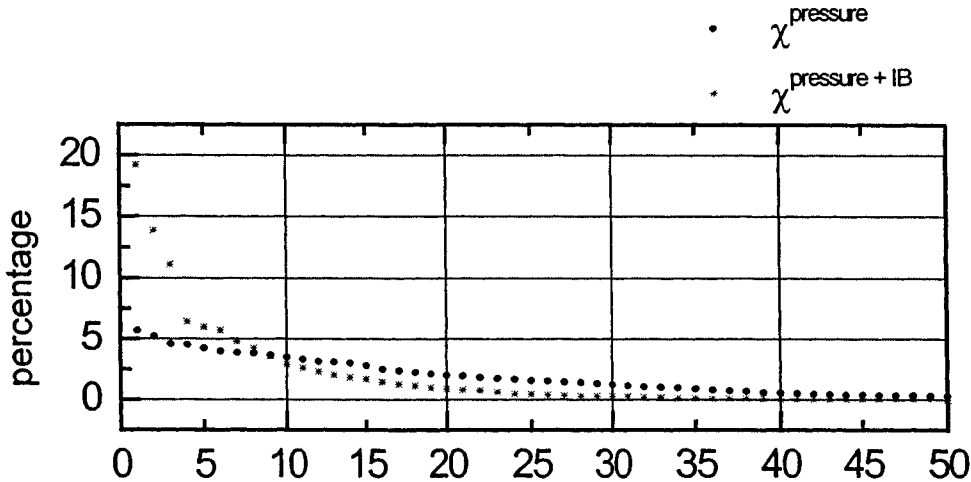


Figure 1. The fraction of the total variance of the atmospheric excitation functions computed in 108 regions explained by the mode for the case of pressure and pressure with the IB. The first 50 modes are shown.

VARIABILITY OF MODES

Figures 2a and 2b display the first complex-valued eigenvectors as maps for both pressure and pressure IB vectorially with the length of the arrow proportional to the magnitude of the eigenvector and direction equal to the eigenvector phase at a sector. Besides arrows, different shadings represent different magnitudes.

For the case of pressure here the first mode can explain only 5.6% of the global variance but reaches strong values over the Gulf of Alaska and North Pacific. The spatial pattern contains also a connection between the regions of the North Atlantic and the Europe; the signal however is weak. Maxima over the Northern Hemisphere might be associated with North Atlantic Oscillation (NAO) and North Atlantic - Eurasia variability. The Southern Hemisphere spatial pattern is characterised by wave trains spanning the South Pacific from Australia to Argentina. The center of the pattern with very strong signals found near 60°S and 90°W. This pattern might be associated with Southern Hemisphere extratropical patterns by Lau et. al. [1993]. It is clear, however, that the modes are not well separated and needs careful study of significance to be useful in studying of atmospheric excitation.

The alternate, with the addition of the IB correction, decreases the overall variance explained but now the proportion in the first mode of this total variance is larger (19.2 %) than the non-IB case, and leads to the dominance of the land areas, with Eurasia especially important. There is also some teleconnection with the Southern Hemisphere even in the IB case.

From Figures 2c and 2d one can see that the second modes magnitudes have generally similar patterns to those for the first modes. In case of pressure there are some differences between the first and the second modes patterns in the Southern Hemisphere. While in the case of pressure + IB one can see in the second mode pattern two maxima over

Europe and Asia instead of one strong maximum over West Europe for the first mode. For the pressure case the second mode explains 5.2 % of the global variance and for pressure with IB this mode can explain 13.2 %.

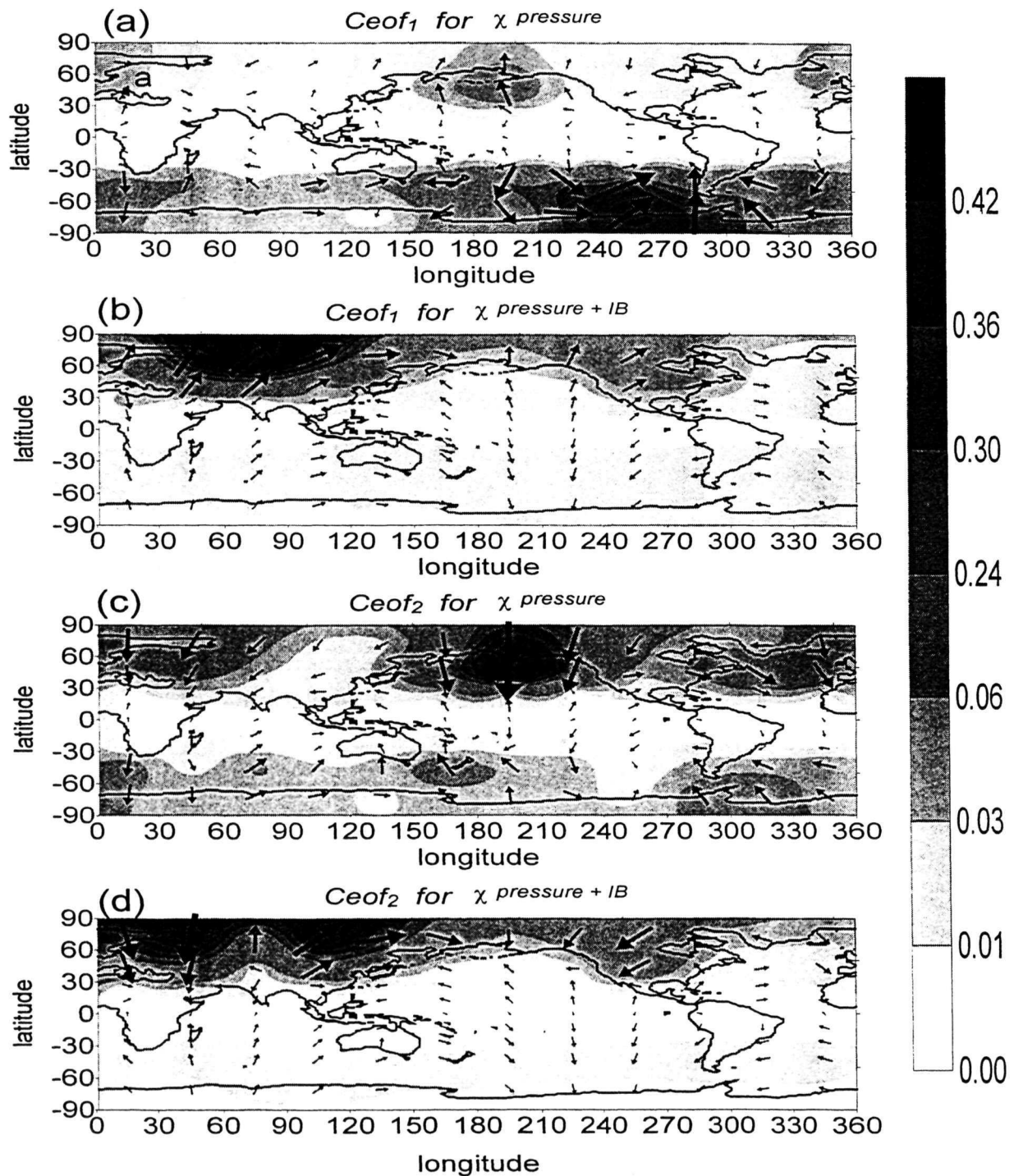


Figure 2. Dimensionless maps of (a, b) first and (c, d) second eigenvector of complex – valued atmospheric (a, c) pressure and (b, d) pressure+IB excitation functions for polar motion for the spectral band 20 – 150 days, expressed in terms of magnitude and phase. Note the changing shadings for the magnitude. Phase are plotted every point indicated by direction of the line segment; the length of the line segment is proportional to the magnitude of the eigenvector.

The phase exhibits large-scale patterns. The patterns for pressure+IB appear to be associated with wave propagation east for the first mode and with both east and west for the second mode (Figs. 2b and 2d). Modes for pressure are difficult to interpret as one wave (Figs. 2a and 2c). The pattern of the first and second modes appears to be one associated with wave propagation both zonally and meridionally.

COMPARISON WITH POLAR MOTION EXCITATION

To determine the extent to which the atmosphere participates in forcing polar motion, we compare the atmospheric excitation function with the function required to explain Earth's observed polar motion. The latter, termed the geodetic polar motion excitation functions $\chi^G = \chi_1^G + i\chi_2^G$ is determined from daily values of geodetic observations of pole position using a time domain deconvolution formula [Wilson, 1985; Nastula & Salstein, 1999]. For our analyses, we used the EOP C04 data set of polar coordinates from the International Earth Rotation Service [IERS, 1999] and a time deconvolution formula [Wilson, 1995] to compute values of χ_1^G and χ_2^G over the period from 1962 to 1999. The geodetic functions were averaged over 10-days and they were high-pass filtered by use of the Butterworth filter for consistency with the atmospheric ones.

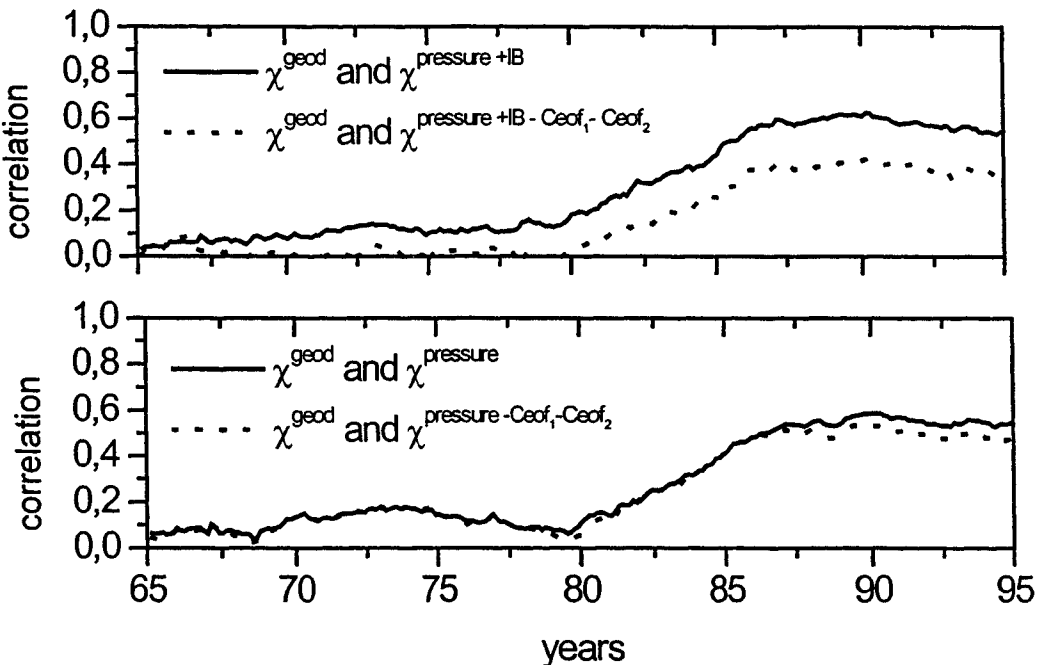


Figure 3. Correlation coefficients between the complex-valued components of geodetic and atmospheric excitation functions for polar motion, computed over five-years intervals, starting each eighth of a year, since 1962. Solid lines show "real" correlation while dotted lines show a partial correlation after two first modes are removed from a relation between polar motion and global atmosphere.

To examine the time variations of the polar motion/atmosphere relation, we calculate correlation coefficients between complex-valued components of geodetic and atmospheric functions. The coefficients were computed over five-year intervals, starting each eighth of a year, since 1962 (Fig. 3). This correlation coefficient will be defined for later purposes as a "real" correlation. In order to estimate influence of the modes on the "real" correlation, we first evaluate time series of expansions coefficients associated with $ceof_1$, and $ceof_2$. Next we eliminate its contributions from the "real" correlation by computation a partial correlations [Panofsky & Brier, 1958].

After considering Figure 3 it is clear that the "real" correlation has improved since 1980's (result also found by Nastula & Salstein, 1999). The IB correction, when included in the pressure term of the atmospheric excitation function, increases the correlation somewhat but does not change the general tendency. These disagreements are likely due to less accurate polar motion or atmospheric data before the period considered here.

Focusing on comparisons between "real" and partial correlations, one can see that two first modes seem to be important in the case of pressure with the IB correction. The "real" correlation between polar motion and atmospheric excitation with IB might be driven by patterns associated with the modes. While in the case of the pressure term, an impact two first modes on "real" correlation seem to be not significant.

CONCLUSIONS

The CEOF technique has proven to be a valuable tool in analysis of relationships between atmospheric excitation for polar motion and climate variability. Further study of the modes significance is needed, however, before relation between the modes of atmospheric excitation variability and climate patterns is fully determined.

For the case of pressure the two first modes contain patterns with strong variations over southern oceans over the Gulf of Alaska and North Pacific. The spatial pattern contains also a connection between the regions of the Northern Hemisphere. The addition of the IB correction leads to the dominance of land areas, with the Eurasia especially important. There are also some teleconnections with the Southern Hemisphere even in the IB case.

Using the CEOF we have reconfirmed the earlier results of Salstein & Rosen [1989] and Nastula & Salstein [1999] who found maxima in the atmospheric excitation function over similar regions.

The modes of pressure with IB terms of atmospheric excitation are more significant for polar motion excitation than those of pressure non-IB; however the non-IB modes may be important indicator for atmospheric variations.

Acknowledgements The research reported here was supported under the Polish State Committee for Scientific Research through project 152/T 12/97/13, and by the United States NASA Earth Observing System Program through NAG5-6309. The NSF International Division facilitated our cooperation through Grant INT-9807014. The authors thank Dr. W. Popinski who helped prepare some parts of the program for the CEOF computation.

REFERENCES

- Barnes, R. T. H., R. Hide, A. A. White, and C. A. Wilson, Atmospheric angular momentum fluctuations, length-of-day changes and polar motion, *Proc. R. Soc. Lond.*, A387, 31-73, 1983.
- Bjornsson, H. and S. A. Venegas, *A manual for EOF and SVD analyses of climatic data*, C2GCR Report 97-1, McGill University, Montreal, Canada, report, 1997.
- Eubanks, T. M., Variations in the orientation of the Earth, *AGU Monograph, Contributions of Space Geodesy to Geodynamics: Earth Dynamics*, Smith and Turcotte eds., Geodynamics Series, Vol. 24, 1 -54, 1993.
- Horel, J.P., Complex principal component analysis: Theory and examples, *J. Clim. Appl. Meteorol.*, 23, 1660-1673, 1984.
- International Earth Rotation Service (IERS), *1996 IERS annual report*, Observatoire de Paris, Paris, France, 1997.
- Marple, S. L. Jr., „Digital spectral analysis with applications”, PRENTICE-HALL, Inc., 1987.
- Nastula, J., The regional atmospheric contributions to the polar motion and EAAM excitation functions, J. Segawa et al. (eds.), Springer-Verlag Berlin Heidelberg, *Proceedings of the International Symposium on Gravity, Geoid and Marine Geodesy*, 1996, Tokyo., 1997
- Nastula, J., W. Kosek, and B. Kolaczek, Analyses of zonal atmospheric excitation functions and their correlation with polar motion excitation functions, *Ann. Geophysicae*, 15, 1439-1446, 1997.
- Nastula, J. and D. A. Salstein, Regional atmospheric angular momentum contributions to polar motion excitation, *J. Geophys. Res.*, 104, 7347 – 7358, 1999.
- Otnes R. K., and L. Enochson, *Digital Time Series Analysis*, New York, John Wiley and Sons, 1972.
- Panofsky, H. A. and G. W. Brier, „*Some Applications of statistics to meteorology*”, The Pennsylvania State University, 1958.
- Ponte, R.M., Stammer, D., and J. Marshall, Oceanic signals in observed motions of Earth's pole of rotation, *Nature*, 391, 476-479, 1998.
- Preisendorfer, R. W., „Principal component analysis in meteorology and oceanography”, C. D. Moleby (eds.), Elsevier Science Publisher, *Developments in Atmospheric Science*, 17, 1988.
- Rosen, R. D. and D. A. Salstein, Variations in atmospheric angular momentum on global and regional scales and the length of day, *J. Geophys. Res.*, 88, 5451 - 5470, 1983.
- Salstein, D. A., and R. D. Rosen, Regional contributions to the atmospheric excitation of rapid polar motions, *J. Geophys. Res.*, 94, 9971 - 9978, 1989.
- Salstein, D. A., D. M. Kann, A. J. Miller, and R. D. Rosen, The Sub-Bureau for Atmospheric Angular Momentum of the International Earth Rotation Service: a meteorological data center with geodetic applications, *Bull. Amer. Meteor. Soc.*, 74, 67-80, 1993.
- Wilson, C. R., Discrete polar motion equations, *Geophys. J. R. Astr. Soc.*, 80, 551-554, 1985.

Imprimé en France par INSTAPRINT S.A.
1-2-3, levée de la Loire - LA RICHE - B.P. 5927 - 37059 TOURS Cedex 1
Tél. 02 47 38 16 04

Dépôt légal 3^e trimestre 2000 - 09005588-700